BEHAVIOR OF STEEL PALLET RACK BEAM TO COLUMN CONNECTIONS AT AMBIENT AND ELEVATED TEMPERATURES

SYED NAVEED RAZA SHAH

THESIS SUBMITTED IN FULFILMENT OF THE REQUIREMENTS FOR THE DEGREE OF DOCTOR OF PHILOSOPHY

FACULTY OF ENGINEERING
UNIVERSITY OF MALAYA
KUALA LUMPUR

2016

UNIVERSITY OF MALAYA

ORIGINAL LITERARY WORK DECLARATION

Name of Candidate: **SYED NAVEED RAZA SHAH**

Matric No: **KHA 130021**

Name of Degree: **DOCTOR OF PHILOSOPHY/ ENGINEERING**

Title of Project Paper/Research Report/Dissertation/Thesis ("this Work"):

BEHAVIOR OF STEEL PALLET RACK BEAM TO COLUMN CONNECTIONS AT AMBIENT AND ELEVATED TEMPERATURES

Field of Study: **STRUCTURAL ENGINEERING & MATERIALS (CIVIL ENGINEERING)**

I do solemnly and sincerely declare that:

(1) I am the sole author/writer of this Work;
(2) This Work is original;
(3) Any use of any work in which copyright exists was done by way of fair dealing and for permitted purposes and any excerpt or extract from, or reference to or reproduction of any copyright work has been disclosed expressly and sufficiently and the title of the Work and its authorship have been acknowledged in this Work;
(4) I do not have any actual knowledge nor do I ought reasonably to know that the making of this work constitutes an infringement of any copyright work;
(5) I hereby assign all and every rights in the copyright to this Work to the University of Malaya ("UM"), who henceforth shall be owner of the copyright in this Work and that any reproduction or use in any form or by any means whatsoever is prohibited without the written consent of UM having been first had and obtained;
(6) I am fully aware that if in the course of making this Work I have infringed any copyright whether intentionally or otherwise, I may be subject to legal action or any other action as may be determined by UM.

Candidate's Signature Date:

Subscribed and solemnly declared before,

Witness's Signature Date:

Name:

Designation:

ABSTRACT

Steel pallet racks (SPRs) are designed to be readily demountable and capable of re-assembly depending upon the volume of storage goods. Therefore, semi-rigid boltless beam-to-column connections (BCCs) are used in these structures which govern the stability of SPRs in the unbraced down-aisle direction. The performance of SPR BCCs relies upon the behavior of the connection device, namely, 'beam end connector' (BEC). The structural behavior of the BEC varies with its configuration and hampers the development of a common analytical model to predict the behavior of all types of SPR BCCs. The behavior of the SPR BCCs becomes more complicated in case of fire. However, the literature completely lacks the studies on the behavior of SPR BCCs subjected to elevated temperatures. This research examines the experimental and numerical behavior of SPR BCCs at ambient and elevated temperatures and consists of two main types of investigation. In the first phase, the experimental testing of SPR BCCs at ambient temperature was performed using double cantilever test setup. Thirty-two tests were performed based on the variation in column thickness, beam depth and number of tabs in the beam end connector to examine the behavior of SPR BCCs. The moment-rotation (M-θ) behavior, load-strain relationship, major failure modes and the influence of selected parameters on the connection performance were investigated. A comparative study to calculate the connection stiffness was carried out by comparing various stiffness design methods available in the literature and the appropriate method is determined. A 3D non-linear finite element (FE) model that simulates the testing protocol was generated using ABAQUS FE software and its accuracy was validated against experimental results. After achieving a good overall agreement between the FE analysis and experimental results, the FE model was further extended to perform parametric analysis. In the second phase, experimental and numerical testing of SPR BCCs subjected to fire were performed. Three different temperature ranges (450 °C, 550 °C and 700 °C) were selected to test

twenty-four connections. For experimental testing at elevated temperatures, the details of specimens and the type of test setup for mechanical loading were same as those used for experimental testing at ambient temperature. The 3D non- linear FE model developed for ambient temperature testing was modified to validate the elevated temperature testing results. The findings showed that the connection performance significantly relies on the sizes of the members constituting the connection. Furthermore, at ambient temperature, the major failure modes were the deformation of tabs, distortion of the BEC and tearing of the column web. Similar failure modes were observed up to the temperature range of 550 °C. However, at 700° C, the out of plane buckling of column web was observed as an additional and dominant failure mode. At ambient temperature testing, the variation in the geometrical features of connection parameters considerably affected the stiffness as compared to the strength of the connection, whereas at elevated temperature testing, variation in material properties exhibited a noticeable degradation in the strength as compared to the stiffness of the connection.

ABSTRAK

Rak keluli pallet (SPR) direka untuk menjadi mudah bagi ditanggalkan dan dipasang semula bergantung kepada jumlah penyimpanan. Oleh itu, sambungan rasuk-ke-tiang (BCC) separa tegar tanpa bolt yang digunakan dalam struktur ini mengawal kestabilan SPRs pada arah lorong bawah tanpa pendakap. Prestasi SPR BCC bergantung pada kelakuan sambungan, iaitu sambungan hujung rasuk (BEC). Struktur BEC dengan konfigurasi pelbagai memberi kelakuan yang berbeza dan ini merencatkan pembangunan model analisis yang umum untuk meramalkan kelakuan semua jenis SPR BCC. Kelakuan SPR BCC menjadi lebih rumit jika berlaku kebakaran. Walau bagaimanapun, rujukan terkini tidak mempunyai kajian mengenai kelakuan SPR BCC pada suhu tinggi. Kajian ini memeriksa kelakuan SPR BCC secara eksperimen dan kaedah berangka pada suhu ambien dan tinggi yang terdiri daripada dua jenis penyiasatan utama. Dalam fasa pertama, ujian eksperimen SPR BCC pada suhu ambien dilakukan dengan menggunakan kaedah julur berkembar. Tiga puluh dua ujian telah dijalankan berdasarkan perubahan dalam ketebalan tiang, kedalaman rasuk dan bilangan tab dalam penyambung hujung rasuk untuk mengkaji kelakuan SPR BCC. Kelakuan momen-putaran (M-θ), hubungan beban-terikan, mod kegagalan utama dan pengaruh parameter tertentu pada prestasi sambungan telah disiasat. Satu kajian perbandingan untuk mengira kekukuhan sambungan telah dijalankan dengan membandingkan pelbagai kaedah rekabentuk kekakuan yang didapati daripada rujukan dan kaedah yang sesuai ditentukan. Model 3D unsur terhingga (FE) tidak linear yang menyerupai protokol ujian dihasilkan menggunakan perisian FE Abaqus dan ketepatannya terhadap keputusan eksperimen telah disahkan. Selepas mencapai keputusan yang seragam di antara analisis FE dan keputusan eksperimen, model FE telah diperluaskan lagi untuk melaksanakan analisis parametrik. Dalam fasa kedua, ujian eksperimen dan kaedah berangka bagi SPR BCC tertakluk kepada beban api telah dijalankan. Tiga julat suhu yang berbeza (450 ° C, 550 ° C dan 700 ° C) telah dipilih

untuk menguji dua puluh empat spesimen sambungan. Untuk ujian eksperimen pada suhu tinggi, butiran spesimen dan jenis persediaan ujian bagi beban mekanikal adalah sama seperti yang digunakan untuk ujian pada suhu ambien. Model FE 3D tidak linear yang dibangunkan untuk ujian suhu ambien telah diubahsuai untuk mengesahkan keputusan ujian suhu tinggi. Dapatan kajian menunjukkan bahawa prestasi sambungan bergantung dengan ketara kepada saiz daripada anggota yang membentuk sambungan. Tambahan pula, pada suhu ambien, mod kegagalan utama adalah ubah bentuk tab, herotan BEC dan pengoyakan web tiang. Mod kegagalan yang sama telah diperhatikan sehingga julat suhu 550 ° C. Walau bagaimanapun, pada 700 ° C, lengkokan web di luar satah diperhatikan sebagai mod kegagalan tambahan dan dominan. Pada ujian suhu ambien, perubahan dalam ciri-ciri geometri parameter sambungan, jauh menjejaskan kekukuhan berbanding kekuatan sambungan, sedangkan pada ujian suhu tinggi, perubahan pada sifat bahan mempamerkan kemerosotan yang ketara pada kekuatan berbanding dengan kekukuhan sambungan.

ACKNOWLEDGEMENTS

At the exciting moment when my thesis is going to be completed, I would like to thank everyone who, in their different ways, gave me guidance, support, help and friendship.

First and foremost, I would like to express my deepest gratitude to my supervisors; Associate Professor Dr. Nor Hafizah Ramli Sulong and Prof. Ir. Dr. Mohd Zamin Jumaat for their guidance and support throughout the whole period of this research. It is really my great fortune to have conducted my PhD research under their supervisions.

I am grateful for the financial support towards this research by the University of Malaya, High Impact Research Grant (HIRG) No. UM.C/625/1/HIR/MOHE/ENG/57 (16001-00-D000057) - ‘‘Behavior and design of steel connection under fire’’.

Many thanks to my friends and colleagues for their help and support, in particular, Dr. Mehdi Shariati, Dr. Rashid Khan, Mr. Muhammed Aslam and Mr. Kafeel Ahmed.

TABLE OF CONTENTS

Abstract iii

Abstrak v

Acknowledgements vii

Table of Contents viii

List of Figures xiii

List of Tables xvii

List of Symbols and Abbreviations xviii

CHAPTER 1: INTRODUCTION 1

1.1 General 1

1.2 Types of steel storage racks 2

1.3 Steel pallet racks (SPRs) 2

1.3.1 Configuration of SPRs 3

1.3.2 Components of SPRs 3

1.3.2.1 Beam-to-column connections (BCCs) 7

1.4 Problem statement 9

1.5 Research objectives 12

1.6 Scope of the study 12

1.7 Significance of the study 14

1.8 Thesis layout 14

CHAPTER 2: LITERATURE REVIEW 17

2.1 General 17

2.2 Classification of SPR BCCs 17

2.3 Classification of the beam end connectors 19

2.4 Existing experimental studies 22
2.4.1 RMI (2012) guidelines 22
2.4.1.1 Cantilever/ Double Cantilever test method 23
2.4.1.2 Portal frame test method 25
2.4.1.3 Cyclic test method 27
2.4.2 EN15512 (2009) guidelines 28
2.4.2.1 Cantilever test method 28
2.4.2.2 Looseness test on beam end connector 29
2.4.2.3 Shear test on beam end connector and connector locks 30
2.5 Analytical and Design Methods 30
2.5.1 RMI (2012) procedure 31
2.5.2 EN15512 (2009) procedure 34
2.6 Comparison of RMI (2012) and EN15512 (2009) guidelines 36
2.7 Various stiffness design methods 38
2.7.1 Initial stiffness method 38
2.7.2 Slope to half ultimate moment 39
2.7.3 Equal area method 40
2.8 Research progress on SPR BCCs 41
2.8.1 Experimental testing of SPR BCCs under static loading 41
2.8.2 Element Modeling of SPR BCCs 45
2.8.3 Component Based Method for the SPR BCCs 49
2.8.4 Influence of BCCs on the behavior of SPRs under seismic loading 49
2.8.5 Influence of connections on global stability 52
2.9 CFS connections under fire 54
2.9.1 Research progress 54
2.10 Chapter summary 59

CHAPTER 3: MATERIALS AND METHODOLOGY 60

3.1 General 60

3.2 Experimental investigations at ambient temperatures 60

3.2.1 Material properties 61

3.2.2 Specimen details 62

3.2.3 Connection arrangement 65

3.2.4 Selection of Test Method 66

3.2.5 Test setup 66

3.2.5.1 Instrumentation 67

3.3 Experimental investigations at elevated temperatures 69

3.3.1 Material properties and specimen details 69

3.3.2 Selection of temperature ranges 69

3.3.3 Test setup 71

3.4 Finite Element (FE) modeling at ambient temperature 76

3.4.1 Connection modeling 76

3.4.2 Surface interaction 77

3.4.3 Loading and boundary conditions 80

3.4.4 Model Discretization 81

3.4.5 Parametric analysis 83

3.5 Finite Element (FE) modeling at elevated temperatures 84

CHAPTER 4: RESULTS AND DISCUSSION 85

4.1 General 85

4.2 Experimental results at ambient temperature 85

4.2.1 Failure modes 85

4.2.2 Load-Strain Relationship 91

4.2.3 Moment-rotation (M-θ) relationship 92

4.2.4 Stiffness 94
4.2.5 Corrections in rotation and stiffness values 96
4.2.6 Effect of parameters on connection performance 97
4.2.6.1 Effect of varying beam depth with constant column thickness and tabs in the connector 97
4.2.6.2 Effect of column thickness on connection behavior 98
4.2.6.3 Combined effect of variation in the geometry of beam end connector and beam depth 99
4.2.7 Ductility 100
4.3 FE analysis results at ambient temperature 101
4.3.1 Failure modes 101
4.3.1.1 Failure of the beam end connector 103
4.3.1.2 Failure of Tabs 104
4.3.1.3 Failure of column 105
4.3.2 Moment-Rotation (M-θ) behavior and stiffness 106
4.4 Parametric analysis 109
4.4.1 Effect of varying column thickness, beam depth and number of tabs in the beam end connector 110
4.4.2 Effect of variation in the thickness of the beam end connector 111
4.4.3 Effect of welding position of beam to the beam end connector 114
4.4.4 Spacing between the tabs in the beam connector 116
4.5 Experimental results of elevated temperature testing 118
4.5.1 Failure Modes 118
4.5.2 Moment-Rotation (M-θ) Behavior and Stiffness 120
4.5.3 Effect of Temperature on Connection Performance 128
4.6 Results of FE analysis at elevated temperature 129

4.6.1 Failure Modes 129

4.6.2 M-θ Behavior and Stiffness 132

CHAPTER 5: CONCLUSION AND FUTURE RECOMMENDATIONS 139

5.1 Design recommendations 143

5.2 Recommendations for future research 144

REFERENCES 145

LIST OF PUBLICATIONS AND PRESENTED PAPERS 153

LIST OF FIGURES

Figure 1.1: Cross-section of the connection components 6

Figure 1.2: Typical SPR structure 7

Figure 1.3: Typical SPR BCC 9

Figure 2.1: Typical SPR BCC 19

Figure 2.2: Tongue and slot design (Markazi et al., 1997) 20

Figure 2.3: Blanking design (Markazi et al., 1997) 20

Figure 2.4: Stud incorporated design (Markazi et al., 1997) 21

Figure 2.5: Dual integrated tab design (Markazi et al., 1997) 21

Figure 2.6: Schematic diagram of Cantilever test setup (RMI, 2012) 24

Figure 2.7: Schematic diagram of double-cantilever test setup (Prabha et al., 2010) 25

Figure 2.8: Schematic diagram of Portal frame test method 26

Figure 2.9: Cyclic test setup RMI (2012) 27

Figure 2.10: Schematic diagram of cantilever test set-up (EN15512, 2009) 29

Figure 2.11: Derivation of connector stiffness RMI (2012) 33

Figure 2.12: Derivation of connector stiffness EN15512 (2009) 35

Figure 2.13: Testing of EU connection according to EU and US codes (Roure et al., 2013) 37

Figure 2.14: Testing of US connection according to EU and US codes (Roure et al., 2013) 38

Figure 2.15: Initial stiffness method 39

Figure 2.16: Slope to half ultimate moment method 40

Figure 2.17: Equal area method 40

Figure 2.18: Typical tearing of column material (Sleczka & Kozłowski, 2007) 43

Figure 2.19: Deformation of beam end connector (Sleczka & Kozłowski, 2007) 43

Figure 2.20: Deformation of tabs (Sleczka & Kozłowski, 2007) 44

Figure 2.21: FE model for double-cantilever test (K Bajoria & Talikoti, 2006) 48

Figure 3.1: Cross-section of column 62

Figure 3.2: Cross-section of beam 63

Figure 3.3: Cross-section of the beam end connector 64

Figure 3.4: Dimensions of tested connection 65

Figure 3.5: Schematic diagram of test set-up 68

Figure 3.6: Reduction Factors for Carbon Steel at Elevated Temperature [EC3 (2005b)] 70

Figure 3.7: Samples of FCP heating elements 72

Figure 3.8: Rock wool 73

Figure 3.9: Cable thermocouples type K for measuring the temperature in the specimens 73

Figure 3.10: Temperature controlling apparatus 74

Figure 3.11: Front view of schematic diagram of test setup 75

Figure 3.12: Isometric view of schematic diagram of test setup 76

Figure 3.13: Geometry of tabs 77

Figure 3.14: Surface to surface interaction among components 79

Figure 3.15: Complete geometry of the modeled connection 80

Figure 3.16: Division of the connection components into a four-sided region 81

Figure 3.17: Discretized components of the SPR assembly 82

Figure 3.18: Meshing of connection 83

Figure 4.1: Connection failure of specimen A 88

Figure 4.2: Deformation of columns 89

Figure 4.3: Deformation of the beam end connector 90

Figure 4.4: Deformation of tabs 90

Figure 4.5: Load-strain graph for specimen ‘A’ 92

Figure 4.6: Average M-θ graphs for each set of specimens 93

Figure 4.7: Effect of varying beam depth with constant column thickness and number of tabs in the beam end connector 98

Figure 4.8: Effect of varying column thickness with constant beam depth and number of tabs in the beam end connector 99

Figure 4.9: Effect of the geometry of the beam end connector 100

Figure 4.10: Comparison of the connection failure 103

Figure 4.11: Comparison of failure of the beam end connector ‘A’ 104

Figure 4.12: Failure of tabs 105

Figure 4.13: Comparison of the maximum deformation of the column at the connection failure 106

Figure 4.14: Four nodes monitored to determine the rotation 107

Figure 4.15: Comparison of the M-θ graphs of the experimental and FE investigations 109

Figure 4.16: Effect of variation in parameters on the M–θ behavior (FE analysis) 111

Figure 4.17: Failure of the beam end connectors 113

Figure 4.18: M-θ graphs of the variation in the thickness of the beam end connector 114

Figure 4.19: Failure modes of the specimens with various welding positions of beam to the beam end connector 116

Figure 4.20: M-θ behavior of specimen N and specimen E 117

Figure 4.21: Typical failure of connection 119

Figure 4.22: Deformation of tabs 119

Figure 4.23: Deformation of the beam end connector 120

Figure 4.24: M-θ curves for tested specimens 125

Figure 4.25: Failure of connection at 700 °C 130

Figure 4.26: Failure of connection at 700 °C 131

Figure 4.27: Failure of column 131

Figure 4.28: M-θ curves comparison of experimental and FE investigations for Specimen 'A' at various temperature ranges 134

Figure 4.29: Normalized strength degradation curves for all eight sets of specimens . 137

Figure 4.30: Normalized stiffness degradation curves for all eight sets of specimens . 137

LIST OF TABLES

Table 2.1: Major experimental research contribution on SPR BCCs 53

Table 3.1: Material properties of specimens 62

Table 3.2: Dimension details and section properties of columns 63

Table 3.3: Dimension details and section properties of beams 63

Table 3.4: Details of specimens' IDs 64

Table 3.5: Details of elevated temperature testing 69

Table 3.6: Reduction Factors for Stress-Strain Relationship of Carbon Steel at Elevated Temperature [EC3 (2005b)] 71

Table 4.1: Average test results 94

Table 4.2: Comparison of the Initial stiffness, Slope to half-ultimate moment and equal area methods 96

Table 4.3: Corrected stiffness and rotation for all eight sets 97

Table 4.4: Comparison of the moment capacity and stiffness of the tested connection in the experimental and FE investigations 108

Table 4.5: Strength and stiffness of the specimens with various welding positions of beam to the beam end connector 116

Table 4.6: M-θ results of the tested specimens 126

Table 4.7: Experimental stiffness and corrections 127

Table 4.8: Comparison of Experimental and FEM results for specimen A 134

LIST OF SYMBOLS AND ABBREVIATIONS

M	:	Moment
θ	:	Connection rotation
M-θ	:	Moment-rotation
F	:	Connection stiffness by RMI
M_{max}	:	Maximum moment capacity of the connection (RMI)
K_0	:	Connection stiffness by equal area method
P	:	Applied Load
P_c	:	Compressive load
L	:	Length between supports
L_b	:	Length of the beam
t_b	:	Thickness of the beam
b_w	:	Width of the beam
h_b	:	Depth of the beam
L_c	:	Length of the column
UT	:	Thickness of the column
b_t	:	Width of column flange
w	:	Width of column web
δ	:	Deflection of the free end of the cantilever
δ_b	:	Deflection of beams
$\delta_{b,av}$	:	Average deflection of beams
δ_2	:	Deflection of column
E	:	Modulus of elasticity
I_b	:	Moment of inertia of the beam
I_c	:	Moment of inertia of the column

H	:	Horizontal load
h	:	Distance of beam top surface from the floor
R_k	:	Characteristic value of the parameter being measured
M_k	:	Characteristic failure moment
M_{Rd}	:	Design moment for the connection
γ_M	:	Partial safety factor for connections
n	:	Variable moment reduction factor selected by the designer ≤ 1
k_{ni}	:	Slope of a line through the origin
k_d	:	Design value of the connector stiffness
k_m	:	Average value of the connector stiffness
v	:	Poisson's ratio
f_y	:	Yield strength
f_u	:	Ultimate strength
T	:	Furnace temperature (°C)
T_0	:	Ambient temperature (20 °C)
t	:	Testing time (minute)
φ	:	Out of plumb coefficient
CFS	:	Cold-formed steel
HRS	:	Hot-rolled steel
SPR	:	Steel pallet rack
BCC	:	Beam to column connections

CHAPTER 1: INTRODUCTION

1.1 General

The manufacturing production throughout the world usually needs warehouses or supermarkets where goods are stored and moved from producer to the consumer. This process essentially needs the storage structures placed along the line in order to utilize the available space and to provide easy access to the stored goods. While earlier storage and warehousing relied on man-to-order shelving and other devices, the need for improvement in storage and in handling efficiency called for increasing mechanization on the one hand and increasing density of storage on the other. Both these requirements could be met only by a highly engineered development of light weight multistory type structures having the capability to be accommodated in relatively less horizontal space. Consequently, during the last few decades, the growing number of industrial warehouses and supermarkets throughout the world has given significant rise to the importance of steel storage rack structures that could solve the storage capacity and goods handling problems in the storage buildings. Nowadays, steel storage racks are used in about 40% of the production-distribution-consumption cycle of all goods (A. M. Freitas, Souza, & Freitas, 2010).

Because of changing storage needs over the years, the effective use of storage racks demands flexibility in the material constituting these racks to permit the handy adjustment and re-assembling of rack elements upon requirement at optimum cost (Sarawit & Pekoz, 2002; Winter & Pekoz, 1973). Cold formed steel (CFS) is therefore favored for the fabrication of these unique structures (Gilbert & Rasmussen, 2009; Gilbert, Rasmussen, Baldassino, Cudini, & Rovere, 2012; Y. H. Lee, Tan, Mohammad, Md Tahir, & Shek, 2014). However, when heavy loads are desired to be supported by storage racks, the Australian Standard for steel storage racking (AS4084, 2012) permits to use hot-rolled steel (HRS) for manufacturing of these structures.

1.2 Types of steel storage racks

The primary categories of steel storage racks are drive-thru racks, drive-in racks and pallet racks (Teh, Hancock, & Clarke, 2004). The sub-categories of steel storage racks are shelving racks, cantilever racks, mezzanine racks, push-back racks, selective pallet racks, narrow aisle racking, double deep pallet racks, gravity flow and pallet flow racks. In the drive-in and drive-thru rack systems, the pallets are placed using the rails moving throughout the depth of the rack structure. Drive-thru pallet rack systems utilize 'first-in-first-out' inventory retrieval. The pallets are loaded from one side and unloaded from the other; permitting the forklift truck to enter from either of the aisles. By contrast, in drive-in racks the pallets are placed on the basis of 'first-in-last-out principle' and the pallets are stored on rail beams one after the other (Gilbert & Rasmussen, 2011c). The depth of drive-in rack minimizes the need for aisles and efficiently utilizes the cubic space. Since the forklift truck has to be permitted to move easily, only horizontal bracing at the top (plan bracing) and vertical bracing at the back (spine bracing) is provided (Gilbert, Teh, Badet, & Rasmussen, 2014). More information about the load transfer behavior and analysis and design of drive-thru and drive-in racks is provided in (Gilbert & Rasmussen, 2011b; Zhang, Gilbert, & Rasmussen, 2011).

1.3 Steel pallet racks (SPRs)

Steel pallet racks (SPRs) are considered as the perfect storage solution and provide sufficient and readily accessible storage when less space is available compared to the high volume of storage items. These three-dimensional structures provide direct and easy access to all the stored items, and depending upon the volume of storage goods, are readily demountable and capable of reassembly.

1.3.1 Configuration of SPRs

In SPRs, most commonly, two perforated lipped channel sections are spaced apart by bolting or welding struts to make a truss frame. However, in some cases, more traditional hot-rolled profiles are used as well as tubular hollow sections. The struts work as cross-bracing and prevent sway in this direction, which is termed as the 'cross-aisle direction'. This direction is usually braced diagonally to avoid the difficulty in supporting the columns against bending about the weak axes (Gilbert & Rasmussen, 2009). Bolted connections between the cross-aisle bracing and columns are usually used in Australia and Europe, while manufacturers in the United States frequently use welded connections (Ng, Beale, & Godley, 2009). The longer direction with different story heights between two pallets is called the 'down-aisle direction'. This direction is left unbraced for quick and unblocked access to the stored goods. The resistance to sway instability in the down aisle direction is provided; collectively, by the beam to column connections (BCCs) and base connections. Thus, SPR BCCs play a critical and significant role to maintain the overall stability of the structure (K. Bajoria & Talikoti, 2006; Baldassino & Bernuzzi, 2000; Bernuzzi & Castiglioni, 2001; André Filiatrault, Bachman, & Mahoney, 2006; André Filiatrault, Higgins, & Wanitkorkul, 2006; A. M. Freitas et al., 2010; Markazi, Beale, & Godley, 1997; Sarawit & Peköz, 2006; Sleczka & Kozłowski, 2007).

1.3.2 Components of SPRs

A typical SPR has several structural members. The initial development of storage racking introduced simple cold-formed perforated lipped channel sections as rack columns. Despite the fact that such sections were structurally beneficial and cost-effective, their shape hampered an efficient connection between the columns and bracing members. Therefore, the spacers were introduced to evade the usage of the lipped flange. The cross-section of recently available columns has perforations and is often similar in shape but more complex than traditional channel sections. Multiple stiffeners, various

perforation shapes, and further material advances assist in optimizing the column sections as per requirement.

The thickness of the columns used in SPRs ranges between 1.5 mm and 3 mm, which is comparatively negligible to the sufficiently greater height of the column. Due to the high slenderness and perforations provided in the column, the critical elastic flexural and flexural-torsional (global) buckling loads are less than the same column without holes, (Casafont, Pastor, Roure, & Peköz, 2011; A. M. S. Freitas, Freitas, & Souza, 2005; Hancock, 1985; Moen & Schafer, 2009). Moreover, local buckling may occur, where the section involves plate flexure alone without transverse deformation of the overall column, or distortional buckling, where the cross-sectional shape changes along the length of the member without transverse deformation (Koen, 2008).

The beams used in these rack structures are normally box, hat or channel sections with sufficient bending capacity (Abdel-Jaber, Beale, & Godley, 2006). The beams used in SPRs are placed perpendicular to the plane of the columns. Current investigations on performance of SPRs concentrate on the stability of pallet beams with opening, to produce simpler design approaches. A connection device, known as 'beam end connector' is attached to the beam at one end which establishes the BCC.

The other components of SPRs are the BCCs and base connection, which are highly responsible for the stability and overall performance of rack structures due to the unavailability of bracing in the down-aisle direction in order to provide the consumer quick and unblocked access to the stored goods. A base connection is an important factor that is responsible for the stability of the unbraced SPRs in the down-aisle direction (Beale & Godley, 2001). The base plate assemblies are used as a bridge in between the column and the floor to transfer upright's axial force to the floor and prevent the buckling of frame in down aisle direction (Gilbert & Rasmussen, 2011a). The strength and stiffness of base

connection depend upon many factors such as floor anchoring arrangement and the axial compressive force in upright (Godley, Beale, & Feng, 1998). Furthermore, a small change in base connection stiffness may significantly change the global elastic buckling load of the rack structure (Lau, 2002). The properties of base plate also influence the end condition of the heaviest loaded bottom portion of the upright (Kilar, Petrovčič, Koren, & Šilih, 2011). This bottom portion mainly governs the ultimate load required for frame instability, because the column is generally constant over its total length (Stark & Tilburgs, 1978). Pinned base connections are used in cross-aisle direction, however, some stiffness exists in the down-aisle direction controlled by the thickness of the base plate and mode of fixation between base plate and floor (A. M. Freitas et al., 2010).

The BCCs are discussed in detail in the next section of this study. The cross-section of the typical SPR column, pallet beam and the beam end connector is shown in Figures 1.1 (a), (b) and (c), respectively. Figure 1.2 presents a typical SPR structure and its components.

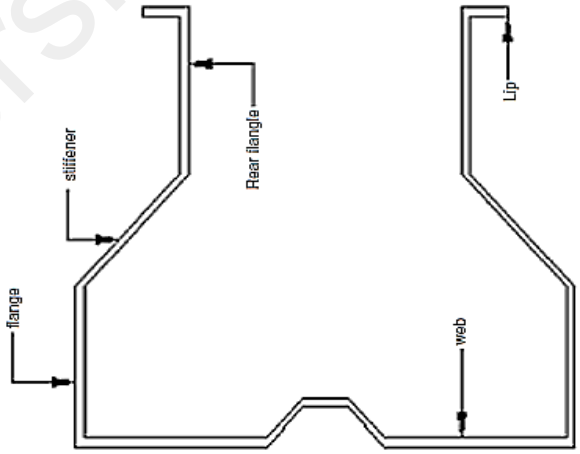

(a)

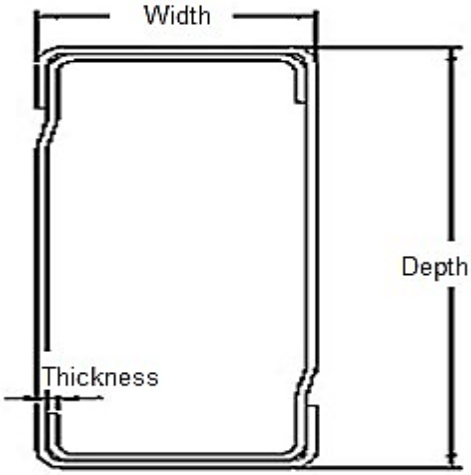

(b)

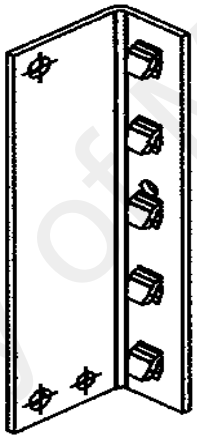

(c)

(a) Column, (b) Beam, (c) Beam end connector

Figure 1.1: Cross-section of the connection components

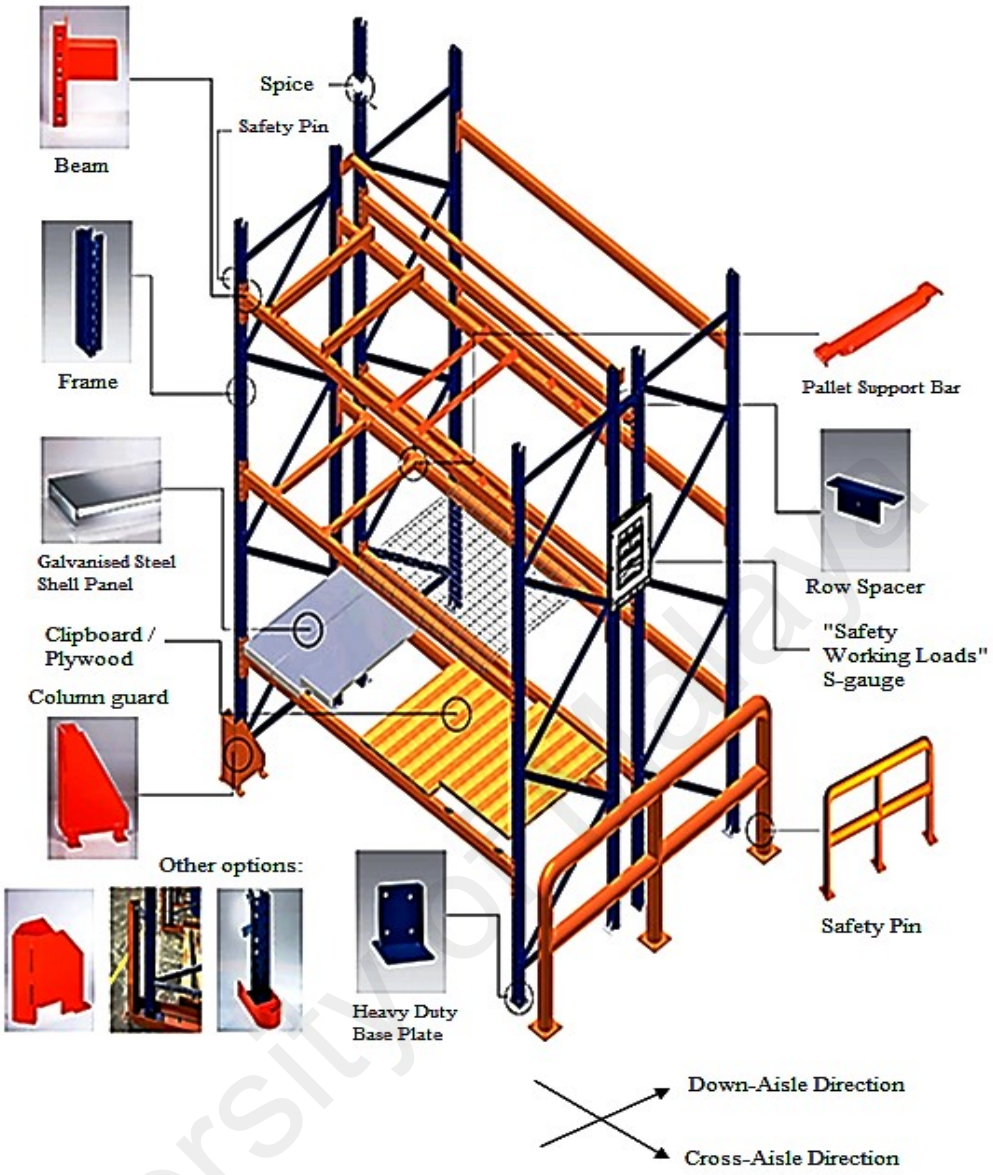

Figure 1.2: Typical SPR structure

1.3.2.1 Beam-to-column connections (BCCs)

BCC in SPRs is mainly established by hook-in beam end connectors inserted into the column holes. The beam end connector may be a fundamental or welded to component of the beam. The important part of the connector is the ‘tab’. The tabs are inserted into the column holes to establish a BCC and serve as a junction between the beam and column. The cost of preparing these connectors may require high expenditure because the tabs need a proper step-by-step manufacturing arrangement. Initially, the connector requires cold forming, punching of tabs to the connector, welding of beam end connector

to the beam and arrangement of locking pin insertion in the connector; in order to assure the proper engagement between the connector tabs and column perforations (Gilbert & Rasmussen, 2009). When locking the beam end connector to the column, the safety lock must be fully inserted into every beam end connector with long leg pointing downward and should be left free to rotate. If the forklift truck accidentally pushes the beam up when lifting the pallets, the beam connector will not disengage. The beam end connectors are tightly attached to the columns through their tabs. A very tight attachment of the beam end connector to the column creates an initial looseness of the joint, which increases the bending moment similar to the bending moments caused by lateral loads. Consequently, the sway effect and shear force on the strength of the whole structure also increases. The connector should have adequate strength to avoid sway failure of the down-aisle direction (K. M. Bajoria, Sangle, & Talicotti, 2010; Gilbert & Rasmussen, 2009; Godley et al., 1998). Furthermore, the properties of the connector also determine the global static and dynamic load-carrying capacity. The stiffness of the connector significantly relies on its rotational demand (K. M. Bajoria et al., 2010; André Filiatrault, Bachman, et al., 2006; André Filiatrault, Higgins, et al., 2006; Andre Filiatrault, Higgins, Wanitkorkul, & Courtwright, 2007; Andre Filiatrault, Higgins, Wanitkorkul, Courtwright, & Michael, 2008; A Filiatrault & Wanitkorkul, 2004; P Sideris & Filiatrault, 2009; Petros Sideris, Filiatrault, Leclerc, & Tremblay, 2010). Figure 1.3 illustrates a typical SPR BCC.

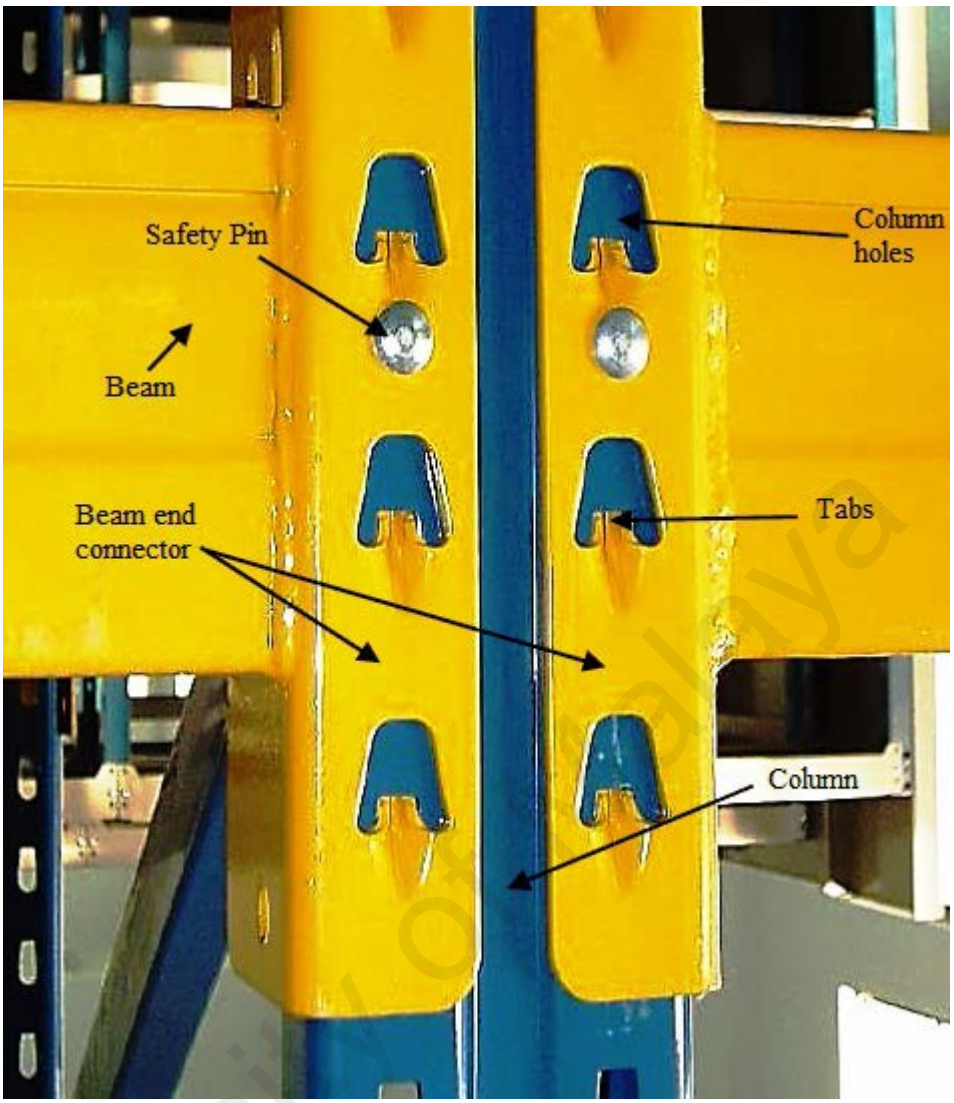

Figure 1.3: Typical SPR BCC

Due to the highly effective role of BCCs in overall stability and performance of pallet racks, the designers and researchers emphasize primarily to develop a common approach to predict the behavior of SPR BCCs. However, an identical and exact nature of this behavior is not well known. This has made it essential to provide a platform for state- of-the-art knowledge about the analysis and behavior of SPR BCCs under different circumstances.

1.4 Problem statement

The main factor that impedes the simple and unified design of SPR BCCs is the diversity in the strength and stiffness of various types of beam end connectors. Therefore,

the recent standards for storage racking design such as Rack Manufacturing Institute (RMI, 2012), European Committee for Standardization (EN15512, 2009) and Standards Australia (AS4084, 2012) suggest experimental testing for each type of beam end connector. Accordingly, due to an aberrant constructional design of various types of beam end connectors available used by rack manufacturers, designers still have a challenge to establish a general analytic design specification for structural properties of these connectors under normal and hazardous conditions. Furthermore, a certain looseness and the relatively small rotational stiffness with regard to the customary connections in steel buildings, are some additional factors that need an accurate estimation of the connection's strength and stiffness for design purposes (Godley & Beale, 2008).

Since, it is difficult to develop a general unified analytical model capable of describing the behavior of all types of SPR BCCs, the prediction of the behavior of any SPR BCC can be made by experimental and numerical testing of any specific BCC and identifying the influence of various parameters on the performance of any BCC. The general concept of parametric influence on the connection's behavior may then be assumed as a benchmark to estimate and improve the performance of any SPR BCC.

It is a well-known fact that warehouse fires are associated with higher average property losses per fire than most other occupancies. Modern high-bay supermarkets and warehouses, with their compact design, their height and densely stored goods in a large number of racks with height up to 40 m create ideal conditions for rapid fire propagation. During fire event, severe deformation occurs in CFS members and the moment transfers from the adjacent members to the connections. In such circumstances, inadequate ductility of connections may result in an early collapse of the frame. Since the stability of SPRs significantly relies on BCCs, the SPR BCCs should be designed to counter the fire effects efficiently. For a flawless fire design of SPR BCCs, it is essential to predict the

effects of gradually increasing temperature on BCCs through experimental investigation. However, literature completely lacks the studies which describe the behavior of SPR BCCs under fire condition.

Though the experimental testing is the most reliable type of investigation to predict the behavior of structural members, however, the experimental investigations are prohibitively expensive and difficult to repeat. Furthermore due to various factors such as imperfections in the specimens, sometimes it is also essential to validate the accuracy of experimental results with several other approaches. The most common and comfortably applicable technique to validate experimental results is finite element (FE) modeling. However, it is necessary to accurately simulate the experimental results to achieve reliable results of FE analysis. In the case of SPR BCCs, a few of previous studies have shown that the FE models developed to validate the moment-rotation (M-θ) behavior of SPR BCCs were failed to capture the same strength degradation in the plastic range observed during experimental testing (Prabha, Marimuthu, Saravanan, & Jayachandran, 2010). The study of Prabha et al. (2010) revealed that the M-θ comparison of experimental and traditional FE failed to capture the failure modes exactly same as observed during experimental investigations, which resulted in overestimated value of ultimate moment *(M_u)*. Furthermore, in the study of Prabha et al. (2010), the tabs of the beam end connector were not modeled and the approach of using axial spring instead of modeling the tabs was used. Thus, the exact deformation behavior of BEC was not observed. In this study, the tabs of the beam end connector have been modeled to observe the exact deformation behavior of the BCC.

This research will help to predict the structural behavior of SPR BCCs at ambient and elevated temperatures and determines the influence of various parameters on the performance of SPR BCCs using experimental and numerical investigations. Various

stiffness design methods are also compared. Furthermore, the recent codes ignore the effect of error due to the deflection of the beam and the beam end connector in the calculation of rotation and stiffness design values. In this study, the effect of the error due to the flexural and shear deformations on the total measured experimental rotation and stiffness values is also calculated in the light of literature and the corrections were applied to achieve precise values of the rotation and stiffness of SPR BCCs.

1.5 Research objectives

The overall objective of the research project described in this thesis is to understand the structural and mechanical behavior of SPR BCCs subjected to ambient and elevated temperatures using experimental and numerical investigations. Specific objectives of this study include:

(i) To examine experimentally the behavior of SPR BCCs at ambient and elevated temperatures.

(ii) To evaluate the accuracy of various stiffness design methods available in the literature.

(iii) To investigate the effects of geometrical properties of connection components on the connection performance through experimental testing.

(iv) To develop and validate a Finite Element (FE) model against the behavior of SPR BCCs tested experimentally at ambient and elevated temperatures.

(v) To perform parametric analysis to predict the effect of those parameters which were not tested experimentally at ambient temperature.

1.6 Scope of the study

The scope of this study covers the experimental testing and numerical analysis of the behavior of SPR BCCs at ambient and elevated temperatures. The connection parameters studied through experimental investigations were (i) column thickness (ii) beam depth

(iii) number of tabs in the beam end connector. The collected observations include the M-θ behavior, load-strain relationship, major failure modes and effects of various parameters on the performance of connection. Instead of the cantilever test method, this study has adopted the double-cantilever test method where thirty-two and twenty-four specimens were tested at ambient and elevated temperatures, respectively. The results of ambient temperature testing were compared with a non-linear 3D FE model developed using the general FE modeling software, 'ABAQUS'(Simulia, 2011). The validated FE model was further extended to include parametric studies. For elevated temperature testing, the scope covers the testing of specimens under an iso-thermal condition and the thermal action was provided by ceramic heaters instead of furnace in order to observe the behavior of SPR BCCs. Only three different temperature ranges (450 °C, 550 °C and 700 °C) were selected based on previous studies. The obtained results were plotted as M-θ graphs and the difference in the strength and stiffness of the connection tested at ambient and elevated temperatures is compared. The non-linear 3D FE model developed for ambient temperature testing was modified and validated against experimental results at elevated temperatures.

There are several limitations associated with this study. One of the limitations is the type of connection testing under elevated temperatures. Most of the design codes for the fire testing of traditional steel connections recommend isolated connection testing (AISC, 2010; BS5950, 1990; EC3, 2005a). This approach has been challenged by the modern research by introducing the performance-based design using full-scale testing. The modern research claims that the actual behavior of CFS connections can be obtained through full-scale testing, however, full-scale testing are difficult and rarely performed due to the high cost and availability of furnaces of required sizes. In the light of the recommendations of codes and other limitations, this study has focused on the isolated testing of SPR BCCs.

For experimental investigations, both at ambient and elevated temperatures, the study was limited to investigate the influence of the column thickness, depth of the beam and number of tabs in the beam end connector using double cantilever test method. For experimental testing at elevated temperatures, this study is limited to the application of iso-thermal condition of fire to SPR BCCs. This study is also limited to the experimental testing of SPR BCCs at selected temperature ranges.

1.7 Significance of the study

A high rise pallet rack may collapse without any prior notice due to an overestimation of structure's strength and stiffness. The rack as well as the goods falling down with the failed rack may result in injuries or fatality of concerned labor or consumer. Since the stability of SPRs significantly relies on the strength and stiffness of BCCs, especially in the event of fire, the incorrect design of connections may results in global collapse of the structure. In previous years, various aspects of SPRs were studied, however, the research focusing on SPR BCCs solely are rarely available. In particular, the behavior of SPR BCCs at elevated temperatures has been ignored completely. The behavior of connection varies proportionally with the variation in temperature. The moments are sustained mainly by the connection instead of attached members. Therefore, modern structural engineering considers that the understanding of behavior of SPR BCCs subjected to fire is essential in order to minimize the sudden failure of the rack structure due to fire. This research will help practicing engineers and manufacturers to understand the behavior of SPR BCCs at ambient and elevated temperature.

1.8 Thesis layout

This thesis investigates the structural behavior of SPR BCCs subjected to ambient and elevated temperatures. This thesis consists of five chapters. Brief details of the chapters are given below:

The first chapter contains an introduction which describes the research background and provides detailed information about the requirement, manufacturing, mechanism, utilization, design demands, types and configurations of storage racks including the components constituting SPRs. Furthermore, a statement of the problem studied, details of the objectives and scope of the research and the complete layout of thesis are also defined in Chapter One. It also briefly explains the proposed research actions to be taken.

The second chapter is based on a critical literature review which explains a number of factors. Initially, it explains the nature of SPR BCCs in the light of design standards as well as the classification of the main types of the existing beam end connectors. Then it proceeds to highlight and compare the pros and cons of various testing methods described in the recent design standards and literature. A comparison of the analytical design approaches recommended by the different design codes. The major failure modes of SPR BCCs observed by the researchers in the past are also discussed. As described previously, the studies focusing on the behavior of SPR BCCs solely are limited, therefore, the information presented in second chapter has been extracted from two types of studies; (i) those which focus on overall analysis of SPRs and partly focus on the contribution of BCCs in rack performance, and (ii) those which investigates the behavior of SPR BCCs solely. Moreover, there is a lack of studies into the behavior of SPR BCCs subjected to elevated temperatures, the studies focused on CFS connections are reviewed and analyzed in second chapter to bring to light the similarity in the behavior of SPR BCCs and traditional CFS connections subjected to elevated temperatures.

The third chapter focuses on the detailed explanation of materials and methodology adopted in this research. This explanation includes the material properties, specimen details, type and description of experimental arrangement at ambient as well as elevated

temperatures. Detailed description of FE modeling at ambient and elevated temperatures is also presented. The parameters considered for parametric analysis are also highlighted.

Chapter Four describes the results of all types of investigations performed at ambient and elevated temperatures. These results are presented in the form of M-θ curves, load-strain relationship graphs and images of observed major failure modes. Chapter four also contains the discussion on the results. The best available method for stiffness design, comparison of the effects of variation in the sizes of most influential parameters tested at ambient temperature, the difference between the experimental and FE results at ambient and elevated temperature testing and the effect of various temperature ranges on the behavior of connection are also highlighted in Chapter Four.

The fifth and last chapter summarizes the findings of this research in the form of conclusion. What achieved from the results, design recommendations for SPR BCCs and recommendations for future research works are provided in Chapter Five.

CHAPTER 2: LITERATURE REVIEW

2.1 General

Despite the reality that the stability of SPRs is dependent of the behavior of BCCs, there is no globally adopted common analytical model for the design of SPR BCCs. It is mainly because of the aberrant and varying design of the commercially available beam end connectors. Although several studies that discuss the overall performance of SPRs are available, limited research has been found that solely focuses on SPR BCCs. Thus, the accurate strength and stiffness characteristics of SPR BCCs have not been exactly identified yet.

This chapter reviews the studies performed into the behavior of SPR BCCs and highlights the contribution of SPR BCCs in global rack performance. The broad classification of various commercially available beam end connectors in the light of literature is also presented. The emphasis is given to find out the key parameters affecting the strength (moment resistance), rigidity (rotational stiffness) and ductility (rotational capacity) of SPR BCCs. The design criteria and testing methods suggested by the recent codes to estimate the design characteristics and corresponding failure modes of SPR BCCs are also highlighted. The limitations of the use of SPR BCCs are identified. As mentioned in chapter one of this study, still there is no study available on SPR BCCs under fire. Therefore, a review of traditional semi-rigid CFS connections subjected to fire is performed that helped in setting the experimental testing of SPR BCCs.

2.2 Classification of SPR BCCs

The BCCs in building structures are traditionally considered to fulfill the conditions of either a pinned or a fixed-end restraint. These behavioral features largely influence the overall frame response. In fact, in nominally pin-jointed frames, the actual connection stiffness leads to a more favorable bending moment in beams, whereas the actual

connection deformability, in nominally rigid frames, adversely influences the frame sensitivity to second-order effects. In both ways, the calculations become simpler, however, in actual conditions SPR BCCs have some finite stiffness which leads to a complication in determining the flexibility of beam end connectors. Eurocode 3 (EC3, 2005a) recommends that a connection that does not fall in the category of a rigid connection or a pin connection should be considered as a semi-rigid connection.

The SPR BCCs are treated as semi-rigid connections. The semi-rigid nature of this connection is primarily due to deformation of the upright flange and/or web, tearing of the upright slots, and distortion of the beam end connector (K Bajoria & Talikoti, 2006). There is no globally adopted common analytical model for the design of SPR BCCs; mainly because of the aberrant and varying design of the commercially available beam end connectors. Most of the recent design codes impose experimental testing to predict the behavior of SPR BCC (AS4084, 2012; EN15512, 2009; RMI, 2012).

It is essential to mention that the SPR BCC is often non-symmetric in both the vertical and horizontal planes. In the vertical plane, usually the non-symmetry is due to the presence of the safety bolt on the upper side of the beam only, and the fact that the beam is fillet welded to the end-connector on three sides only, thereby leaving the lower flange un-welded. In the horizontal plane, non-symmetry is due to the shape of the beam end connector that has hooks on one side only, and is obtained by cold forming of a thin plate that is bent in the shape of an L as a stiffened edge (the same edge where tabs are present). A non-symmetric response is hence to be expected under hogging and sagging bending moments. The typical M-θ curve of the SPR BCCs is shown in Figure 2.1.

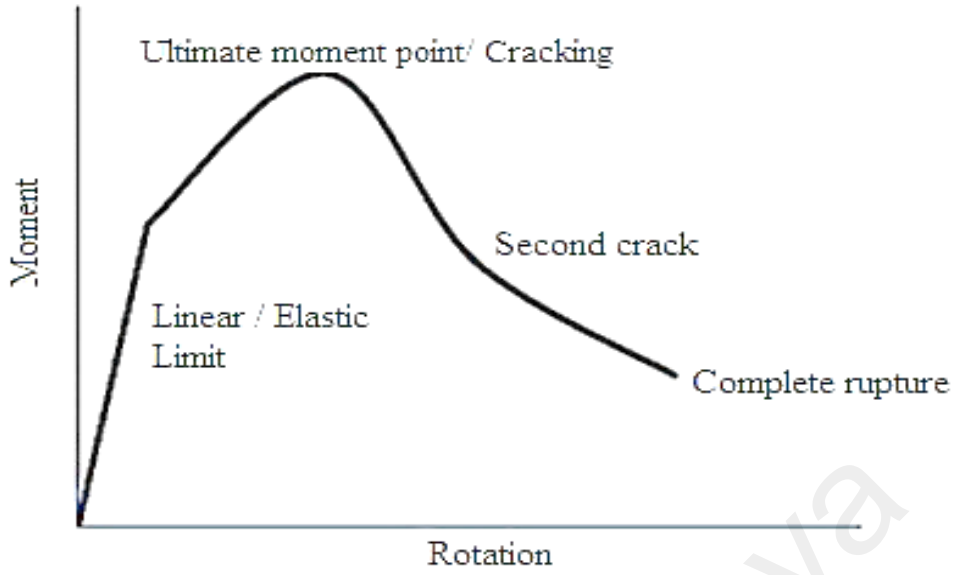

Figure 2.1: Typical SPR BCC

With increasing load, the connection deformation starts and the curve tends to become non-linear up to the Mu value or the failure of connection corresponding to the column wall cracking or the connection top tab failure. After achieving the peak moment value, the strength of connection gradually decreases and the connection may be subjected to another type of failure; and, finally, ruptures completely.

2.3 Classification of the beam end connectors

The function of the beam end connector may be considered, up to some extent, similar to that performed by customary bolted semi-rigid connections in heavy steel buildings. The beam end connector is made up of hot rolled alloy steel and comprises particular types of hook punched into the connector, which serves as a beam-column junction. These hooks are called 'tabs', 'lugs' or 'lips'. These beam end connectors are broadly classified depending on their shape and constructional function into four categories (Markazi et al., 1997). In the ‘tongue and slot design’, (Figure 2.2) the integral tabs are connected to the flange or web of the rack column. In the ‘blanking design’, (Figure 2.3) the connector is interconnected either parallel or perpendicular to the column web. In the ‘stud-incorporated design’ of the connectors (Figure 2.4), holes of constant size are punched

into the bracket to permit the adjustment of the studs or non-integral tabs. In the 'dual integrated tab design', (Figure 2.5) the non-cantilever tabs are used. These tabs are manufactured and punched out of the bracket with an arrangement of their permanent link to the bracket at two spots. This type has a single set of tabs and the connector-column connection is established at the web or flange of the column.

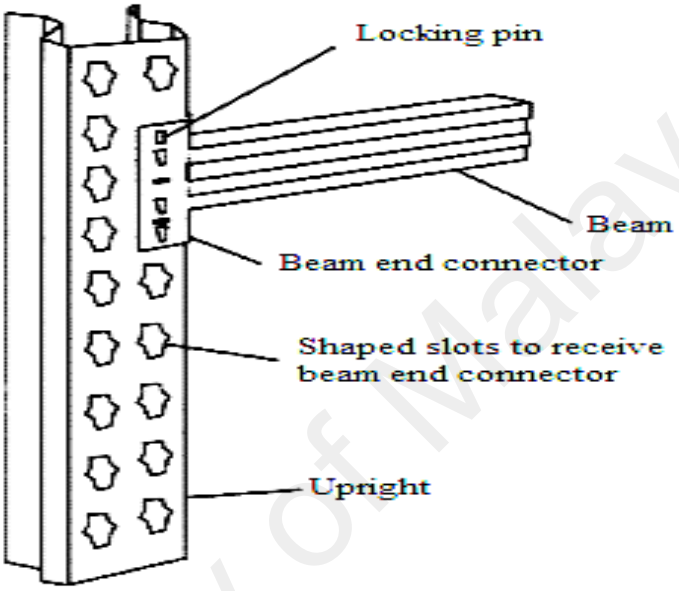

Figure 2.2: Tongue and slot design (Markazi et al., 1997)

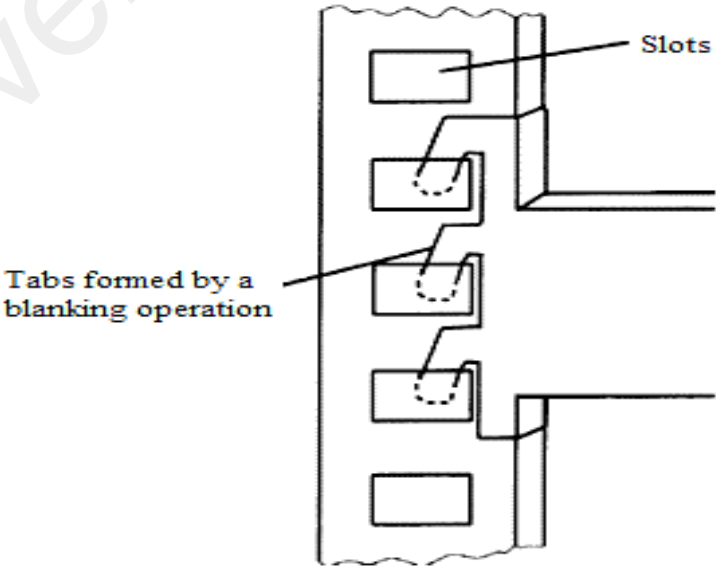

Figure 2.3: Blanking design (Markazi et al., 1997)

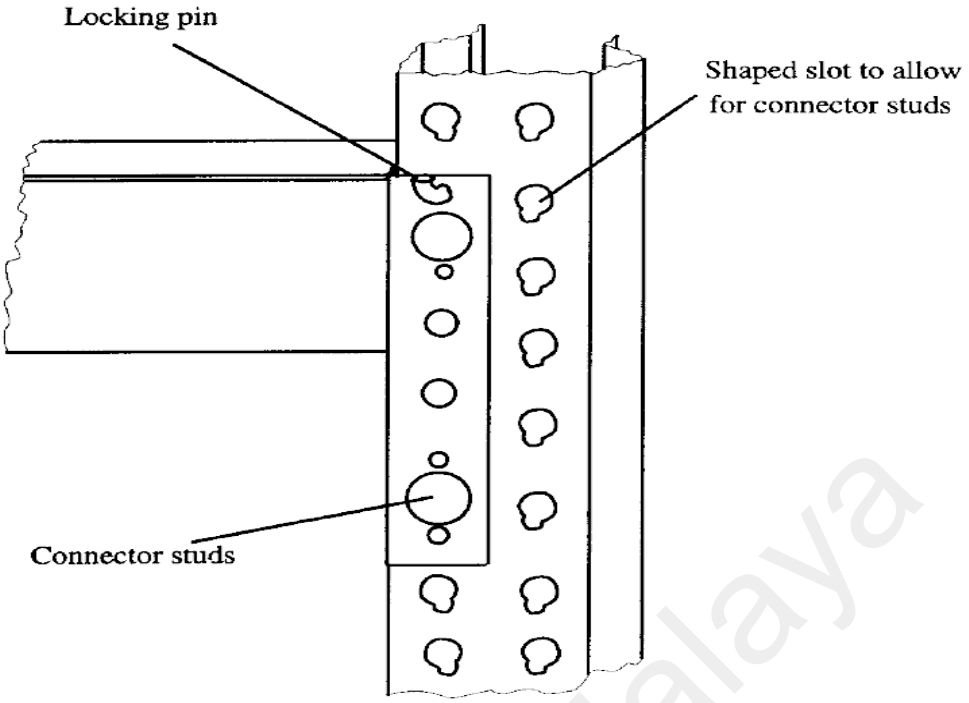

Figure 2.4: Stud incorporated design (Markazi et al., 1997)

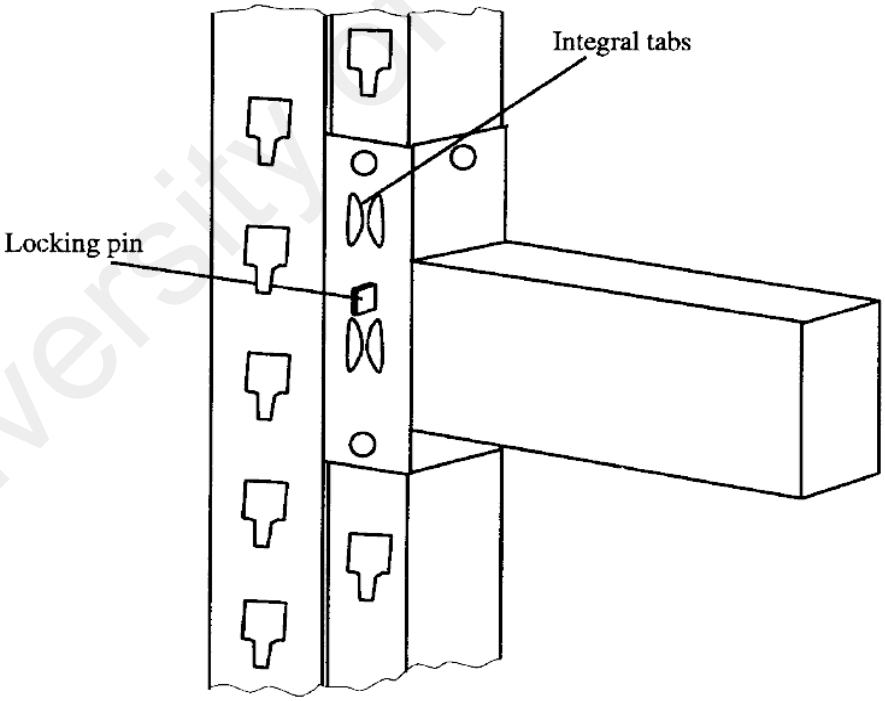

Figure 2.5: Dual integrated tab design (Markazi et al., 1997)

2.4 Existing experimental studies

The exact prediction of the performance of SPR BCCs and obtaining the M-θ curves through numerical or analytic approaches is highly complex. Several factors exist which are impossible to quantify through numerical or analytic approaches such as: the contact within claws and perforations, the yielding of claws and perforations due to local contact stresses, the influence of the tolerances in the thickness and geometry of the components, and the initial looseness. Thus, the experimental investigation is the basic practical approach to obtain M-θ curve for the connection (Roure et al., 2013; Wang, Zhao, & Chen, 2010). However, the secondary approaches should be used to support the experimental results (Mahoney, 2008).

To predict the performance of the beam end connector, the recent design standards for storage rack design (AS4084, 2012; EN15512, 2009; RMI, 2012) recommend alternative testing methods. Previous studies revealed that the test setups defined in the design codes have marginal differences in the position of loading and instrumentation (Harris, 2007; Harris & Hancock, 2002). For instance, the testing provisions provided by AS4084 (2012) are mainly based on EN15512 (2009). Therefore, only the detailed review of experimental methods suggested by the RMI (2012) and EN15512 (2009) are focused in this section.

It should be noted that prior to connection testing, all the storage-racking design codes recommend the material properties of members to be obtained by means of tensile coupon tests.

2.4.1 RMI (2012) guidelines

To investigate the behavior of the beam end connector, the RMI (2012) specification suggests the use of “cantilever testing method”, “portal frame testing method” and “cyclic test method”. This section presents the critical overview of these procedures.

Primarily, the cantilever test was introduced as a test setup to evaluate the moment capacity of the connection (M_{max}), and the portal test as a test setup to evaluate the connection stiffness (F). Later on, a formulation was proposed to calculate the stiffness of the connection through the cantilever test. The testing procedures recommended in the RMI (2012) specification principally propose the use of a suitable spring constant for the end fixity of load beams. A review of number of studies showed that this procedure is not illustrative of most types of rack arrangement with difficulties in implementation and may not be satisfactorily repeated. However, the testing procedures defined in RMI (2012) are considerably effective from modeling point of view.

2.4.1.1 Cantilever/ Double Cantilever test method

The cantilever testing method is considered to be an efficient method to predict the strength characteristics of SPR BCC (Abdel-Jaber et al., 2006). It precisely determines the connection moment capacity. In this method, both ends of the column are kept rigidly fixed. The end of the pallet beam having the beam end connector is inserted in the perforations through tabs at the center of the column and the other end is left in cantilever. A lateral restraint is provided to prevent the twisting of the beam end and the beam is left free to move in the loading direction. Loading should be applied 610 mm from the face of the column to the top of the beam. The consequent displacement in the line of action of the applied load and/or the rotation near the connector is observed. The rotation is measured by either transducers or inclinometers. To investigate the BCC behavior, several researchers used cantilever test method (K. Bajoria & Talikoti, 2006; Baldassino & Bernuzzi, 2000; Bernuzzi & Castiglioni, 2001; Krawinkler, Cofie, Astiz, & Kircher, 1979; Markazi et al., 1997; Zhao, Wang, Chen, & Sivakumaran, 2014). The details of the above mentioned investigations are presented later in this study. A typical schematic arrangement for the cantilever test setup is shown in Figure 2.6.

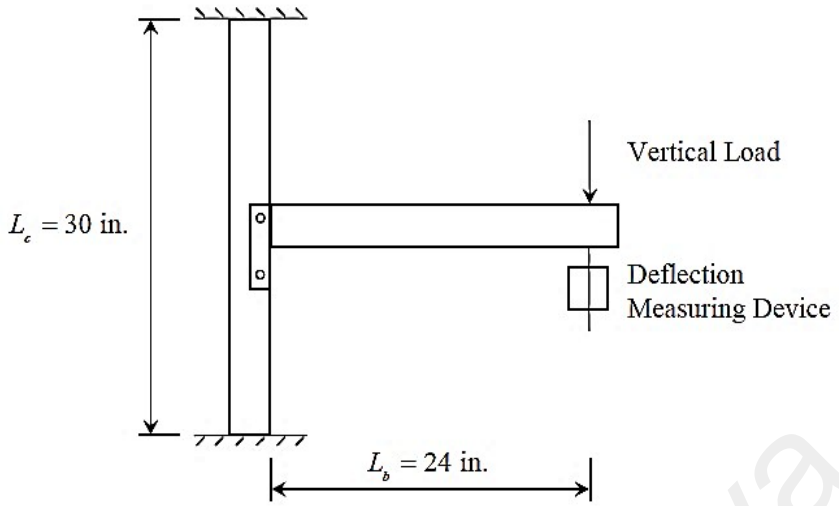

Figure 2.6: Schematic diagram of Cantilever test setup (RMI, 2012)

The cantilever test can be further extended by attaching one more beam to the other side of the column, and, hence, is called the double cantilever test method. Although the double cantilever test method is not presented in any of the design codes, however, this method resembles to the cantilever test method; therefore, presented in this section of the study. The literature has proven the efficiency of this method (K. Bajoria & Talikoti, 2006; Prabha et al. 2010). The study of K. Bajoria and Talikoti (2006) showed that the results obtained from the double cantilever test method and the results obtained from full rack structure tests were in perfect agreement with each other, while the variances with the standard cantilever test were minor (<1%). Prabha et al., (2010) investigated eighteen connections with varying parameters experimentally and with FE, using the double cantilever test setup and achieved reliable results.

The experimental arrangement of this test method is similar to the cantilever test method, with the only difference being that the unconnected ends of the beams on either side of the column are kept pin connected to two vertical sections. These are usually channels, to restrain the lateral movement of the beam, and the load is applied at the top of the column. It is important to mention that the double cantilever test is capable of

achieving more precise results about the connection behavior. The column is only allowed to move in the up and down direction and the only deformation is the deformation of the connector. Moreover, the connector is subjected to moment, shear and axial pull similar to the actual frame, and, hence, provides a better estimation of the shear and moment ratio (K. Bajoria & Talikoti, 2006). Simulation of this test method accurately gives the stiffness of the connection (K. Bajoria & Talikoti, 2006). A typical schematic diagram of the double-cantilever test setup used by Prabha et al. (2010) is shown in Figure 2.7.

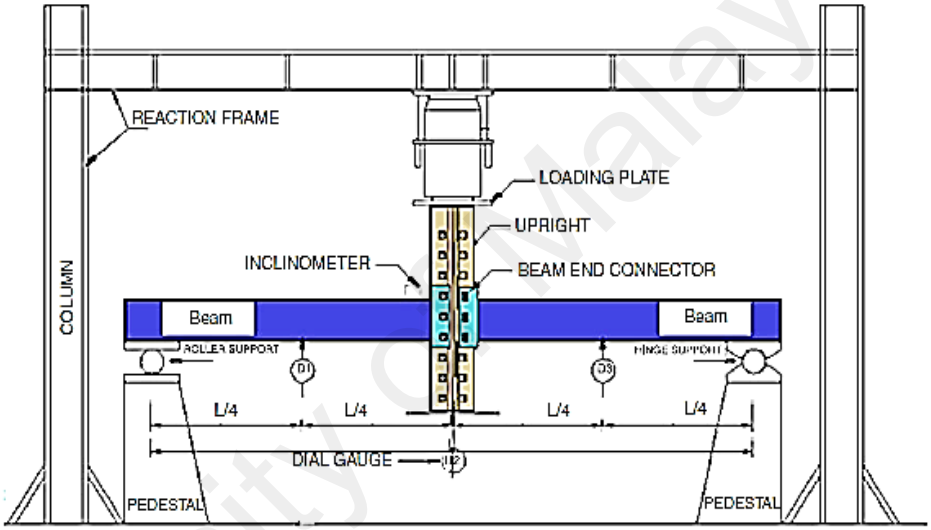

Figure 2.7: Schematic diagram of double-cantilever test setup (Prabha et al., 2010)

2.4.1.2 Portal frame test method

The M-θ curves achieved through the cantilever test method significantly depend on the moment-to-shear ratio applied to the BCC. In fact, this ratio differs constantly throughout the process of applying lateral load in the down-aisle direction of the SPR. For better representation of the bending moment-to-shear force ratio in a BCC, the portal test method was proposed. The portal testing method is considered to be a precise method to calculate the stiffness characteristics of the beam and the beam end connectors. The portal frame provides an average stiffness of one connector closing down and one opening up. Harris & Hancock (2002) compared the two test setups. The findings revealed that

the cantilever test gives the stiffness values half of those obtained from the portal frame test method. However, in some cases, the variable behavior of the beam end connectors placed on either side of the portals cannot be distinguished and the moment reversal condition is also difficult to predict with this test method because RMI (2012) does not define the connection stiffness for the unloading paths. The results of the portal frame test method are usually used for sway analysis (Abdel-Jaber et al., 2006).

In this method, a pinned base portal frame is constituted by attaching both ends of the beam to two different lengths of column. The vertical load equivalent to the service load of the pallet beam is applied with the help of two equal size pallets. A horizontal load is applied at the top surface level of the pallet beam and the displacements are measured at this height. The RMI (2012) recommend that the applied load should be twice that of the horizontal design load. The RMI (2012) further recommends the use of the portal test when stiffness measurement is required to find the value of connection spring constant to analyze a semi-rigid frame. The stiffness values obtained for the beams and column should be reduced by a factor of 2/3. The evaluation of M-θ curves through portal frame test method requires the consideration of the P-delta effects which leads to a careful design procedure. A portal test arrangement is shown in Figure 2.8. The study of Krawinkler et al., (1979) efficiently portrays the experimental setup and the accuracy of the results obtained by the portal test method.

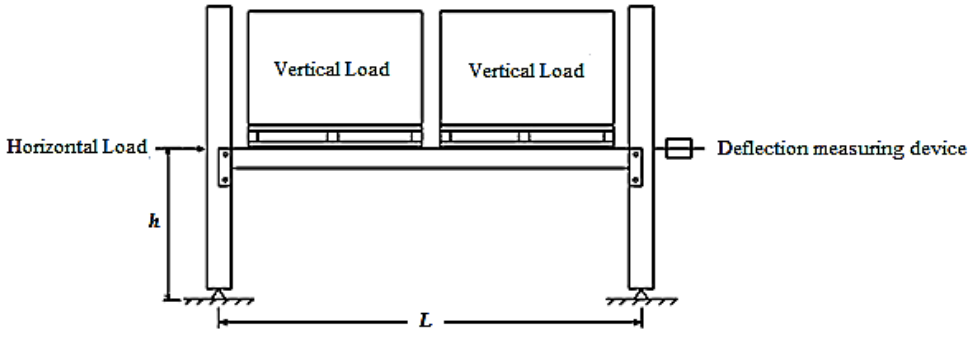

Figure 2.8: Schematic diagram of Portal frame test method

2.4.1.3 Cyclic test method

The cyclic test was first introduced in the latest RMI specification (RMI, 2012). In the cyclic test, two full size pallet beams with the beam end connectors at one end are connected at the center of the column. Before applying the cyclic load, a persistent downward load, *Pc*, of one kip is applied to each beam segment adjacent to each connector on both sides of the BCC in order to simulate the design downward acting gravity pallet loads that serve to fully engage the beams and their connectors into the columns receiving them. The cyclic loading is applied in accordance with the loading guidance available for the moment-resisting frames. For special cases, other types of loading, similar or better than moment frame cyclic loading, may also be applied. By governing the peak drift angle imposed on the test specimen, qualifying tests are performed. The results of the tests should be capable of predicting the median value of the drift angle capacity for the performance states of strength degradation and ultimate drift angle capacity. The schematic diagram of cyclic test method is presented in Figure 2.9.

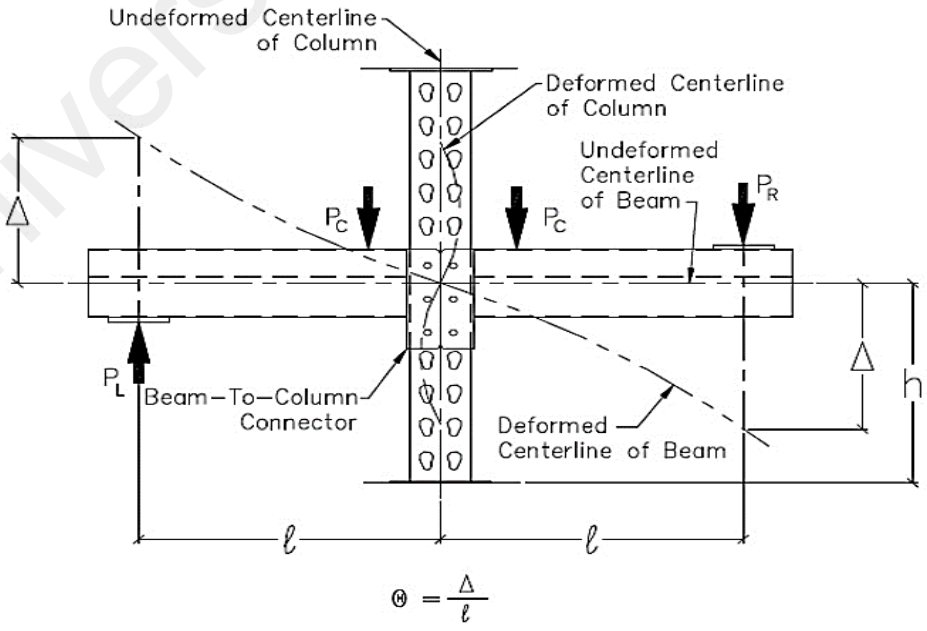

Figure 2.9: Cyclic test setup RMI (2012)

2.4.2 EN15512 (2009) guidelines

The EN15512 (2009) suggests only the cantilever test method to obtain the M-θ characteristics of the BCC. EN15512 (2009) specification not only defines the test protocols and techniques for obtaining the connector stiffness and strength values for design purposes; it also defines testing procedures to determine the connector looseness and the shear in the beam end connectors and connector locks.

2.4.2.1 Cantilever test method

The test method for obtaining the M-θ behavior of BCCs is described in EN15512 (2009) in Annex A.2.4. The code specifies that the free length of the column should verify: h ≥ beam connector length + 2 x column face width (For the connections tested, h varies between 406 and 420 mm). The lateral movement of the beams should be prevented. The loading apparatus should be 750 mm between pin ends. The distance between exposed edge of column and the loading apparatus should be 400 mm. The load intensity should be monitored through computer. The transducers or inclinometers should be used to measure the rotation of beam. The exact location of transducers or inclinometers is not specified in the code, however, it is suggested that the instrumentation should be placed close to the beam end connector. EN15512 (2009) recommends that a pre-load of 10% of the probable failure load should be applied to the connection to calibrate the transducers and to align the column vertically below the apparatus. A gradual increment in load is applied after resetting the transducers until the failure of the connection. Although this approach over estimates the deflection, the code model gives excellent prediction of moment capacity (Abdel-Jaber et al., 2006; Godley, 1997). The recorded data should be used to plot the M-θ curve. A correction factor is applied for the material thickness or the differences in the yield stress values of material. The cantilever test set-up according to EN15512 (2009) is presented in Figure 2.10.

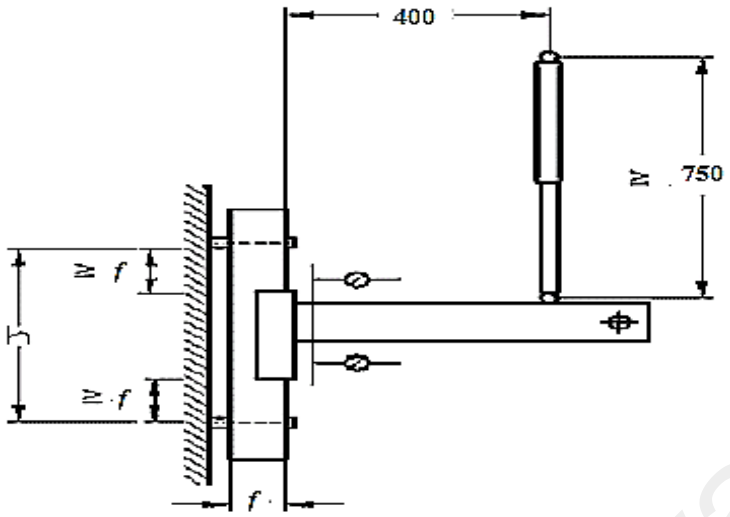

Figure 2.10: Schematic diagram of cantilever test set-up (EN15512, 2009)

2.4.2.2 Looseness test on beam end connector

SPR BCCs may perform better if the joints show their full rotational stiffness immediately after the connection is established. However, in practice, an initial looseness of the connection may produce a highly non-linear M-θ behavior. Due to the initial looseness of the joints, the rack tends to behave as an out-of-plumb frame. The EN15512 (2009) includes an out-of-plumb, φ, for the analysis, which combines the influence of looseness together with the frame imperfections. Thus, the results of a cyclic test with only one cycle combines the calculations for the looseness and M-θ relationship.

In order to determine the looseness in the beam end connector, EN15512 (2009) suggests the use of the same test arrangement as for the measurement of the strength and stiffness of the beam end connector, except that the loading jack should be double acting and capable of applying the load in the reverse direction. The connector should not disengage from the column during the reversal process.

Regarding the SPR BCCs, the phenomenon of the initial looseness of joints has been declared critical by many researchers (Baldassino & Bernuzzi, 2000; Godley & Beale, 2008; Godley, Beale, & Feng, 2000; Markazi, Beale, & Godley, 2001). Godley and Beale

(2008) determined the initial looseness of the connector using a cyclic test with a single cycle.

2.4.2.3 Shear test on beam end connector and connector locks

According to EN15512 (2009), in a shear test on the beam end connector and connector locks, a short column is fixed to a relatively infinitely stiff frame, with a beam connected to it through the connection under investigation. The load is applied to the connection with a pin-ended jack, placed as close to the column as possible. The free end of the beam is restrained by a pinned support at least 400 mm from the face of the column. This support is adjusted in the vertical direction to keep the beam constantly horizontal. To test the connector lock, the specimen is installed in the inverted position and loading is applied to the top surface of the beam in a direction normal to the face of the column, such as to pull the beam end connector away from the face of the column.

2.5 Analytical and Design Methods

A critical review of literature revealed that after achieving the results from experimental testing, various analytical models could be adopted. The lateral stiffness of SPR in the down-aisle direction is greatly influenced by the distortions at the BCCs. For analytical modeling purposes, these distortions are represented by simple rotational spring elements inserted between the beam ends and the center line of the column. The rotational spring constant to be used in a numerical model can be obtained from the M-θ relationships between the beam end and the column using the existing experimental methods. As evidenced by the experimental testing procedures, the response of SPRs in the down-aisle direction is strongly affected by the nonlinear M-θ response of the BCCs. The analytical research related to the behavior of SPRs can be divided into two different types of model:

- Linear models for which the M-θ response of BCCs is linearized by simple linear rotational springs representing secant properties at the anticipated response level of the racks. For dynamic analysis, an equivalent linear viscous damping model is also used to represent the energy dissipation of these same connections during inelastic actions.

- Nonlinear models for seismic analysis, in which the nonlinear response of BCCs is followed over the time-history response of racks by the use of nonlinear M-θ hysteretic rules. This nonlinear modeling is mainly used for research purposes and rarely used in design situations.

Efforts have been made to develop a uniform analytical rule to obtain the M-θ behavior of the SPR BCCs to determine the design values for the moment resistance, rotational stiffness, and rotational capacity as well as to minimize the effect of the initial looseness of the connection. These studies were carried out using different types of test set up. The experimental and numerical results were used to develop analytical equations to determine the strength, stiffness and ductility of the SPR BCCs. In this respect, the recent design codes suggest equations with a slight difference in the parameters.

2.5.1 RMI (2012) procedure

In the procedure suggested by RMI (2012) to calculate the connection stiffness in the cantilever test, it follows that the connection stiffness, F, associated with the moment, M, and the corresponding rotation, θ, is given by:

$$F = \frac{M}{\theta} \tag{2.1}$$

The rotation of the joint, θ, is obtained by measuring and subtracting the contribution of column and beam rotation:

$$\theta = \frac{\left(\delta - \frac{PL_b^3}{3EI_b}\right)}{L_b - \frac{M.L_c}{16EI_c}} \tag{2.2}$$

Where δ is the deflection ($0.85x\delta_{max}$), P is the value of load ($0.85xP_{max}$), E is the modulus of elasticity, L_b and L_C are the length of the beam and column segment, respectively, and I_b and Ic are the moments of inertia of the beam and column segment, respectively.

Rearranging Eqs. 1 and 2, gives the required stiffness value as:

$$F = \frac{RF}{\frac{\delta}{PL_b{}^2} - \frac{L_c}{16EI_c} - \frac{L_b}{3EI_b}} \tag{2.3}$$

Where RF is the reduction factor which should be taken as 1 or 2/3.

The portal test requires the application of a certain force value prior to the calculation of the connection stiffness. By applying an additional horizontal load and measuring the corresponding lateral deflection, F can be computed from the following expression:

$$\delta = \frac{Hh^2}{2}\left\{\frac{h}{3EI_c} + \frac{L}{6EI_b} + \frac{1}{F}\right\} \tag{2.4}$$

Where H denotes the applied horizontal load on the beam, which is multiplied by 2 because of the use of two beams in this test; thus, H becomes $2H$, δ denotes the lateral deflection due to the applied horizontal load, h is the distance of beam top surface from the floor, and L denotes the center-to-center distance of the two columns parallel to the shelf beam. In solving Eq. 2.4 for F, the following is obtained:

$$F = \frac{1}{\frac{2\delta}{Hh^2} - \frac{h}{3EI_c} - \frac{L}{6EI_b}} \tag{2.5}$$

According to the RMI (2012) specification, the F resulting from Eq. 2.5 is the value of the connection stiffness during the sway analysis. The stiffness should be experimentally calculated for both the vertical design load and ultimate load. An equal distribution of the vertical load over the whole row of pallets is considered as a uniformly

distributed force. This force initiates some moments in the joints prior to the application of the horizontal load and can be determined by:

$$M = \frac{wL^3}{24EI_b\left\{\frac{h}{3EI_c}+\frac{L}{2EI_b}+\frac{1}{F}\right\}} \tag{2.6}$$

With $M=PL_b$ and F known, the stiffness can then be determined from Eq.2.1 for each load step. The resulting moment and rotation relationship is illustrated in Figure 2.11. According to the RMI (2012) specification, the stiffness of the connection required for linear analyses is F determined from Eq. 2.3 with P equal to 0.85 times the ultimate load and δ equal to the deflection at that load.

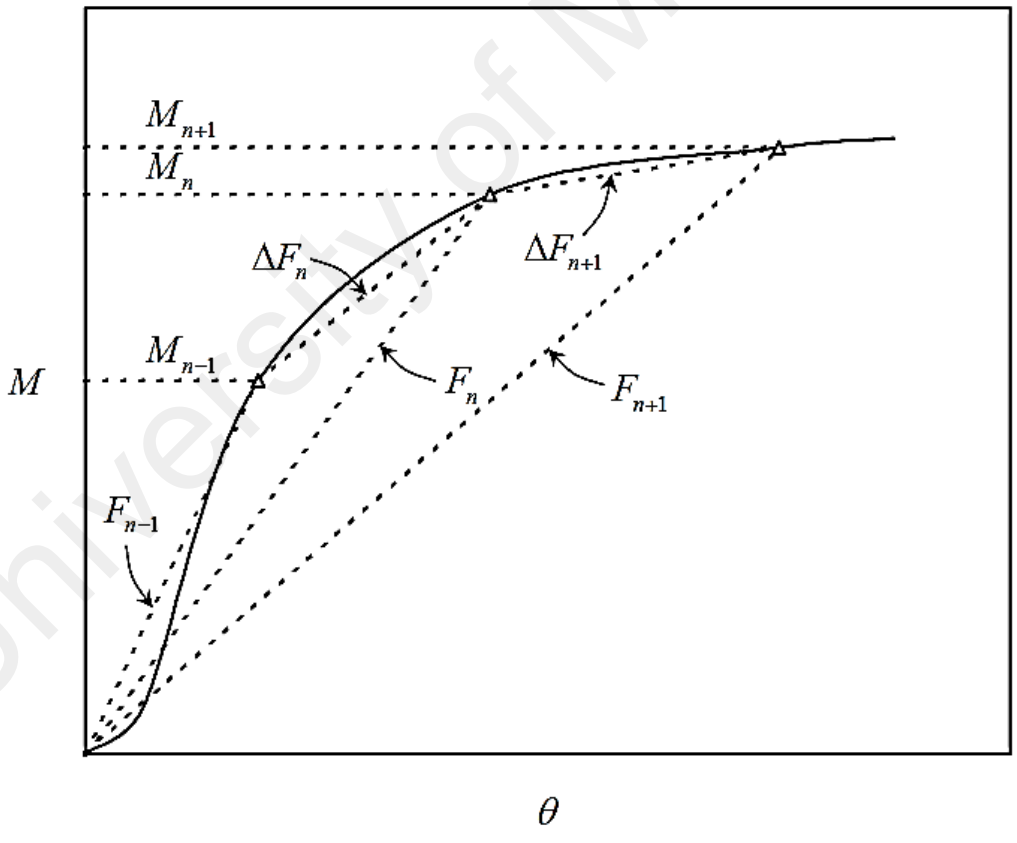

Figure 2.11: Derivation of connector stiffness RMI (2012)

2.5.2 EN15512 (2009) procedure

After correcting the individual results of a group of tests for the variations in the thickness and yield stress, section 13.3.3 of EN15512 (2009) provides guidance to determine the characteristic value of the parameter being measured, R_k, as well as the characteristic failure moment, Mk. The design moment for the connection, M_{Rd}, is then calculated by:

$$M_{Rd} = n\frac{M_K}{\gamma_M} \tag{2.7}$$

Where;

γM= partial safety factor for connections

n= variable moment reduction factor selected by the designer ≤ 1

Regarding the rotational stiffness, EN 15512 (2009) provides an opportunity to plot the bi-linear, average and multi-linear curves. The rotational stiffness of the connector can be obtained as the slope k_{ni} of a line through the origin, which isolates equal areas between it, and the experimental curve below the design moment corrected to yield and thickness, M_{Rdc}, provided that:

$$k_{ni} \leq 1.15\ \frac{M_{Rd}}{\theta_{ki}} \tag{2.8}$$

The design value, k_d, of the connector stiffness should be taken as the average value, k_m where:

$$k_m = \frac{1}{n}\sum_{i=1}^{n} k_{ni} \tag{2.9}$$

This provision is designed to limit the difference between the rotation at failure assumed in the model and that indicated by the test by up to 15% in the cases where the

connector behaves non-linearly. The derivation diagram of the connector stiffness is presented in Figure 2.12. The average curve is derived from the results of the tests on the relevant beam and connector combination. The average curve is obtained by plotting the mean value of the rotation at each moment increment up to the value of the design moment *(M_{Rd})* using the M-θ curves after correction. The multi-linear curve is obtained by replacing the average curve with a series of straight lines, which always lie below it. It is assumed that the M-θ characteristic is also valid for the negative rotations.

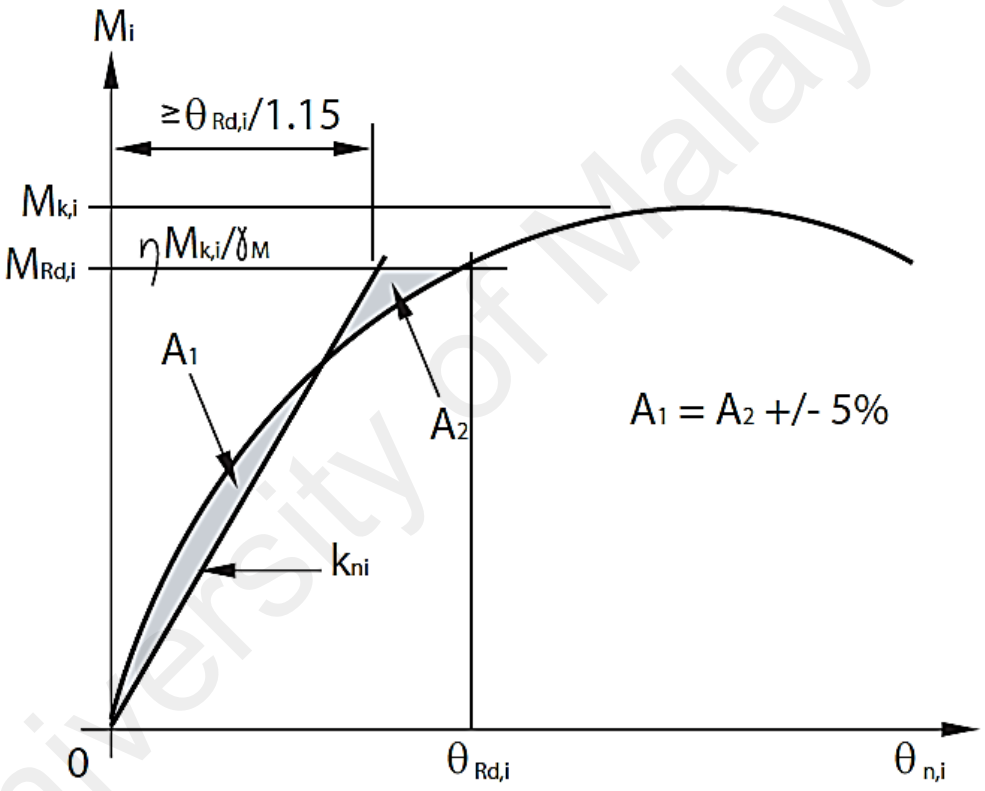

Figure 2.12: Derivation of connector stiffness EN15512 (2009)

The ductility of BCC plays a significant role in minimizing the intensity of deformation in the joint itself as well as the larger deformations projected on the surface near the connection (K. M. Bajoria et al., 2010; Sangle, Bajoria, & Talicotti, 2012). At lower rotations, high non-linearity develops in the beam end connector that influences the static ability of structure. At larger rotations, the inelastic rotation capacity of BCC is substantial, and, for some connections, can exceed 0.20 radians (Filiatrault et al., 2006). However, due

to the relatively shorter height of the racks, the BCC needs greater rotational capacity than building moment-resisting connections. Almost all the design standards support the use of elastic design for pallet beams; however, the EN15512 (2009) specification has a provision for moment redistribution at the connection provided that the connection has its own sufficient ductility. However, in real cases, the connection has less bending strength compared to the attached members. This allows the formation of hinges in the beam end connector prior to its attachment to the beam. A sufficiently ductile connection may prevent the formation of hinges, as a mechanism is fully formed when the beam reaches its ultimate moment (Harris & Hancock, 2002).

The analysis based design of unbraced pallet racks with a focus on the suitability of a selection of methods of analysis and essential improvements in European design practice is recently presented (Bernuzzi, Gobetti, Gabbianelli, & Simoncelli, 2015a, 2015b). A lack of uniformity in the European codes design rules was identified. Moreover, a few methods suggested by the European codes for buckling check and elastic critical load were also found to be unreliable.

2.6 Comparison of RMI (2012) and EN15512 (2009) guidelines

Roure et al. (2013) tested the SPR BCCs used in the US and Europe according to both the RMI (2012) and EN15512 (2009) guidelines. The M-θ curves obtained for the European connection using both test arrangements (RMI (2012) and EN15512 (2009) resulted in same failure moment. However, the stiffness obtained with the EN15512 (2009) arrangement was clearly higher than that obtained through RMI (2012) procedure. The M-θ curves obtained for the US connection using both test arrangements (RMI (2012) and EN15512 (2009) showed that the failure moment obtained with the RMI (2012) method was higher, but the stiffness was practically the same with both arrangements. The shear-to-moment ratio between the two types of design guidelines was also analyzed.

The main difference in the US and European design code is the distance from the load point to the face of the column. Tests were carried out on the US and European connections by varying the distances for medium and heavy connections. The results showed that in both types of connection, increasing the moment-to-shear ratio in the test arrangement produces a small increment in the stiffness value. It was concluded that the test arrangements for the single cantilever test of BCCs proposed by RMI (2012) and EN15512 (2009) are very similar, but not identical, and the characteristics of the connections obtained with them show some differences.

Figure 2.13 shows the M-θ curves obtained for the EU connection using both test arrangements (RMI, 2012; EN15512, 2009). The M_{max} is the same with both arrangements, but the stiffness obtained with the EN arrangement is clearly higher.

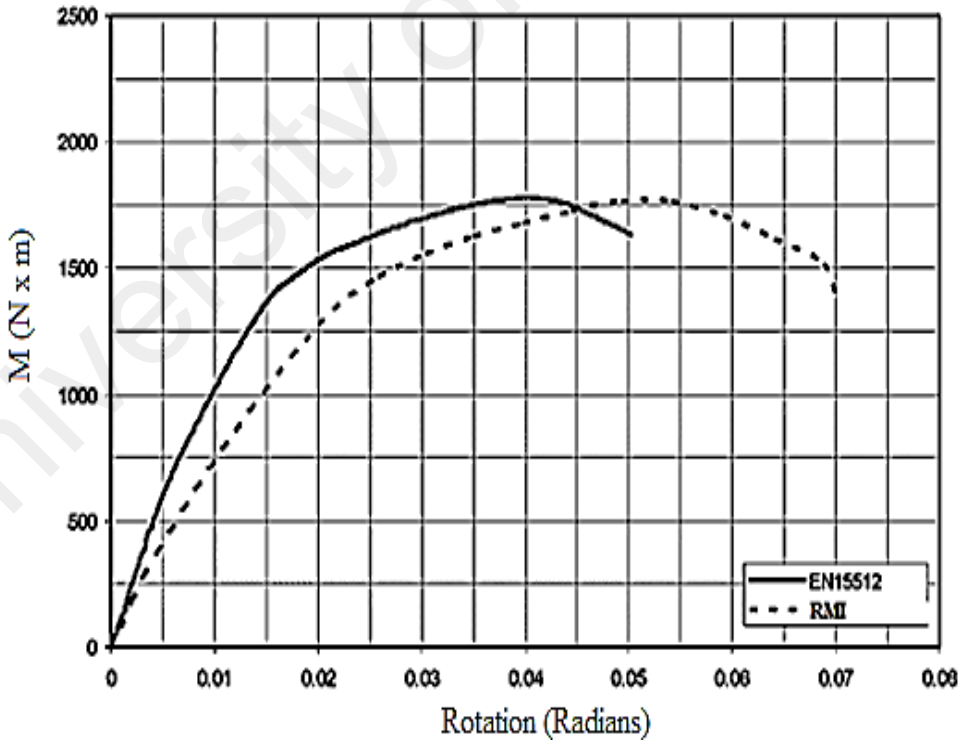

Figure 2.13: Testing of EU connection according to EU and US codes (Roure et al., 2013)

Figure 2.14 shows the M-θ curves obtained for the US connection using both test arrangements (RMI, 2012; EN 15512, 2009). The M_{max} obtained with the RMI method is higher, but the stiffness is practically the same with both arrangements.

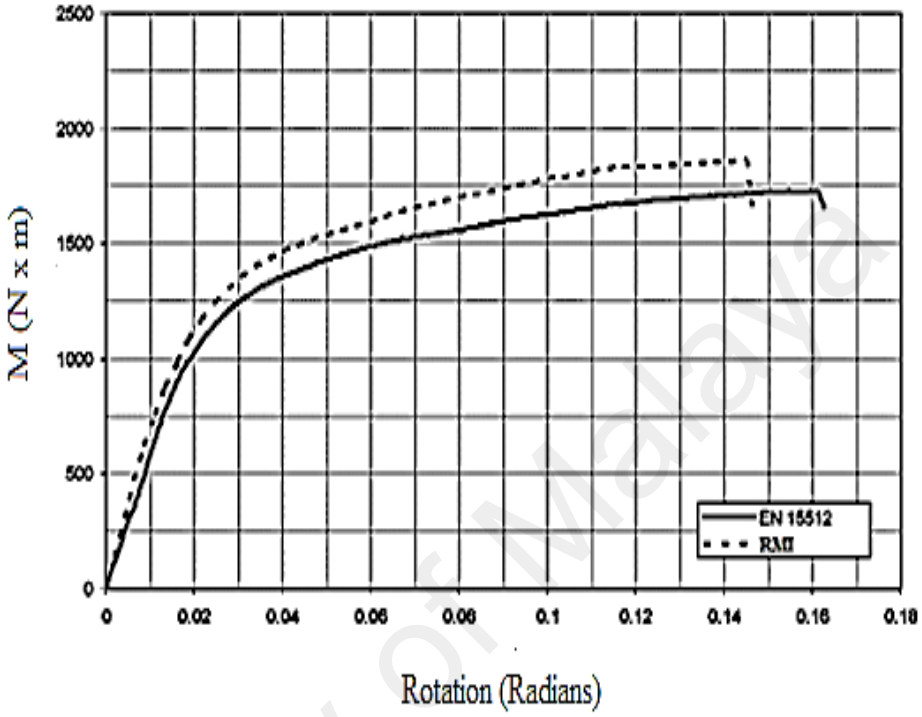

Figure 2.14: Testing of US connection according to EU and US codes (Roure et al., 2013)

2.7 Various stiffness design methods

For designing the structure, the performance of the connector is essential and thus the calculation methods require an accurate estimate of the beam end connector's stiffness and strength. A variety of methods are available to measure the stiffness of the beam end connector. This study compares three different methodologies; the initial stiffness, slope to half-ultimate moment and equal area methods, which were introduced in the literature for arriving at the connection stiffness of any SPR BCC (Godley, 1991).

2.7.1 Initial stiffness method

It is the simplest and easiest method of arriving at connection stiffness where the slope of the initial straight line curve of the M-θ plot is measured, by imposing a best fit straight

line; as shown in the Figure 2.15. However, this method can lead to over-optimistic values if the characteristic is not linear for a substantial part of the range.

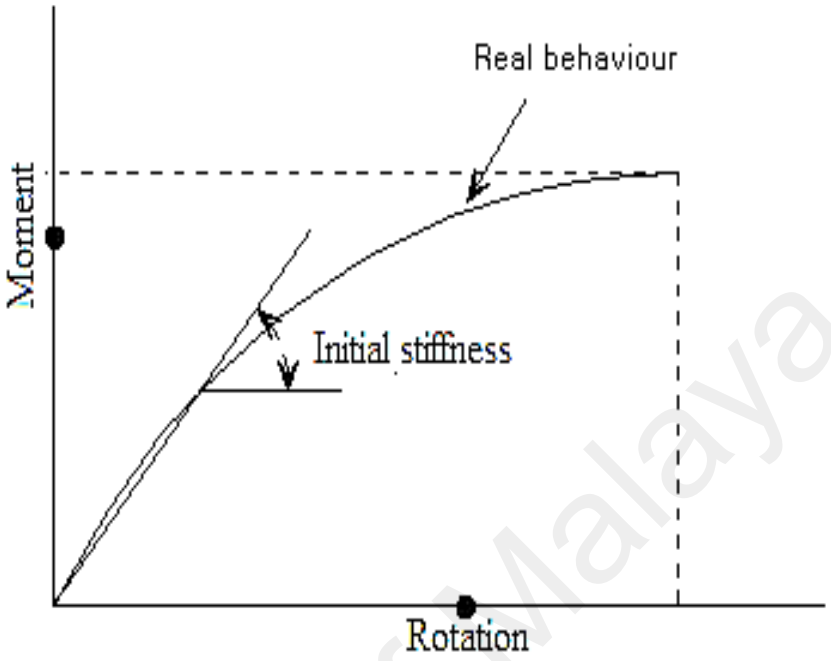

Figure 2.15: Initial stiffness method

2.7.2 Slope to half ultimate moment

Slope to half ultimate method or 0.5 M_u slope as it is otherwise called is a more conservative alternative method of arriving at joint stiffness. The stiffness is arrived by taking the slope of the line passing through the origin and the point at which the working moment of 0.5 M_u (i.e. half of ultimate moment) is reached. It eliminates the need to estimate the slope by fitting the straight line to the curve. Figure 2.16 shows slope to half ultimate method.

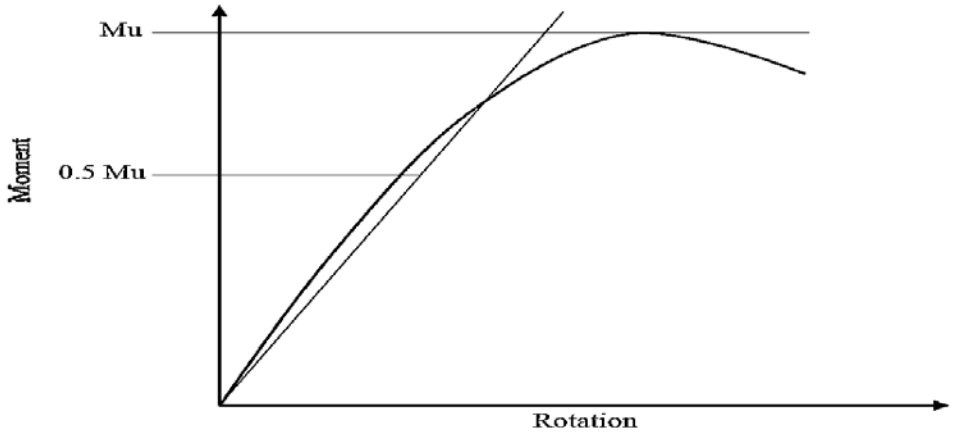

Figure 2.16: Slope to half ultimate moment method

2.7.3 Equal area method

This method represents the true curve by an idealized characteristic comprising two straight line, placed so that the work done to failure in the idealized case is the same as in the actual case. The rotational stiffness is taken as the slope of line passing through the origin which isolates equal areas between it and the experimental curve, below the design moment as shown in the Figure 2.17.

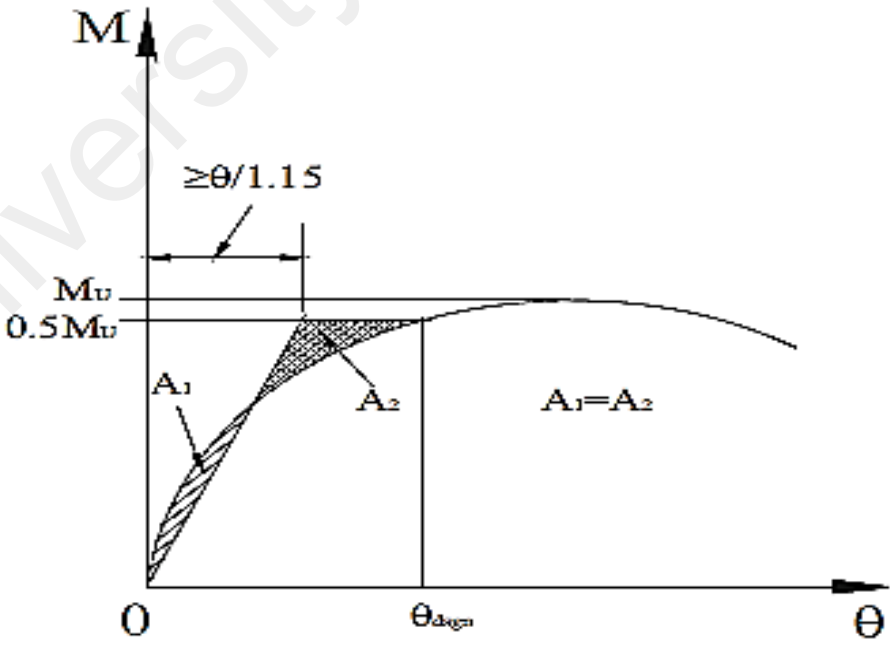

Figure 2.17: Equal area method

Where

M = Moment, θ = Rotation, Mu = Ultimate moment, M_θ = Design Moment = 0.5 Mu

2.8 Research progress on SPR BCCs

2.8.1 Experimental testing of SPR BCCs under static loading

Krawinkler et al., (1979) tested twenty SPR BCCs using cantilever test method. Two different types of tabs were tested. These tabs were hooks (Type A) and button grips (Type B). The experimental results indicated that because of local deformations at the BCC, the M-θ hysteretic loops have a pinched shape similar to that obtained for the reinforced concrete elements with high shear. Low cycle fatigue phenomena may also affect the strength and ductility of the BCCs. The strength of the Type A connectors was limited by the capacity of the hook-type grips that started to pull out of the column perforations. In the Type B subassemblies, fracture of the fillet weld between the beam and the beam end connector limited the moment capacity.

Markazi et al., (1997) performed bending tests on several types of commercially available beam end connector and determined the parameters governing an efficient BCC design. The parameters enhancing the strength and stiffness of the beam end connector were the increased number of tabs, high strength of connector material, interactive connector design, increased gauge of beam end connector and column, increased column thickness, welding method of beam and beam end connectors, and the increased number of contact planes between the beam end connector and the column. Most of the connections failed due to the narrow contact area between the tabs and the column. The study focused on the rotation of beam axis only and ignored the effects of the rotation of the column. However, the study determined that if measurements of the rotation were made using displacement transducers attached to the beam, the flexibility of the beam needed to be taken into account in order to obtain the true M-θ relationship. Bernuzzi & Castiglioni (2001) tested two different types of beam end connector under monotonic and

cyclic loading to estimate the connection behavior on the overall performance of storage rack. The failure modes observed were the deformation of tabs and the deformation of nodal zone. The type of loading and the connector design influenced the connection performance. The study indicated that a simple bi-linear model with the same properties assumed for both the clockwise and anti-clockwise rotations at the joints may not be applied to all SPR structures. However, the results were non-dimensionalized and the maximum moment in all tests was unity. K. Bajoria & Talikoti (2006) compared the cantilever and double cantilever test methods to evaluate the flexibility of SPR BCCs in actual conditions. The research observed some imperfections in the specimen and the specimen failure occurred due to the tearing of the column flange, which may lead to the collapse of the whole structure. The imperfections in the specimens increase the non-linearity in the connection's behavior.

Sleczka & Kozłowski (2007) performed cantilever tests on SPR BCCs with double-sided (internal column) and one-sided (external column). The main aim of the experimental tests was to obtain M-θ characteristics of tested joints and also the observation of behavior of joint components under loading and finally failure modes. A component method was proposed to identify the weakest component in the connection. Three types of failure were observed; (i) tearing of column material (Figure 2.18), (ii) deformation of beam end connector (Figure 2.19), and (iii) deformation of tabs in the connectors (Figure 2.20). The failure modes observed by Sleczka & Kozłowski (2007) were the typical failure modes which have been observed in most of the studies focusing on cantilever testing of SPR BCC.

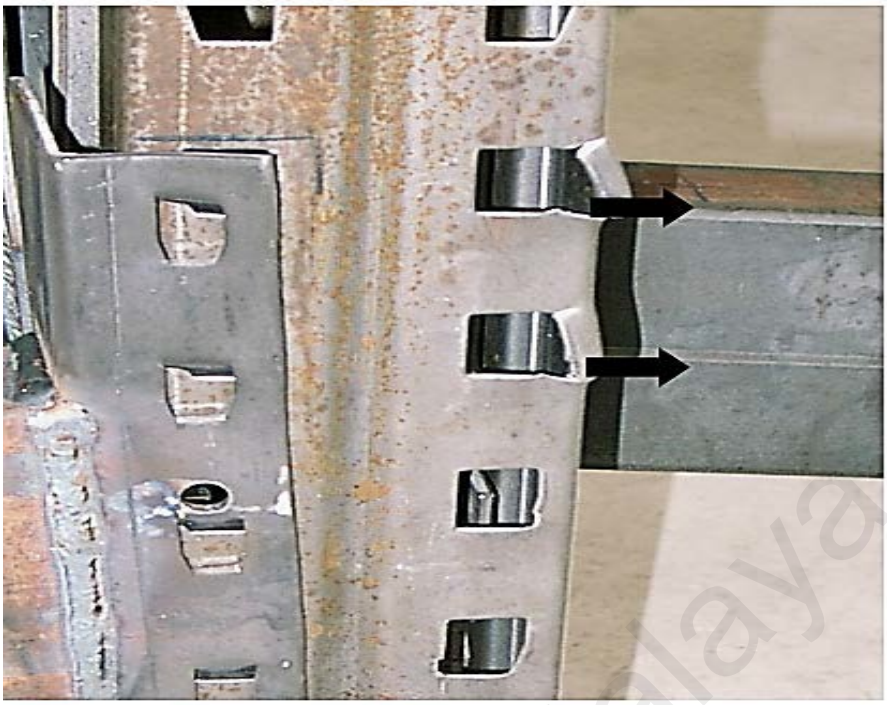

Figure 2.18: Typical tearing of column material (Sleczka & Kozłowski, 2007)

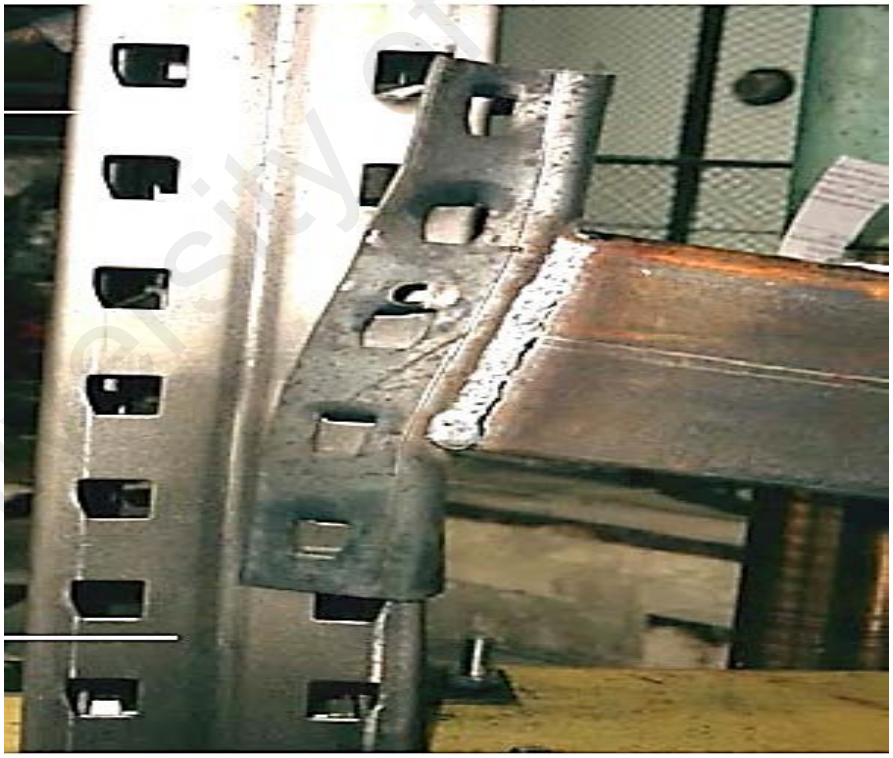

Figure 2.19: Deformation of beam end connector (Sleczka & Kozłowski, 2007)

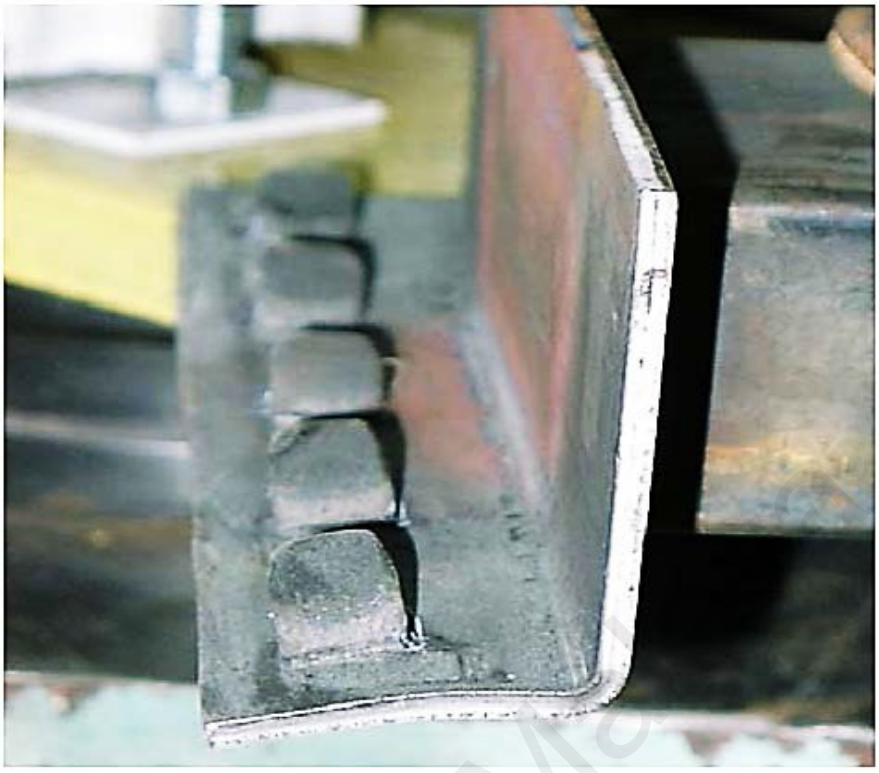

Figure 2.20: Deformation of tabs (Sleczka & Kozłowski, 2007)

Prabha et al., (2010) tested SPR BCCs and the failure modes were governed by the deformation of the column and the tabs. The study demonstrated that the M-θ curve is significantly dependent on the thickness of the column, the depth of beam and the geometry of the beam end connector. In support of this opinion, EN15512 (2009) also declares that the parameters affecting the performance of the beam end connector are the thickness of the column, the profile of the beam, the position of the beam on the connector, the connection of the beam and the beam end connector, the type of bracket and the properties of the beam end connector material.

Zhao et al., (2014) investigated the flexural behavior of storage rack BCCs under monotonic, static, hogging loading in a cantilever test setup. The effect of various influencing parameters, such as column profile and thickness, pallet beam profile and the number of tabs in the beam-end-connector were investigated. One of the significances of the research was the study about the rotation component of the column which was not included in previous studies. The major failure modes were the cracking of the tabs and

the yielding of column. The M-θ curve showed significant changes with variation in column thickness, depth of the beam and the beam end connector.

It should be noted that the pullout capacity of the beam end connector also influences the mode of collapse when the bottom of the column is subjected to forklift truck impact (Gilbert & Rasmussen, 2009). Low pull out capacity leads to confined collapse whereas high pull out capacity tends towards progressive collapse. Welding failure between the beam and the beam end connector and failure of the bracket are frequently reported in the literature (Bernuzzi & Castiglioni, 2001; Godley et al., 2000; Markazi et al., 1997).

2.8.2 Element Modeling of SPR BCCs

The high costs on the experimental testing, non-linear behavior of various types of beam end connector and the possibility of systematic and random errors in the experimental investigations directed researchers towards the use of FE modeling of SPR BCCs. The FE modeling, which was developed by using various types of analysis software, has proven itself to be a reliable tool to achieve a more predictable performance of the connections and the effects of various parameters on the overall performance of rack structures. The FE modeling of connections typically has two phases, the modeling phase and the analysis phase.

For a numerical analysis, the stiffness of the beam end connector is calculated through either a tangent method or a secant method. If a continuous non-linear rotational spring is used during the analysis procedure, tangent method may provide feasible solutions. However, the secant method is more practical and easier than the tangent method. These connectors often have different stiffness, when rotating clockwise or anti-clockwise. In this case, the minimum stiffness may be used as a limitation in the design process. As each connection can be specified independently, changes in the rotational stiffness, due

to the applied shear caused by the vertical load on the beam that occurs in these joints can be incorporated (SEMA, 1985).

Historical practice of seismic analysis of SPR BCCs using numerical modeling relies on the suggestions of a study performed by (C. Chen, Scholl, & Blume, 1980). They compared the results of shake table tests with two-dimensional non-linear numerical models. Bilinear M-θ hysteretic rules were considered for the BCCs. The local deformations witnessed during experiments were simulated by adjusting the stiffness values of the connection in the model. The researchers observed a significantly nonlinear behavior of M-θ curves and suggested that the spring constants should be used for FE modeling, which replicates the original shake table drifts happen during experiments. However, the spring constants were not able to represent the exact low amplitude natural periods and showed that the connection stiffness at greater vibration were only 25%–33% of the small displacements.

Markazi et al., (2001) developed an eight noded, three-dimensional, isoparametric, hexahedron element FE model with three linear translatory displacements at each corner. The effect of spring stiffness on the rotational stiffness of the beam end connector was examined. However, the flexibility of members and rotation component of column were not taken into account.

Abdel-Jaber et al., (2006) investigated the difference in two unlike approaches to measure the beam rotation and introduced suitable corrective equations which were based on the postulation that the beam end connector must be in the elastic state. In another study, the researchers examined the moment-reversal behavior of BCC in a two story one bay frame (Abdel-Jaber, Beale, & Godley, 2005). A single multi-linear model with reversal loading and two traditional bi-linear models were developed to define the M-θ behavior of the connection. The parameter investigated was the variation in the ratio of

side load to axial load. The models were compared with (i) the experimental results and (ii) the calculations mentioned in some of the old standards for storage rack design (FEM, 1997; SEMA, 1985) specifications. The multi-linear model produced accurate moment and deflection behavior; however, the two bi-linear models failed to correctly model the moment-reversal phenomenon.

A number of studies was presented on the FE modeling of SPRs and the BCCs were modeled to investigate their influence on overall stability of rack structures (K. Bajoria & McConnel, 1984; K. Bajoria & Talikoti, 2006; K. M. Bajoria et al., 2010; Kwarteng, Beale, Godley, & Thomson, 2012; Sangle et al., 2012). Bajoria & Talicoti (2006) compared their experimental results with an elasto-plastic FE model. The FE simulations were performed for both cantilever and the double-cantilever test method. This FE model was the first model simulating the double-cantilever test method, as shown in Figure 2.21. The entire test assembly was modeled using ANSYS. SHELL63 element was used to represent the column and the box beam section. Contact surfaces were defined using CONTA173 element between the connector plate and the column to represent their interaction. The tabs were modeled by the use of SOLID43 element to provide connection between the connector and the column. Geometry, boundary and loading conditions of the finite element model were made as close to the double cantilever test as possible. The far ends of the beam were pin connected and the ends near the column were modelled with SOLID43 element to represent beam end connector. The hook in end connector was subjected to moment, shear and axial tensile forces. The failure occurred due to the tearing of the column flange because of the axial pull. The results of the double cantilever tests were found to be in perfect relation with the experimental setup.

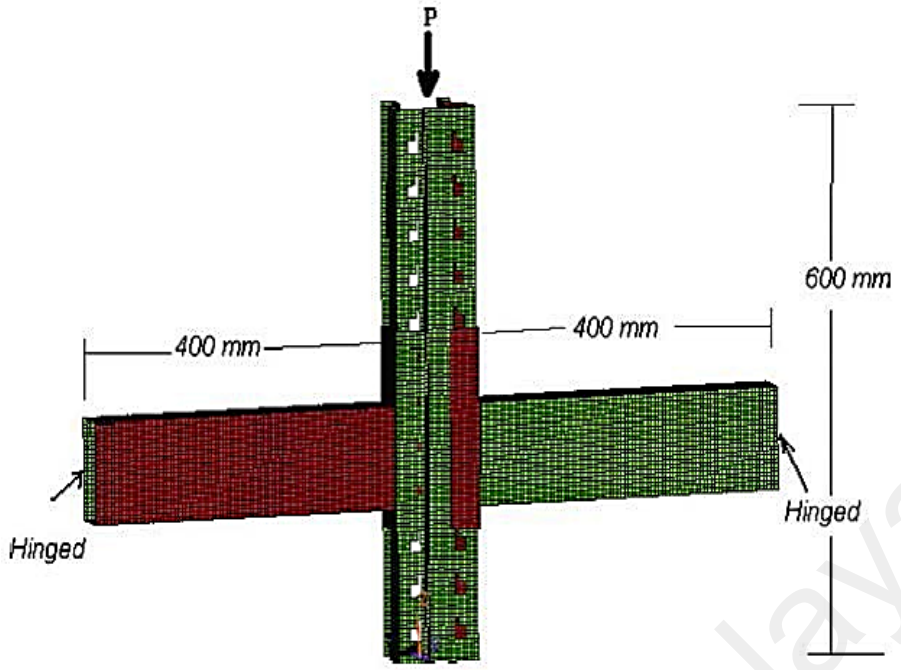

Figure 2.21: FE model for double-cantilever test (K Bajoria & Talikoti, 2006)

Prabha et al., (2010) developed the contact between the column and the beam end connector by using a frictionless surface-to-surface contact algorithm. This element did not carry any force itself and was only able to transfer the forces. Due to the complexity in modelling, the tabs of the end connectors were not modeled and appropriate boundary conditions according to the experimental setup were assigned at the connection. This approach neglects the actual field deformation behavior of tabs which is the most important aspect in connection's performance. A non-linear axial spring was modeled to control the initial looseness of the connection. The connection failure was initiated by the tabs trying to cut the column web. Bajoria et al., (2010) used shell elements to model the angle shaped connectors. One leg of the beam end connector was directly connected to the beam end. For the other leg, three hooks in connectors were designed as a solid element and connected to the four corners of the perforations in the column. The model provided good guidance for the prediction of M-θ curve.

2.8.3 Component Based Method for the SPR BCCs

The recent design codes and research performed in the past on the SPR BCCs are mostly based on experimental-theoretical philosophy. However, an in depth analysis of past research reveals the possibility of using the component method to evaluate the main connection response: moment resistance, initial stiffness and rotation capacity of SPR BCCs (Kozłowski & Ślęczka, 2004). However, the component based method has not been frequently applied for the analysis of rack joints.

The basic concept of the component-based model is to treat a connection as a combination of several basic components. The application of the component method is usually performed in three stages. The first stage is identification of the components in the analyzed joint, in which the joint is subdivided into components. The second stage is the prediction of the initial stiffness, strength and deformation capacity of each component. The third stage is evaluation of the flexural strength and rotational stiffness of the whole joint.

Kozłowski & Ślęczka (2004) introduced a preliminary component method model for the SPR BCCs, which they compared with the available experimental findings. The results of both investigations were in good relationship with each other. The components identified in the study were: column web in tearing, column web in bearing, column web in tension and compression, tabs in shear, connector in bending and shear, connector web in tension and compression, and beam flange in tension and compression. A comparison of the predicted component method results with those obtained from the tests showed a high level of accuracy for both the stiffness and flexural resistance.

2.8.4 Influence of BCCs on the behavior of SPRs under seismic loading

The common problem that is faced by rack systems is vibration load during loading and unloading of materials on the racks. The seismic zone experiences these loading

vibrations and therefore; the connection must have the ability to prove the adequacy of seismic design guidelines (Aguirre, 2005).

Harris & Hancock (2002) introduced an innovative testing rig able to apply up to 500 kN vertical load under both loading and unloading conditions to test the lateral stability of high rise racks. Higher deflection in the members resulted in greater BCC rotation. The research showed that the size of structural members plays an important role in controlling the deflections, and, consequently, the rotation of the connection.

Aguirre (2005) observed that the moment capacity of the SPR BCCs is three times higher than the normal semi-rigid BCCs. In his study, the seismic behavior of the pallet racks was determined and several component tests were conducted to predict the behavior of the BCCs. The connection failure was dependent on insufficient thickness of the column and the beam depth. The second reason was the asymmetry in the inclined hooks and the presence of the safety-bolt on the upper side of the beam end connector. The similarity in failure modes of both the static and the cyclic specimens demonstrated that the failure of the connection was initiated by the failure of the outermost hook. Later, a progressive failure initiated heading towards the neutral axis of the beam. To counter this phenomenon, the use of an inverted beam with bolts, strong tabs or greater beam depth may be feasible.

Filiatrault, et al., (2006) and Mahoney (2008) used a shake table test setup to observe the rotational stiffness of the connectors under static loading with the help of previously calculated dynamic values at minor vibrations and high magnitude of earthquake loading. The behavior of the connection was initially linear and the connector stiffness gradually reduced with an increase in vibration and showed a considerable reduction during the strongest shake and regained the initial stiffness after the completion of each test. From

the research, it can be concluded that the high stiffness may be achieved by using a beam with sufficient depth.

Several investigations were performed using down-aisle shake table tests on full-scale steel pallet-type storage rack specimens (André Filiatrault, Bachman, et al., 2006; André Filiatrault, Higgins, et al., 2006; Andre Filiatrault et al., 2007; Andre Filiatrault et al., 2008; A Filiatrault & Wanitkorkul, 2004; P Sideris & Filiatrault, 2009; Petros Sideris et al., 2010). The collective results indicated that the BCCs exhibit ductile and stable behavior with rotational capacities beyond the values observed during the shake-table tests and expected from a design seismic event. However, the hysteretic responses of some of the tested BCCs exhibited significant pinching similar to those tested by Bernuzzi & Castiglioni (2001).

During sway analysis of a spliced pallet rack, it was reported that a considerably high moment, rotation and displacement might occur depending on the location of the splices either above or below the junction (Beale & Godley, 2004). Further, the computer algebra program developed by authors may help to precisely determine the limiting cases of splices with zero rotation stiffness near the beam-column junction (Beale & Godley, 2004).

Kwarteng et al., (2012) performed tests on SPR BCCs in order to obtain the M-θ curve of the connection including the reduced capacity after repeated cyclic loads. The M-θ curve relations were then used in ANSYS computer models to determine the behavior of down-aisle SPRs under seismic loads. The results of the analyses showed that the reduced moment capacity of the connection does not significantly affect the overall structural behavior of SPRs as the rotations required for effect to occur does not normally occur under earthquake simulations.

2.8.5 Influence of connections on global stability

The collapse of a rack may occur due to overloading, incorrect design, or wrong manufacturing or installation. Several studies have been presented that investigate the reasons for the collapse of storage racks (Affolter, Piskoty, Wullschleger, & Weisse, 2009; Ng et al., 2009; P Sideris & Filiatrault, 2009; Petros Sideris et al., 2010). The role of the BCC was discussed to avoid the buckling phenomenon. The researchers, collectively, worked on the relationship that, to some extent, the beam could be utilized to restrain the deformation and to replace bracing. To support this relationship, lateral constraint was provided at the BCC in the end frame only. The size of the beam was critically important. When a considerable out-of-plane force was developed due to the member deflections at the BCC closest to the ground, the translational restraint was eliminated.

Table 2.1 shows the major contributions available in the literature regarding the testing of SPR BCCs under different circumstances and for investigating the influence of different parameters and types of loadings.

Table 2.1: Major experimental research contribution on SPR BCCs

Researchers	Test Type	Parameters investigated	Dominant Failure Mode
Stark & Tilburgs (1978)	Cantilever Test, Cross set-up test	Differences in test set-up; Type of beam end connectors	Deformation of tabs
Krawinkler et al., (1973)	Cantilever Test, Portal Test	Geometry of the connector tabs	Deformation of tabs
Markazi et al., (1997)	Cantilever Test	Member sizes, gauge difference, geometry of the beam end connector	Deformation of tabs, yielding of the beam end connector, deformation of the column
Bernuzzi, & Castiglioni (2001)	Cyclic Test	Seismic loading	Deformation of tabs, Deformation of nodal zone
Filiatrault et al., (2004)	Cantilever Test	Geometry of the connector, Material differences	Deformation of tabs
Filiatrault et al., (2006)	Pull back Test, White noise Test, Shake Table Test	Geometry of the connector, Type of loading	Deformation of tabs
Bajoria & Talikoti (2006)	Cantilever Test, Double-cantilever Test	Difference between test methods	Deformation of tabs
Sleczka & Kozlowski (2007)	Cantilever Test	Geometry of the members, Types of the beam end connector	Deformation of tabs, yielding of the beam end connector, deformation of the column
Prabha et al., (2010)	Double-cantilever Test	Thickness of column, Depth of beam, Depth of the beam end connector	Deformation of tabs, yielding of the beam end connector, deformation of the column
Kwarteng et al., (2012)	Cantilever Test, Cyclic Test	Seismic effects	Weld between the beam and the beam end connector. Deformation of the beam end connector and tabs
Roure et al., (2013)	Cantilever Test	Types of full assembly, Efficiency of US and EU testing procedures	Deformation of the beam end connector and tabs
Zhao et al., (2014)	Cantilever Test	Geometry of the members, Types of the beam end connector	Deformation of tabs, Deformation of column
Mohan et al., (2015)	Cantilever Test	Thickness of column, Depth of beam, Depth of the beam end connector	Deformation of tabs, yielding of the beam end connector, deformation of the column

2.9 CFS connections under fire

2.9.1 Research progress

Fire forms a significant threat for any structural buildings that can cause a major damage to the lives and properties. It is a general concept that as compared to other materials when CFS members become exposed to fire, due to the high slenderness, less resistance to buckling and high value of thermal conductivity, fire gives a rapid rise to the temperature and decreases the properties of material constituting the structural members which results in rapid loss of strength and stiffness of whole structure and leads to an early and unwanted collapse of the structure. In this case, the thermal forces induced on beams and columns are strongly affected by the detail of the BCCs, such as the connection type (simple, semi-rigid, rigid) and the connections become significantly responsible to maintain the global stability.

Connections are critical in understanding the performance of cold-formed structures under elevated temperatures. At elevated temperatures, a significant body of literature exists on the behavior of traditional steel connections (K. Al-Jabri, 2004; K. Al-Jabri, Burgess, Lennon, & Plank, 2005; K. Al-Jabri, Burgess, & Plank, 2000; K. Al-Jabri, Seibi, & Karrech, 2006; Khalifa Saif Al-Jabri, 1999; Khalifa S Al-Jabri & Al-Alawi, 2007; Khalifa S Al-Jabri, Davison, & Burgess, 2008; Bravery, 1993; Burgess, Davison, Dong, & Huang, 2012; Cai & Young, 2014, 2015, 2016; da Silva, Santiago, & Real, 2001; Garlock & Selamet, 2010; Hu, Davison, Burgess, & Plank, 2009; Laím & Rodrigues, 2016; Laím, Rodrigues, & Craveiro, 2016; Lawson, 1990; Leston-Jones, 1997; Mao, Chiou, Hsiao, & Ho, 2009; Spyrou, Davison, Burgess, & Plank, 2004a, 2004b; Stoddart, Byfield, & Tyas, 2012; Sun, Burgess, Huang, & Dong, 2015; Yu, Burgess, Davison, & Plank, 2008).

Past research on mechanical properties at elevated temperatures was mainly focused on HRS. However, in recent times some studies have been carried out on the reduction of mechanical properties of CFS at elevated temperatures (Abreu, Vieira, Abu-Hamd, & Schafer, 2014; J. Chen & Young, 2006, 2007; Ellobody & Young, 2005; Kaitila, 2002; Kankanamge, 2010; Kankanamge & Mahendran, 2011; Laím et al., 2016; J. H. Lee, Mahendran, & Makelainen, 2003; Makelainen & Miller, 1983; Outinen & Makelainen, 2001; Ranawaka & Mahendran, 2006, 2009a, 2009b, 2010; Sidey & Teague, 1988; Wei & Jihong, 2012).

Despite the availability of significant literature on the fire behavior of CFS connections, a serious lack of studies focusing on the fire behavior of SPR BCCs exists in the literature. Since the knowledge base is similar, therefore, a number of studies into the fire behavior of traditional cold-formed semi-rigid steel connections have been reviewed in this section to strengthen the investigation methodology of this research.

Sidey and Teague (1988) stated that the strength reduction of CFS at elevated temperatures may be 20% higher than that of HRS. Lawson (1990) experimentally examined eight semi-rigid steel BCCs at elevated temperatures under varied moment. The connections sustained up to two-thirds of their design moment capacity in fire conditions. Leston-Jones (1997) tested the influence of semi-rigid connections on the performance of steel framed structures in fire. The study was limited to smaller sized section sizes. Al-Jabri et al., (2000) conducted testing of five steel connections with different configurations at elevated temperature. In total, twenty tests were conducted at different load levels. The main purposes of testing were to identify the influence of parameters such as member size and type and thickness of end-plate on the connection response in fire, and to review the degradation characteristics of bare-steel and composite connections and the general outcomes from the performed tests. Da Silva et al., (2001) extended the

component model that was widely accepted in cold design to predict the response of steel joints under fire loading. Spyrou et al., (2004a; 2004b) investigated the tension and compression zones within an end plate steel joint at elevated temperatures. Al-Jabri (2004) developed a component based model for flexible end-plate connections at elevated temperatures. In this model the elements of the connection were treated as springs with known stiffness and the overall connection response is obtained by assembling the stiffness of individual elements in the tension and compression zones. This method is valid up to the point at which the bottom flange of the beam comes into contact with the column (Khalifa Saif Al-Jabri, 1999). Lee et al. (2003) predicted the mechanical properties of light gauge steel subjected to elevated temperatures and compared the differences with high strength steel. They derive accurate reduction factors for mechanical properties in fire safety design and presented the empirical equations for the reduction factors and a stress–strain model at elevated temperatures for light gauge steel members.

Al-Jabri et al., (2005) tested five different semi-rigid connections to establish the M-θ-temperature (M-θ-t) relationships for semi-rigid connections. A variety of full-scale flush end-plate and flexible end-plate steel BCCs using a portable furnace. A linear temperature ramp (at a rate of about 10 °C per minute) achieving 900 °C in 90 min was adopted. The results of these tests provided valuable knowledge. A curve-fitting of the test results in Ramberg–Osgood expressions (Ramberg & Osgood, 1943) of M-θ curves was performed. In general, this technique requires the availability of a large number of M-θ curves suitable only to connections that would behave in a similar way to those that have been used to generate the curve-fitting expressions. Al-Jabri et al., (2005) were later verified their experimental test results using FE modeling (K. Al-Jabri et al., 2006). Degradation of steel properties with increasing temperature was assumed in accordance with Eurocode (EC3, 2005b) recommendations. The obtained simulated failure modes

and M-θ-t characteristics of the connections compared well with the experimental data. While examining the differences between the behavior of corner and flat parts of the CFS members.

Ellobody and Young (2005) investigated the structural performance of CFS high strength steel columns using FE analysis on duplex stainless steel columns having square and rectangular hollow sections. The column strengths and failure modes as well as the load-shortening curves of the columns were obtained using the finite element model. The results of the parametric study showed that the design rules specified in the American, Australian/New Zealand and European specifications are generally conservative for cold-formed high strength stainless steel square and rectangular hollow section columns, but unconservative for some of the short columns.

Chen and Young (2006) reported that the mechanical properties of the corner parts being different from the flat parts. Later, in another study of them, Chen and Young (2007) performed experimental investigations on the behavior of CFS members at elevated temperatures. Steady and transient tensile coupon tests were conducted at different temperatures ranged approximately from 20 to 1000 °C for obtaining the mechanical properties of CFS structural material. Curves of elastic modulus, yield strength obtained at different strain levels, ultimate strength, ultimate strain and thermal elongation versus different temperatures are plotted and compared with the results obtained from the Australian, British, European standards and the test results predicted by other researchers. The findings revealed that the yield strengths predicted by the Australian, British and European standards are conservative, except for G550 1.0 mm steel from 450 to 970 °C and G450 1.9 mm steel at 660 °C. Hence, the standards provide unconservative predictions for high temperatures. An equation was proposed to rectify the errors in codes and validated against the experimental results.

A review of the fire behavior of HRS connections was performed by Al-Jabri et al., (2008) and very useful information was provided. A comparison of strength and stiffness degradation of CFS members and HRS members showed that at elevated temperatures, the strength degradation CFS members occurs at very higher rate as compared to HRS members. Mao et al., (2009) studied the fire response of steel semi-rigid BCCs connections made with H-shape beam and H-shape column. A finite element model was developed and showed a good agreement with previously available experimental results. The numerical results show that the applied moments have significant effects on the stiffness of steel moment connections in addition to material properties and connection geometry. Hu et al., (2009) developed a simplified component model for flexible end-plate connections subjected to fire and under variable loads. The proposed component model well predicted the tying resistance and critical components of failure for steel connections in fire and showed a close agreement with experimental results. Garlock & Selamet (2010) validated the single plate shear connection by a full-scale building fire tested in Cardington (Bravery, 1993). The Cardington connection was redesigned using the single and double angles using American Institute of Steel Construction (AISC, 2010) provisions. Burgess et al., (2012) efficiently described the role of connection in steel structures subjected to fire. Stoddart et al., (2012) performed blast modeling of steel connections and proposed a frame modeling approach that should be able to achieve a realistic treatment of connection response without significantly increasing the computational requirements. Wei & Jihong (2012) discussed the mechanical properties of G550 CFS steel members under transient and iso-thermal temperature states and declared that a noticeable difference exists between the transient and steady state method for G550 steel. The steady state test results of G550 may result in an overestimate of the fire resistance of CFS structures.

Aberu et al. (2014) provided a comprehensive information on the behavior of various CFS members subjected to fire as well as the effect of various types and scenarios of fire on the behavior of any specified CFS member. Cai & Young (2014, 2015, 2016) provided useful information on the fire behavior of cold-formed stainless steel single and double shear bolted connections.

The literature has revealed that the degradation of CFS members at elevated temperature is different from the degradation of HRS members; mainly due to the high slenderness and being thin-walled mebers. Therefore, the CFS members become more susceptible to lateral torsional buckling or distortional buckling at very early stage of being heated at low temperatures.

2.10 Chapter summary

The literature review presented in this chapter was initiated to cover the scope of the study and to achieve the desired objectives. The other important purpose of review was to extract the information and to achieve better understanding on performing experimental and numerical investigations into the behavior of SPR BCCs under ambient and elevated temperature. A number of observations for instance, the selection of test method, the parameters which may be influential on connection performance and various types of failure modes noticed from the literature review has helped to adopt experimental testing setup and other arrangements, methodology about the FE modeling of SPR BCCs under discussion. The findings of literature review are applied in the investigations which are presented in the next few chapters of this study.

CHAPTER 3: MATERIALS AND METHODOLOGY

3.1 General

This study attempts to evaluate the behavior of SPR BCCs under static loading and subjected to ambient and elevated temperatures, experimentally and numerically. The M-θ behavior, load-strain relationship and major failure modes are observed. At ambient temperatures, it was also desired to understand that how the variation in most influential parameters, such as depth of beam, the thickness of the column and the number of tabs in the beam end connector, could improve the performance of SPR BCCs. The experiments were carried out by means of the double cantilever test method. A comparative study to calculate the connection stiffness using the three different methods namely, the initial stiffness method, slope to half-ultimate moment method and the equal area method was also carried out to suggest the relatively appropriate method for stiffness design. In order to find out the more appropriate method, the mean stiffness of all the tested connections and the variance in the values of mean stiffness according to all three methods were calculated. The experimental results are further validated with a non-linear 3D FE model. After achieving a close agreement between the two types of observations, the validated FE model is further extended to parametric analysis in order to observe the influence of those parameters on SPR BCCs which are not considered in experimental investigations.

The experimental and numerical testing of SPR BCCs at elevated temperature is also performed and the results are compared with experimental testing performed at ambient temperature. This chapter comprehensively explains the materials' details and the methodology adopted to achieve the objectives of this research.

3.2 Experimental investigations at ambient temperatures

The design of CFS members and assemblies are normally carried out on the basis of theoretical provisions prescribed by the code of practice. But in the case of perforated

CFS members used in the rack system, the design is carried out based on the initial test on the members and their behavior. It is the same case when adequate design method is not available for some structural members. Adequate design procedures are not available for SPR BCCs and hence design has to be carried out based on the results of experiments conducted on members and/or the assemblies. The design specifications of international standards such as RMI (2012) and EN15512 (2009) recognize the importance of investigating individual component characteristics, and they have almost similar approaches to understand the behavior of members and connections. The purpose of the experimental program presented in this section is to investigate the semi-rigid characteristics of SPR BCCs by varying the column thickness, depth of beam and number of tabs in the beam end connector. Experimental investigations are performed on selected SPR BCCs. As mentioned in the previous chapter of this study, it is essential to obtain the material properties of the specimens before conducting experimental testing.

3.2.1 Material properties

The RMI (2012) and EN15512 (2009) codes recommend that the material properties of pallet rack sections to be accurately determined by means of tensile coupon test. For this study, CFS sections were used for columns and beams. The beam end connectors are made of HRS. The material properties of members and beam end connectors were provided by the manufacturer; obtained using the tensile coupon test. According to the manufacturer, three tension coupon specimens were fabricated for upright and the beam end connector with various depths. The coupons were obtained from the start, middle and the end of mother coil. The material properties provided by the manufacturer are given in Table 3.1.

Table 3.1: Material properties of specimens

Member	Young's Modulus (E) (GPa)	Poisson' ratio (ν)	Yield strength (f_y) (MPa)	Ultimate strength (f_u) (MPa)	Plastic strain at Ultimate Tensile Strength
Column	210	0.3	459	575	0.2272
Beam			353	497	0.3275
Beam-end-Connector (Four tabs)			214	343	0.4712
Beam-end-Connector (five tabs)			263	365	0.4182

3.2.2 Specimen details

A total of 32 tests are carried out, composed of four trials of each set of specimens, which are distinguished by two different column thicknesses, four different beam depths and the number of tabs in the beam end connector being either four or five. The section sizes selected for experimental testing were based on the commercial practice in the area where this research has been performed. The column specimens are distinguished by means of their thickness. Column 'A' has a thickness of 2.0 mm and column 'B' has a thickness of 2.6 mm. The height of the column was kept constant throughout the investigation and was limited to 500 mm. The cross-section of the column is illustrated in Figure 3.1. The details of the dimensions and section properties of the columns are given in Table 3.2.

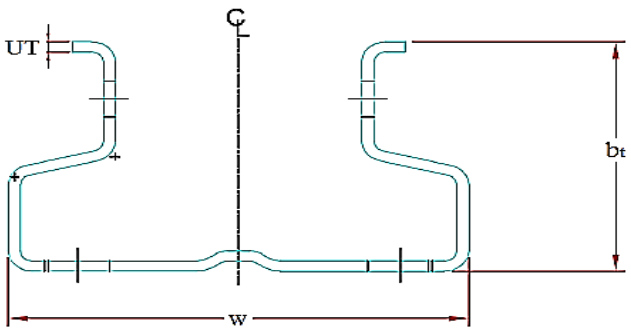

Figure 3.1: Cross-section of column

Table 3.2: Dimension details and section properties of columns

Column	A	B
Thickness ‘ t’ (mm)	2.0	2.6
Flange width ‘b_t’ (mm)	67.6	68.3
Web ‘w’ (mm)	112.2	113.1
Height ‘h’ (mm)	500	500
Cross section area ‘A’ (cm^2)	5.73	7.48

Box-beams with four different depth values, namely B1, B2, B3 and B4 were used in the experimental testing. Beams B1 and B2 have a four tab beam end connector, while for B3 and B4, the connector has five tabs. The cross section of the box-beam is represented in Figure 3.2. The dimensions and section properties of the beam sections are given in Table 3.3.

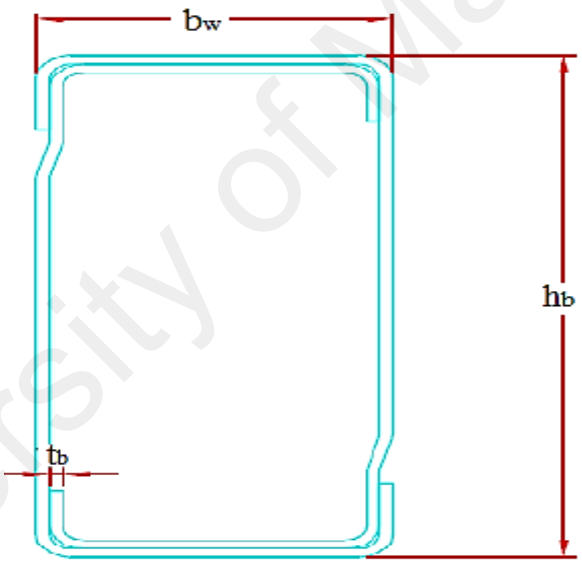

Figure 3.2: Cross-section of beam

Table 3.3: Dimension details and section properties of beams

Type of beam	Width ‘bw’ (mm)	Depth ‘hb’ (mm)	Thickness ‘tb’(mm)	Cross-sectional Area ‘A’ (mm^2)	Center of Gravity ‘CG’ (mm)		Moment of Inertia ‘M’(cm^4)		Section Modulus ‘S’ (cm^3)	
					(x-x)	(y-y)	(x-x)	(y-y)	(x-x)	(y-y)
B1	40	92	1.5	387	20	46	42.197	11.5	9.173	5.75
B2	40	110	1.5	441	20	55	65.945	13.5	11.99	6.75
B3	50	125	1.5	516	25	62.5	102.6	24.6	16.415	9.862
B4	50	150	1.5	591	25	75	162.11	29.06	21.615	11.62

The geometry of the beam end connectors is distinguished by the number of tabs in the beam end connector. Connector 'A' has four tabs and connector 'B' has five tabs. The depth of connectors 'A' and 'B' is 200 mm and 250 mm, respectively. The cross-section of the beam end connector is shown in Figure 3.3. All the dimensions of the specimens are the measured values.

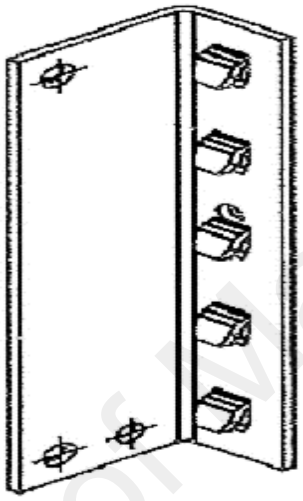

Figure 3.3: Cross-section of the beam end connector

For a clarified representation of the specimens under investigation, each specimen was given a specific specimen ID and a letter, which is listed in Table 3.4 along with details of the number of tests performed. For example, in the specimen ID '2.0UT-92BD-4T', 2.0UT represents the column thickness as being 2.0 mm, 92 BD represents the depth of beam as being 92 mm and 4T represent the number of tabs in the beam end connector, which is four.

Table 3.4: Details of specimens' IDs

Letter assigned to specimens	Specimen details	Number of tests performed
A	2.0UT-92BD-4T	4
B	2.0UT-110BD-4T	4
C	2.0UT-125BD-5T	4
D	2.0UT-150BD-5T	4
E	2.6UT-92BD-4T	4
F	2.6UT-110BD-4T	4
G	2.6UT-125BD-5T	4
H	2.6UT-150BD-5T	4

3.2.3 Connection arrangement

A sketch of tested specimen D with its dimensions is shown in Figure 3.4. The connection shows a beam end connector of 4-mm is welded to one end of the beam with tabs punched into it. The leg of the angle with tabs is in contact with column web after assembly, while there is a 2-mm gap between the second legs, perpendicular to the column web. The tabs were reversely inserted into the column holes.

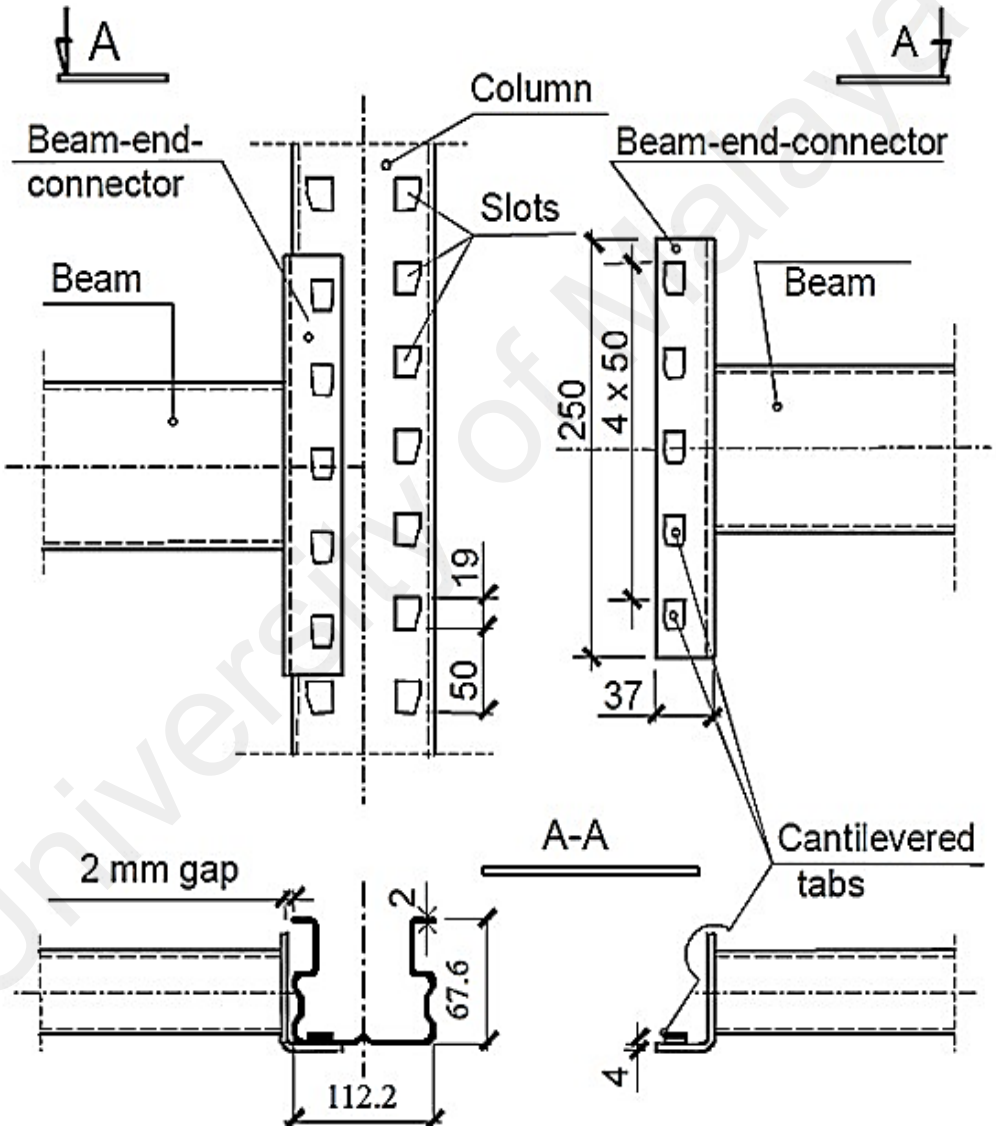

Figure 3.4: Dimensions of tested connection

3.2.4 Selection of Test Method

To investigate the behavior of the beam end connector, RMI (2012) suggests alternative testing methods. These methods are the 'portal frame testing method' and 'cantilever testing method'. However, the EN15512 (2009) only suggests the cantilever testing method.

The cantilever test can be further extended by attaching one more beam to the other side of the column, which accordingly, is called the double cantilever test method. Though, this test method has not been described in any of the standards yet, however, the literature has proven that when compared to full scale rack testing, the double cantilever test predicts the connection behavior more effectively than cantilever test method (K. Bajoria & Talikoti, 2006). The main advantage of this type of set-up is the column moves only up and down as a rigid body and a far better shear-to-moment ration can be achieved compared to the simple cantilever test. The entire beam deformation is only by the connection deformation. In double cantilever test, the connector is subjected to three types of forces namely moment, shear, axial pull thus representing the actual field conditions.

3.2.5 Test setup

In this study, the double-cantilever test method was adopted to predict the M-θ behavior of the connection. Initially, the column is placed and aligned below the actuator. Two beams are connected at the center of the column on both left and right sides. The lateral movement of beams is restricted by restraining them by means of two rectangular hollow sections welded to the angle sections and bolted to the strong floor. The unconnected ends of the beams are supported by roller supports on the left and right sides. The effective distance between the roller supports is 2 m. The tabs of the beam end connectors are reversely hooked in the column perforations. A locking pin is used to avoid any change in the position of the column or the connector due to accidental uplift. In

accordance with EN15512 (2009), to minimize the effects of initial looseness, a load equal to 10% of the anticipated failure load is applied as a pre-load initially and the displacement measuring devices are installed. When a tab is not properly engaged with the column, a larger initial rotation in the connection may occur; therefore, it is required to give an initial loading to make sure the beam end connector properly engages with the column.

In contrast to the traditional test set-ups where the beam transmits the load to the connected column, the load is applied to the top of the column in a displacement control based method. The load is applied using a 50 kN hydraulic actuator controlled by the computer at a rate of 3 mm/min until the connection failure. The load is applied to the top of the column which caused compression in the top of the beam end connector and tension at the bottom. The test continued until a drop of 1 kN load is observed or the deformation of the specimen is so large that it is unsuitable to carry load, whichever happened earlier.

3.2.5.1 Instrumentation

In order to achieve a set of information about the behavior of the connection throughout the entire range of applied loading, three different types of measurement were recorded in the tests besides loading. Strain readings were fitted to monitor the yielding of steel, displacements were measured to obtain the load-deflection behavior and rotation measurements are taken to obtain the M-θ characteristics. For rotation measurements, EN15512 (2009) suggests that the rotation can be measured by either: (i) displacement transducers bearing onto a plate fixed to the beam close to the connector, but with enough clearance to allow for connector distortion, and/or (ii) inclinometers connected to the beam close to the connector. In this study, two digital inclinometers were placed on the top flanges of the beams on either side at a distance of 50 mm from the face of the column to directly record the rotation of beams in degrees, which reduces the manual

computational efforts and provide precise results in terms of rotation. Deflection measurements using linear variable differential transducers (LVDTs) having a measurement range from 50 mm-200 mm were also installed. In order to measure any deflection in beams due to the applied load, two LVDTs were installed at a distance of L/4 from the center of roller support, on the beams on either side. One LVDT is placed at the bottom of the column to observe central deflection.

For the tests involving beams B1 and B2, three strain gauges were installed. One strain gauge (S1) was placed in the column web near the top surface of the beam end connector estimate the tensile strain. The other two strain gauges (S3 and S4) were placed near the bottom slot of the beam end connector in the tension region. For beams B3 and B4, four strain gauges were installed. Three strain gauges were fixed in the same position as for B1 and B2, whereas an additional strain gauge (S2) is placed in the lower portion of column web near the bottom surface of the beam end connector. Readings from the strain gauges and LVDTs were recorded onto the computer system through data logger. The schematic diagram of test set-up and the locations of instrumentation are presented in Figure 3.5.

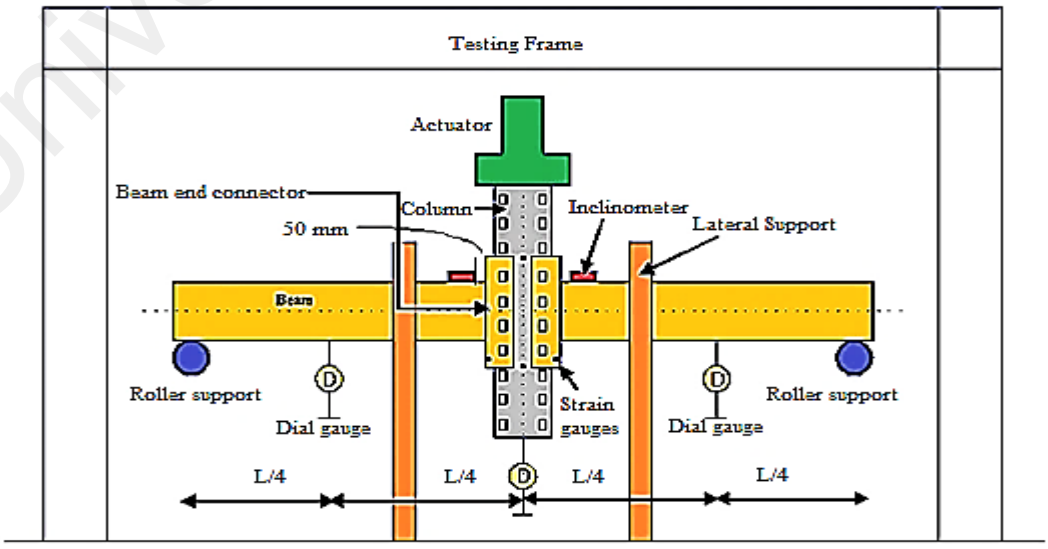

Figure 3.5: Schematic diagram of test set-up

3.3 Experimental investigations at elevated temperatures

3.3.1 Material properties and specimen details

The specimens used for elevated temperature testing have the material properties, the dimensional details of specimens and cross-sectional shapes same as those used for the specimens tested at ambient temperatures. Similar to the ambient temperature testing, eight sets of specimens (A to H) were identified and each specimen is tested on three different temperature ranges. In total, twenty-four tests were performed at elevated temperatures. Table 3.5 shows the details of elevated temperature testing of specimens.

Table 3.5: Details of elevated temperature testing

Specimen set	Specimen ID	Temperature ranges No. of tests performed		
		450 °C	550 °C	700 °C
A	2.0UT-92BD-4T	1	1	1
B	2.0UT-110BD-4T	1	1	1
C	2.0UT-125BD-5T	1	1	1
D	2.0UT-150BD-5T	1	1	1
E	2.6UT-92BD-4T	1	1	1
F	2.6UT-110BD-4T	1	1	1
G	2.6UT-125BD-5T	1	1	1
H	2.6UT-150BD-5T	1	1	1

3.3.2 Selection of temperature ranges

Mechanical properties play an important role in the fire safety design of CFS structures since temperature rise in steel members reduces the mechanical properties such as yield strength and elastic modulus. This reduction of mechanical properties greatly affects the structural behavior of CFS members and reduces the load carrying capacity at high temperatures. Therefore the mechanical properties at elevated temperatures are required for the fire safety design of steel members. Hence it is important to have a good knowledge and understanding of the reduction of mechanical properties with increasing temperatures. Eurocode 3 (EC3, 2005b) provides reduction factors for both yield strength and elastic modulus for carbon steel. These reduction factors can be used for both CFS

and HRS despite the fact that the reduction of mechanical properties of both types of steel is considered different (Kankanamge, 2010).

Though studies discussing the fire behavior of SPR BCCs solely are not available, however, a collective review of the studies available on cold formed thin walled steel structures suggests that for a thorough observation of the fire behavior of connections, temperature range should be kept in between 300-900 °C. However, the strength reduction factor defined by EC3 (2005b) at different temperatures provides no noticeable degradation at 300 °C but after this temperature, the strength degradation becomes noticeable and the behavior of members and/or connections varies with different types of deformations. To support this statement, the reduction factors for stress-strain relationship of steel at elevated temperature according to EC3 (2005b) are shown in Figure 3.6 and Table 3.6.

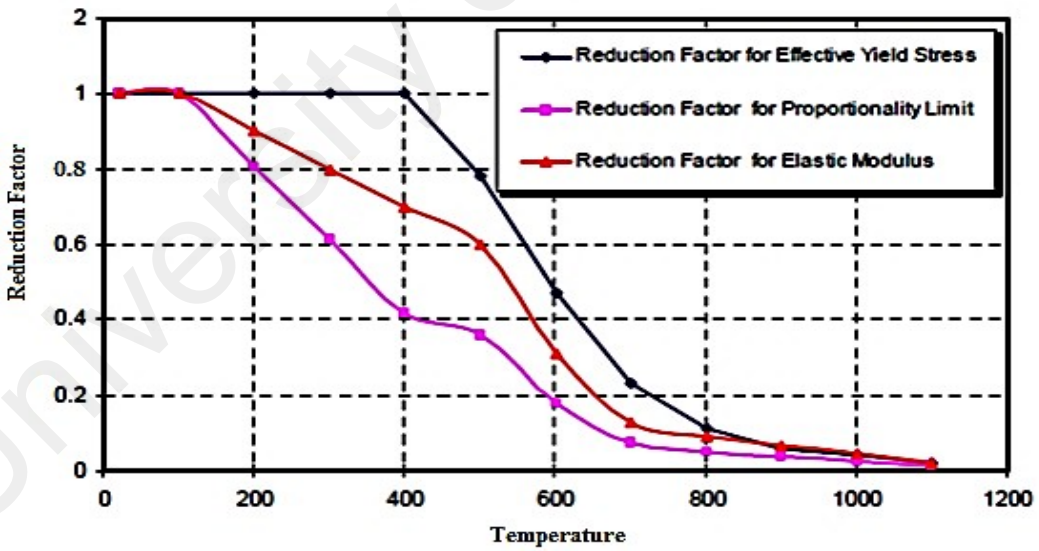

Figure 3.6: Reduction Factors for Carbon Steel at Elevated Temperature [EC3 (2005b)]

Table 3.6: Reduction Factors for Stress-Strain Relationship of Carbon Steel at Elevated Temperature [EC3 (2005b)]

Temperature (°C)	Effective yield stress $K_{yT} = f_{yT} / f_y$	Modified factor for yield strength $Kx_T = f_{yT} / f_y$	Proportionality limit stress $K_{pT} = f_{yT} / f_y$	Elastic modulus $K_{ET} = E_T / E$
20	1.000	1.000	1.000	1.000
100	1.000	1.000	1.000	1.000
200	1.000	0.922	0.807	0.900
300	1.000	0.845	0.613	0.800
400	1.000	0.770	0.420	0.700
500	0.780	0.615	0.360	0.600
600	0.470	0.354	0.180	0.310
700	0.230	0.167	0.075	0.130
800	0.110	0.087	0.050	0.090
900	0.60	0.051	0.0375	0.0675
1000	0.40	0.034	0.0250	0.0450
1100	0.20	0.017	0.0125	0.0225
1200	0.000	0.000	0.000	0.000

3.3.3 Test setup

The basic test setup used for elevated temperature testing is similar to the test set-up used for ambient temperature testing, i.e., the double-cantilever test method. However, some modifications are made in the loading setup and instrumentation.

For elevated temperature testing, the load is applied using the Universal Testing Machine (UTM) to the top of the column. Both the applied load and the corresponding deflection readings are recorded by the computer connected to the UTM.

Due to the high temperature effects in the connection region, the strain gauges and inclinometers were removed. In order to obtain the rotation, LVDTs were placed close to the connector. To assess the end rotations of the beams, two LVDTs were used at each beam. The end rotations of the beam were obtained as the relative LVDTs' displacements divided by the separation between them. However, it was essential to save the LVDTs from the temperature effects. For this purpose, initially two thick long steel plates coated with fire retardant Intumescent coating were fixed at the back side of the beam in

perpendicular direction and at the horizontal axis of symmetry of the beams on either side. LVDTs D1 and D2 were placed on the plates at the right and left hand sides, respectively, 100 mm from the face of the column. LVDTs D3 and D4 were placed at a distance of 200 mm from LVDTs D1 and D2, on the right and left hand sides beams, respectively. This arrangement excluded the relative slippage between the column and the beam end connector. The LVDTs were connected to a computer operated data logger, which recorded the readings on the computer.

To produce thermal action in the specimens, an isothermal fire condition was applied to observe the deformation of connections at various magnitudes of temperature. The thermal action on the connection components was applied through flexible ceramic pad (FCP) heating elements (Figure 3.7) mounted on the specimen surface. To minimize heat loss, the entire surface of the specimen was insulated with rock wool, with a density of 128 kg/m3 (Figure 3.8). The heating process was controlled by K-type cable thermocouples (Figures 3.9) placed in a position that covered the entire connection. The thermocouples were connected to an electrical transformer (ET) (Figure 3.10a) for heating. A temperature recorder was also calibrated to the ET (Figure 3.10b).

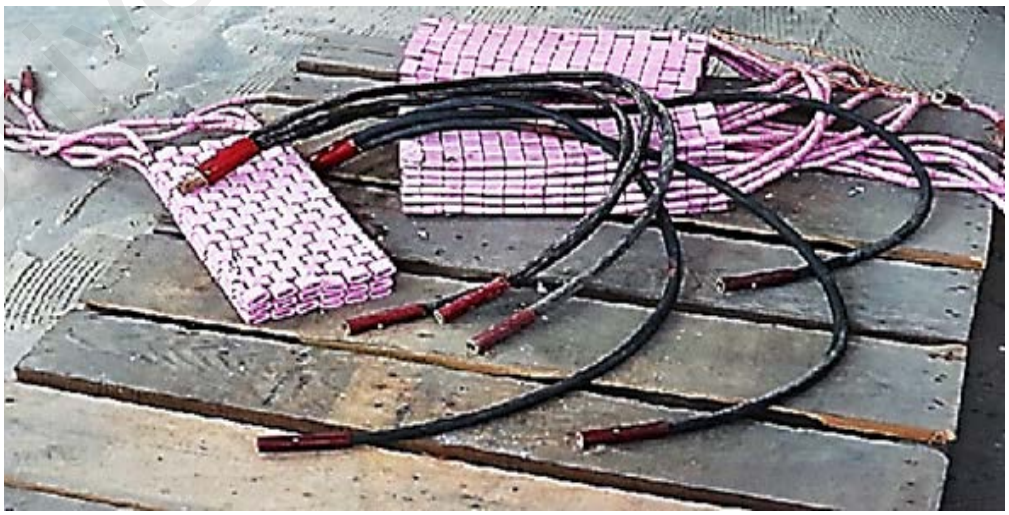

Figure 3.7: Samples of FCP heating elements

Figure 3.8: Rock wool

Figure 3.9: Cable thermocouples type K for measuring the temperature in the specimens

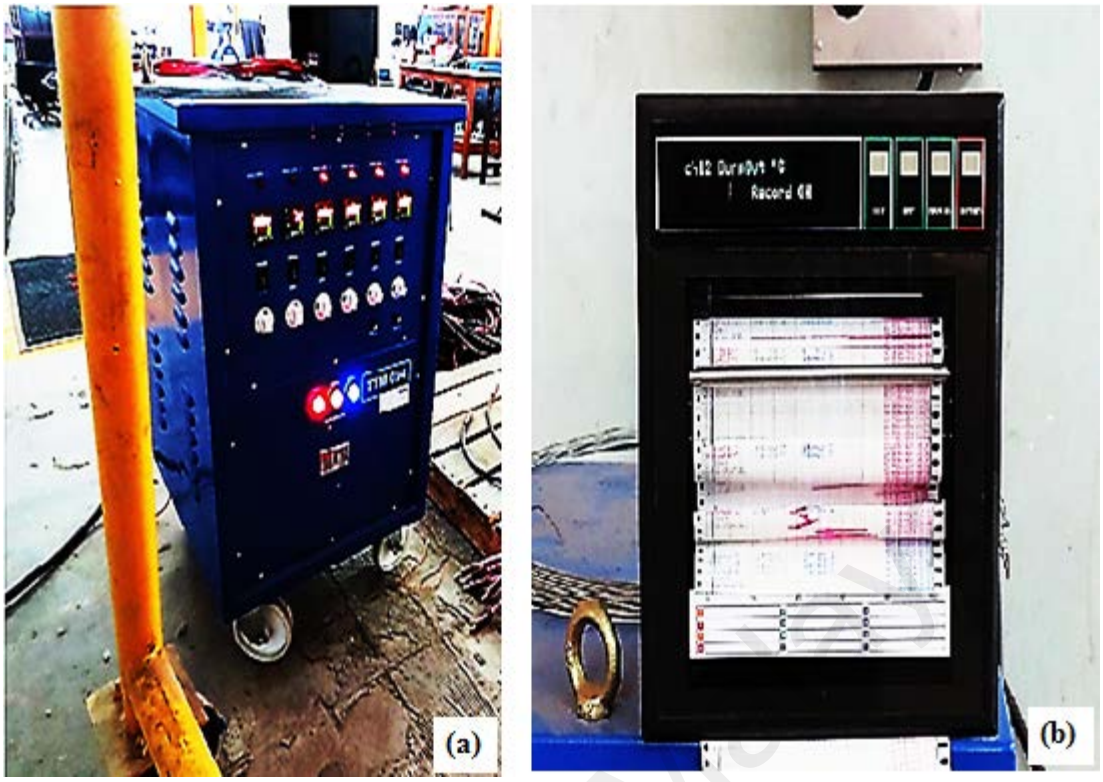

(a) Electrical transformer for heating recorder (b) Calibrated temperature

Figure 3.10: Temperature controlling apparatus

There are three different methods of assessing the fire safety of structures: time domain, temperature domain, and strength domain. This research is based on the strength domain used in fire safety design. Fire safety in the strength domain is verified by comparing the applied load at the time of the fire with the minimum load capacity of structural members during the design fire event.

In order to produce thermal action in the specimens, an iso-thermal fire condition is applied to observe the deformation of connections at various magnitudes of temperature. The temperature was applied to the desired temperature range and kept constant. The load was then applied using a universal testing machine (UTM) in a displacement controlled method at a rate of 3 mm/min until the occurrence of a connection failure. The UTM was connected to the computer, and the application of load and corresponding central deflection was observed using the computer readings. The load was applied to the top of the column, which caused compression at the top of the beam end connector and tension

at the bottom. Figure 3.11 presents the front view of the schematic diagram of the test setup for elevated temperature testing, and Figure 3.12 illustrates the isometric view of the test setup.

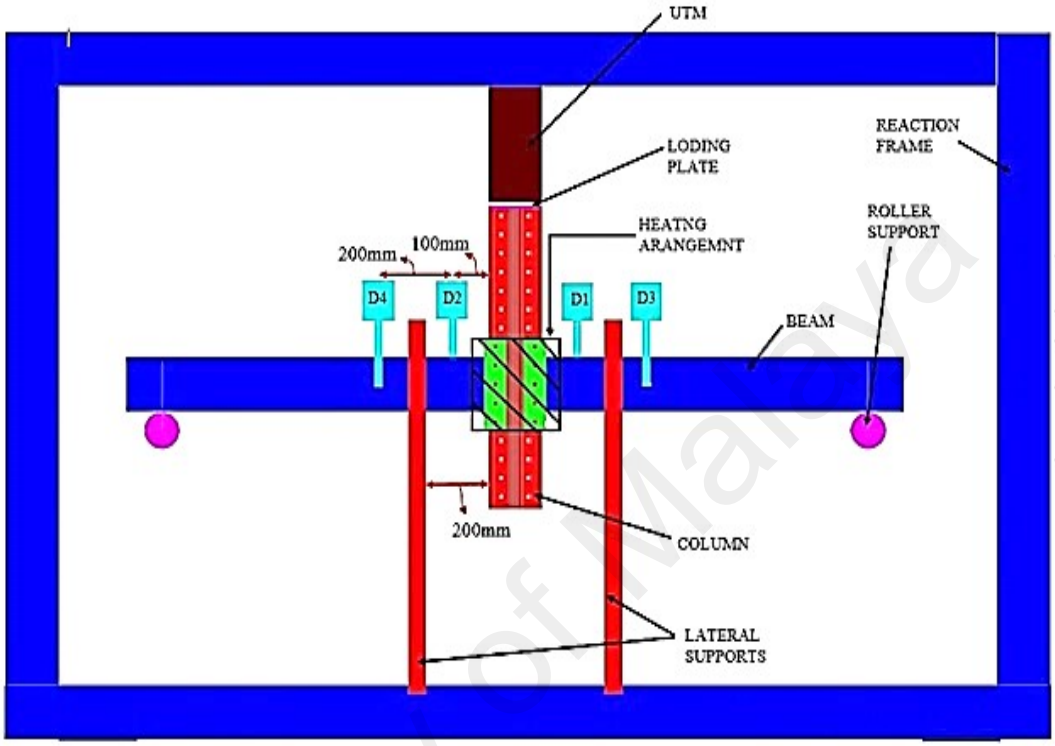

Figure 3.11: Front view of schematic diagram of test setup

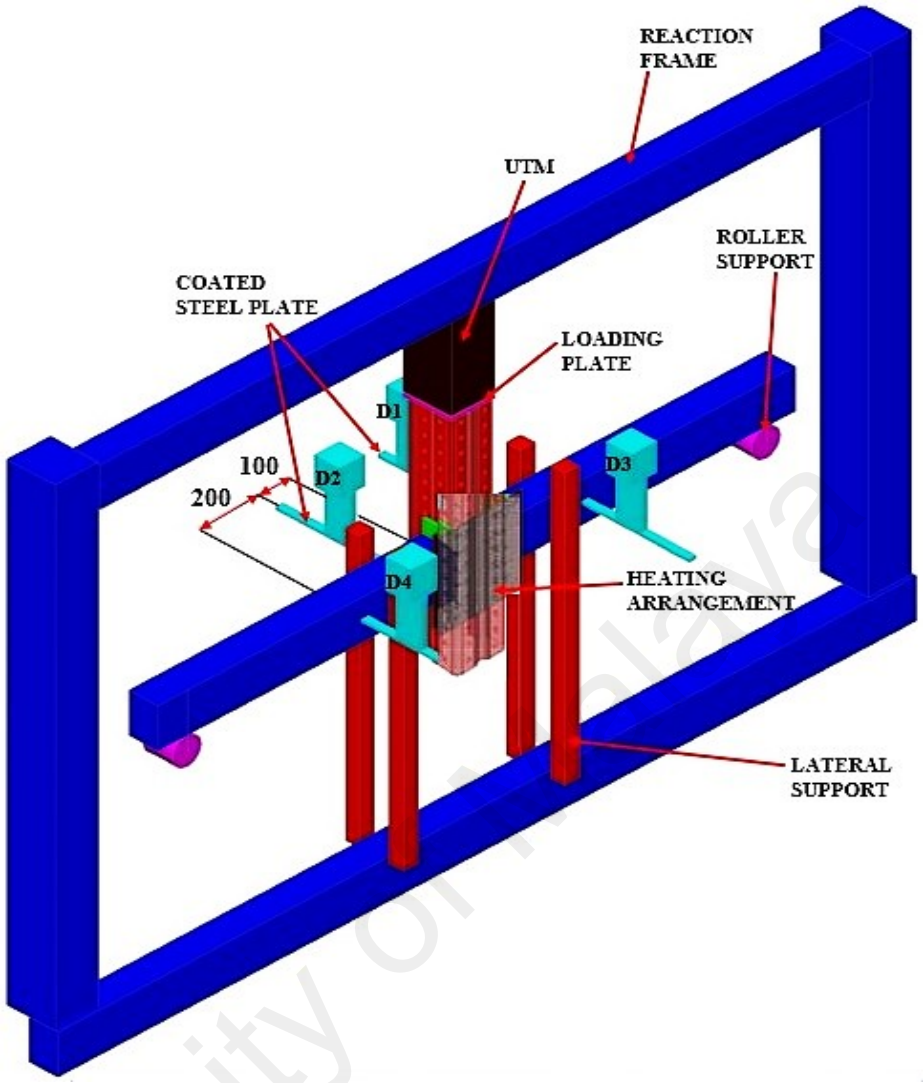

Figure 3.12: Isometric view of schematic diagram of test setup

3.4 Finite Element (FE) modeling at ambient temperature

FE simulations were performed to evaluate the structural behavior of SPR BCCs. A 3D nonlinear FE model of the column, beam, and beam end connector assembly was developed using the commercial FE software ABAQUS (Simulia, 2011) for both four- and five-tab connectors.

3.4.1 Connection modeling

Four- and five-tab beam end connector assemblies were modeled. Element C3D8R (i.e., continuum 3D with eight nodes and reduced integration) was used for all the three parts of an assembly. The number of elements in each beam/beam end connector were 18812 whereas in column, the number of element was 46404. A bilinear elasto-plastic

material model was adopted to estimate the deformation behavior of the column, beam, and beam end connector assemblies. Distortion energy density criterion or von Mises yield criterion is used to predict yielding. The material properties of all the three components listed in Table 3.1 were used for FE modeling (FEM). Plastic strain (Table 3.1) was calculated through the Ramberg–Osgood method (Ramberg & Osgood, 1943). It should be noted that the few of previous studies (Prabha et al., 2010) did not consider the modeling of tabs that hampers to obtain realistic modeling of the strength and deformation behavior of connector tabs which were the most crucial element of SPR BCCs. In this study, the tabs of the connector were modeled using solid elements with a thickness of 4 mm (Figure 3.13) to replicate the original experimental conditions. Considering tabs as a solid element complicated the FE model. However, this approach replicated an actual system, and thus, the deformation behavior of tabs could be predicted.

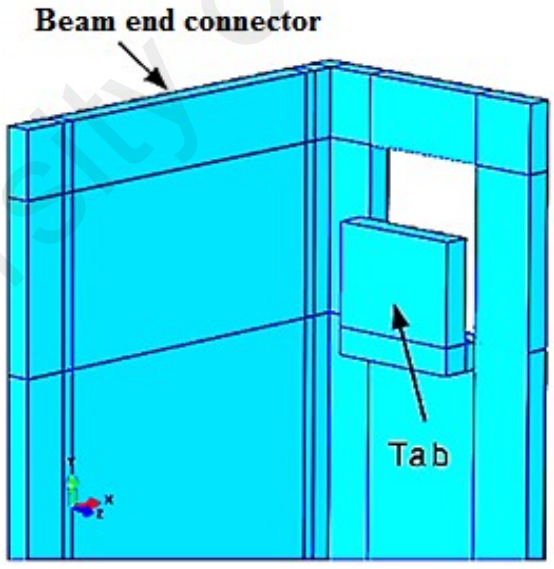

Figure 3.13: Geometry of tabs

3.4.2 Surface interaction

Contact nonlinearity is incorporated into the FE model by defining the interactions among column, beam end connectors, and tabs. The surface-to-surface interactions (front and side) between the column and the beam end connector are defined through tangential

frictionless behavior, as shown in Figure 3.14 (a). Similarly, the surface-to-surface interactions between the column and the tabs are defined in two ways: (i) normal hard contact, as shown in Figures 3.14 (b) and (c), and (ii) tangential frictionless contact, as shown in Figure 3.14 (d). The former is defined to avoid the relative movement between the surfaces of the column and the tab, whereas the latter is defined to restrain the sideways movement (normal to longitudinal axes) of the column. Future research may incorporate precise surface-to-surface tangential contact through the Coulomb friction model. The weld between the beam end connector and the beam is modeled using the BEAM element which simulates the welded connection. In future works, more advanced analysis can be performed through coupling elements that replicates the exact type of welded connections in structures. The complete geometry of the modeled connections is presented in Figure 3.15.

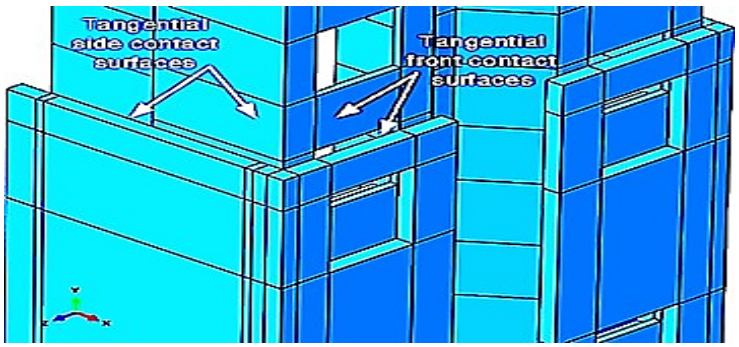

(a)

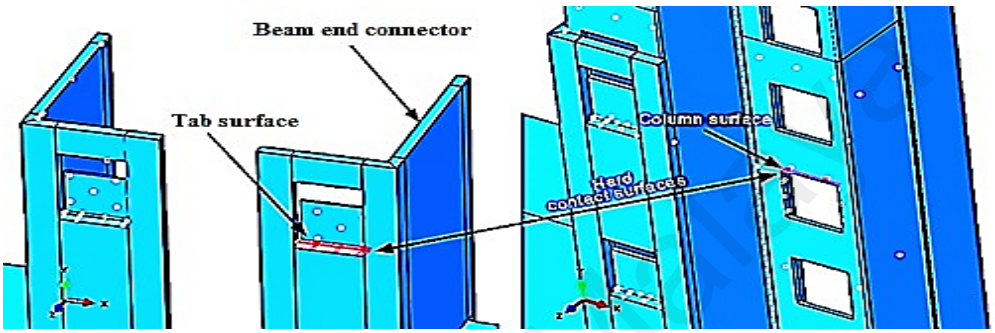

(b)

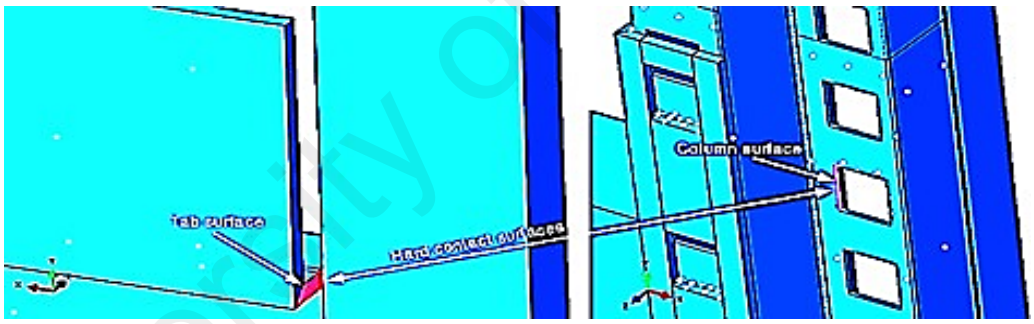

(c)

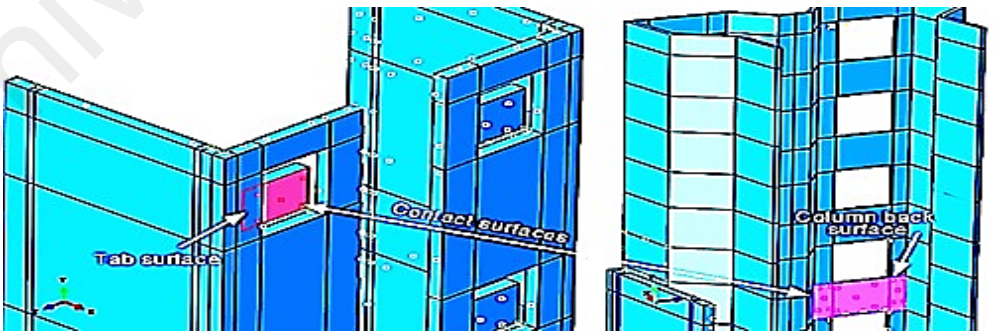

(d)

Figure 3.14: Surface to surface interaction among components

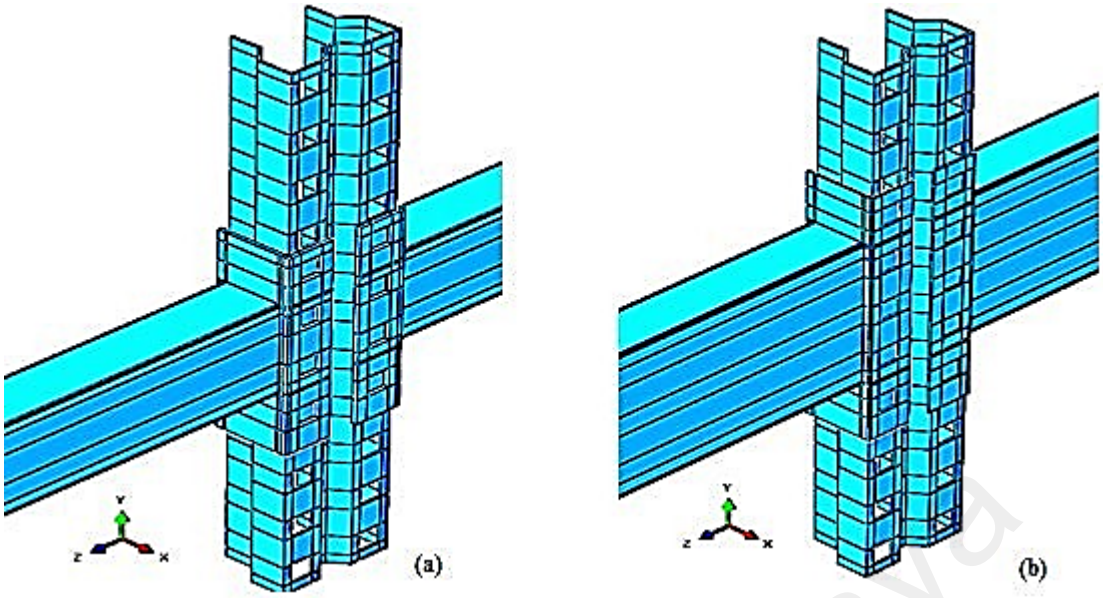

(a) Connection with four tab beam end connector

(b) Connection with five tab beam end connector

Figure 3.15: Complete geometry of the modeled connection

3.4.3 Loading and boundary conditions

In the experimental setup, the roller and lateral supports were used to restrain the vertical and lateral movements of beams, respectively. Further, in double-cantilever test setup, the column moves only up and down as a rigid body. Therefore, similar boundary conditions are applied to the end of beams and the column. During test setup, a displacement controlled loading was applied. Similar loading procedure is adopted for FE analysis. Displacement is applied in 10,000 steps and controlled by providing the logical limits of time (step size) from 0 to 1. This made the every sub-step equals to 1/10,000. The step size was further sub-divided and this undertaking resulted in a displacement rate of 70×10−4 mm/sub-step size. This small value is selected to avoid strain rate effects on deformation behavior. A displacement controlled loading is applied on the top surface of the column in the negative y axis.

3.4.4 Model Discretization

All components of the SPR assembly were discretized using the mapped discretization scheme to enhance computational accuracy. Mapped discretization was achieved by efficiently dividing individual components into a four-sided region, as shown in Figures 3.16 (a) and (b).

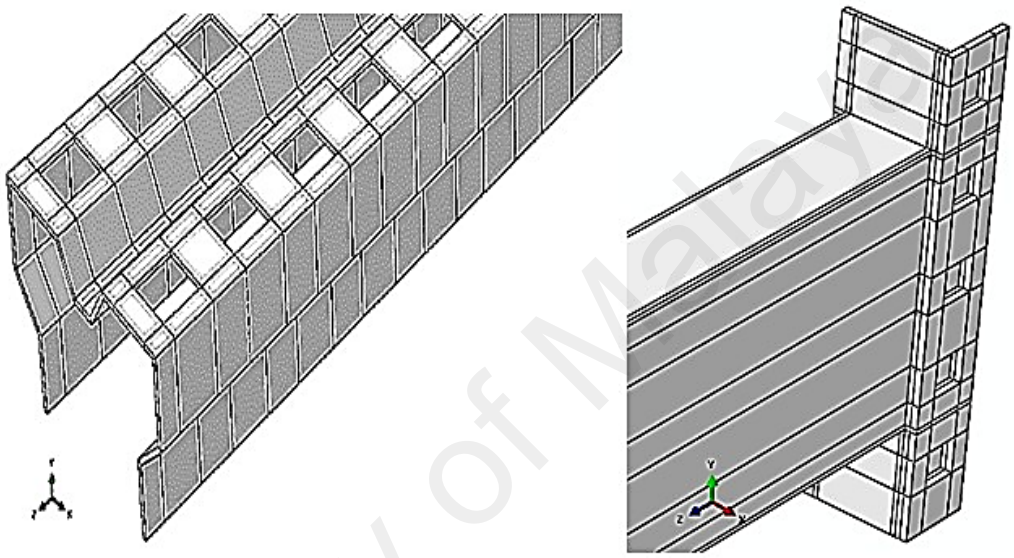

(a) Division of the column (b) Division of the beam end connector

Figure 3.16: Division of the connection components into a four-sided region

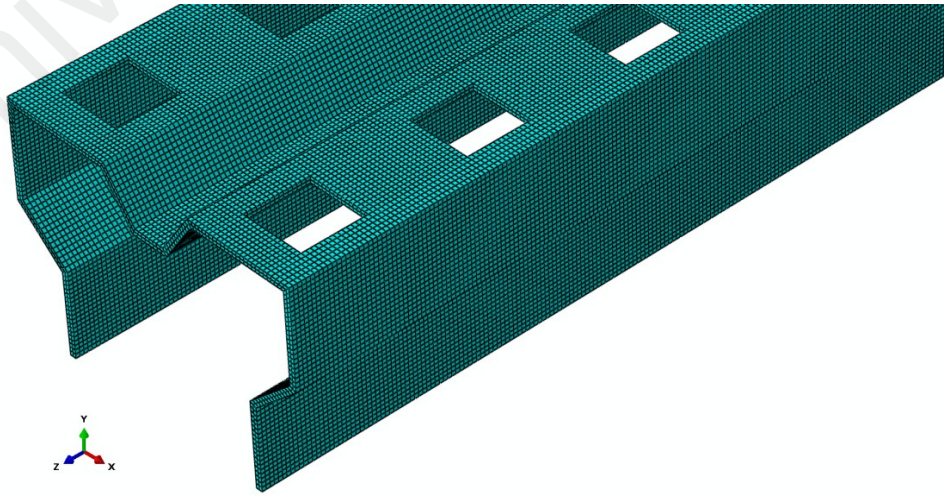

(a)

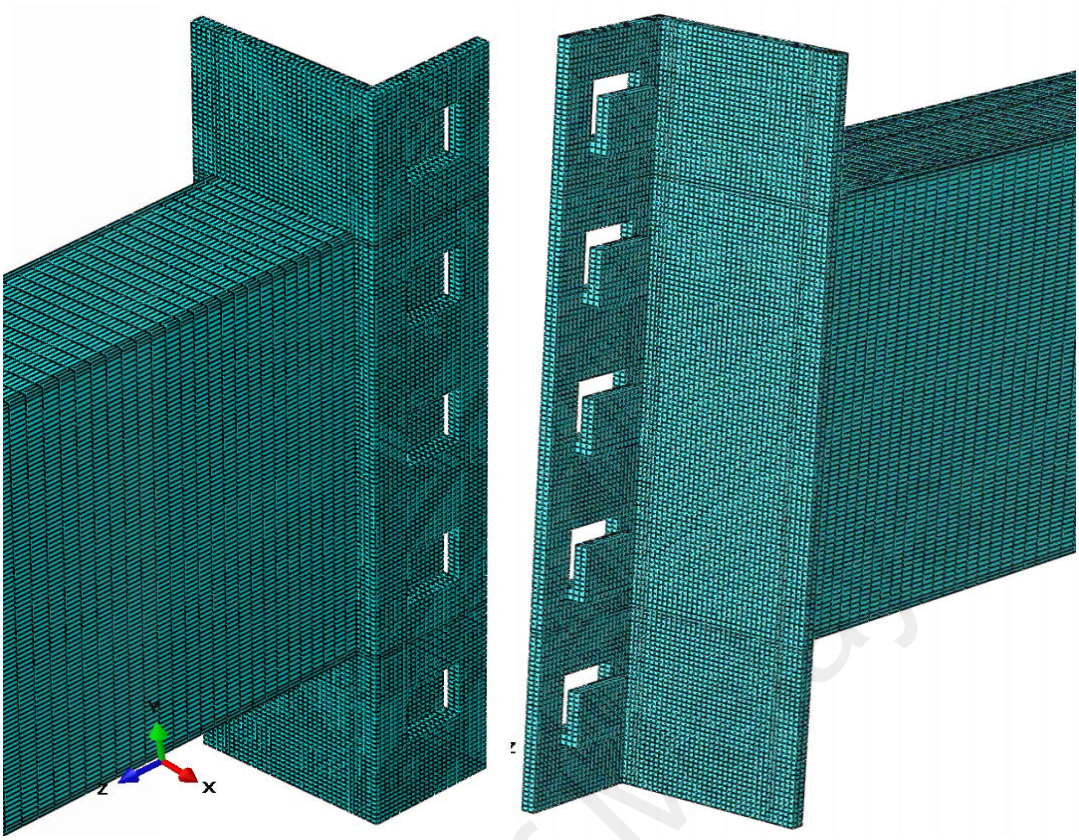

(b) (c)

(a) Column, (b) front view of the beam end connector, (c) back view of the beam end connector to show tabs

Figure 3.17: Discretized components of the SPR assembly

Convergence criterion is required to terminate the iterative loop once the solution is assumed sufficiently accurate. The convergence criterion is based on the variation of two-norm for equivalent stress, T. If the two-norm of the residuals is less than prescribed tolerance then the incremental solution is considered converged. Otherwise, the trial value must be updated iteratively until the residue satisfies the convergence criterion. The prescribed tolerance for solution convergence of equivalent stress is defined as 10e-5. Iterations are carried out unless and until the variation in the two-norm of the residuals for T_{n+1} satisfy the following conditions:

$$|T_{n+1} - T_n|_2 \, |T_n| < (10^{-5})$$

A time sub-stepping algorithm is used to control the time step size. The advantage of using time sub-stepping in an iterative procedure is to improve the convergence of a solution by reducing the time increment once needed. In addition, time sub-stepping algorithm must also be capable of increasing the time step size at a material point where convergence can easily be achieved in order to reduce the computational time. Thus, convergence issues in the simulations because of contact, geometric and material nonlinearities were successfully resolved by reducing time step size and increasing mesh density in critical regions. Figure 3.18 shows the meshing of the entire connection.

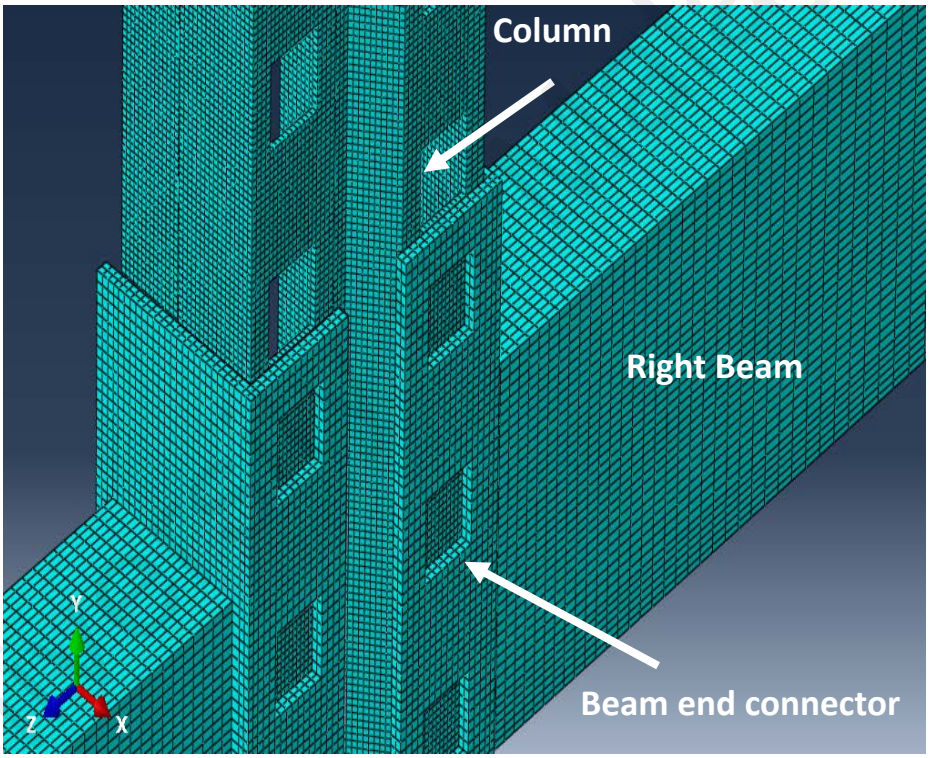

Figure 3.18: Meshing of connection

3.4.5 Parametric analysis

The FE model that was developed to validate the experimental testing was further extended for parametric analysis. The analyzed parameters were as follows: variation in column thickness, beam depth and number of tabs in the beam end connector, variation in the thickness of the beam end connector, variation in the welding position of beams to

the beam end connector, and variation in the spacing between the tabs to keep the depth of the connector similar to that during the experimental test. Different sizes of specimens were chosen for parametric analysis to observe the connection response for various connection types. The discussion on parametric analysis is presented in the next chapter of this study.

3.5 Finite Element (FE) modeling at elevated temperatures

The FE model developed for ambient temperature analysis was further modified in terms of material modeling to validate the results of experimental testing of SPR BCCs subjected to elevated temperature. To obtain the steel material characteristics a tensile coupon test was performed at ambient temperature by the manufacturer. Elevated-temperature characteristics are not tested directly by tensile coupon test. The stress–strain relationships at the respective temperatures are derived from the ambient temperature coupon test. Elastic regions of the relationships are defined by reduction factors for yield strength and elastic modulus recommended in the EC3 (2005b). This methodology has been previously applied by a number of studies to obtain the numerical behavior of CFS connections subjected to fire. Definitions of the relationships after yielding followed a methodology introduced by (Renner, 2005) where a plastic strain rate under steady-state heating condition for three loading rates was obtained. Material models were converted to true stress and logarithmic plastic strain curve for the different temperatures. These true stress and plastic true strain curves were specified in ABAQUS (Simulia, 2011). The bi-linear FE model developed for ambient temperature testing was modified to multi-linear FE model.

CHAPTER 4: RESULTS AND DISCUSSION

4.1 General

In this chapter, based on the materials and methodology described in Chapter Three, the behavior of cold-formed SPR BCCs at ambient and elevated temperatures was investigated based on experimental tests and extensive FE analysis.

This chapter presents the detailed results of investigations conducted to evaluate the behavior of SPR BCCs under ambient and elevated temperatures. A discussion on the achieved results is also presented. For easy understanding, this chapter is divided into two parts. The first part presents the results and discussion of experimental testing and parametric FE analysis on SPR BCCs tested at ambient temperature. The second part presents results and discussion of the experimental and numerical behavior of SPR BCCs tested at elevated temperatures. This part also compares the results of ambient testing of SPR BCCs with elevated temperature testing.

4.2 Experimental results at ambient temperature

The main focus of the experimental testing was to find out three major characteristics of SPR BCCs. These characteristics include: (i) major failure modes (ii) load-strain relationship (iii) M-θ behavior. An emphasis is also given to compare various stiffness design methods and the relatively appropriate method to calculate the stiffness of SPR BCCs is highlighted.

4.2.1 Failure modes

In this study, collectively, among all the experiments, three failure modes were observed: (i) tearing of the column material, (ii) yielding of the beam end connector, and (iii) fracture or yielding of the tabs. Not identical, but similar failure modes were observed by previous studies (Markazi et al., 1997; Prabha et al., 2010; Sleczka & Kozłowski, 2007).

In most of the specimens, immediately after applying the load, a minor initial looseness of the beam end connectors was noticed due to the absence of bolts or welds in the connection, which induced lateral deformation in the specimens. As the loading continued, the gap between the connector's surface and the column's flange in the compression zone was closed and the space between the tension zone of the beam end connector and the column's flange increased proportionally.

In the specimens 'A' and 'B' (relatively shallow beams and thin column), the pre-dominating failure mode was the failure of the tabs. Initially, the top tabs on both sides in compression zone (connected to the first slot of column making the connection) initially tried to tear the column web slots causing drop in the load. However, a complete rupture of the top tab on both sides occurred before they distort the column web. This failure mode was dissimilar to a few of other studies (Prabha et al., 2010; Sleczka & Kozłowski, 2007). This is because the failure of connection in this study is considered either at a drop of 1 kN or when the connection is severely damaged and unable to sustain further load. However, the connection was able to sustain the load even after the complete rupture of top tabs. As the loading continued, the bottom two tabs in tension zone slit the column slots and came out by tearing the column flange and a considerable drop in load was observed. At this stage, connection failure was considered. The bottom two tabs were not completely ruptured, however, a noticeable deformation was observed. At failure, the beam end connector experienced a noticeable twist. This failure phenomenon was different in the case of specimens 'C' and 'D'. No complete rupture of top tabs was observed. The tabs in the tension zone were not deformed similar to the tabs in the specimens with relatively shallow beams. This may be attributed to the increase in the size of both; the beams and the beam end connector. However, tearing of the column flange by bottom tabs on both sides was also observed in this case.

In the tests conducted on specimens ‘E’ and ‘F’, the failure initiated due to the failure of tabs in both compression and tension zones. Increased column thickness removed the complete rupture of top tabs, however, the deformation of bottom tabs and the beam end connector was similar to the specimens ‘A’ and ‘B’. The two tabs in the tension zone came out by tearing the column flange. When compared to the specimens ‘A’ and ‘B’, the noticeable difference was the increased failure load which can be attributed to the increased column thickness. The distortion in column flange was minor in the case of specimens ‘G’ and ‘H’. The last tabs in the tension side initially disengaged and finally came out of the column slots, completely. The deformation of the beam end connector was also not similar to the specimens with four tabs connector. No beam failure was observed in any specimen. It was noticed that an increase in the thickness of the column, made the tabs on the beam end connector experience larger deformation due to the in-plane moment.

There was a variety in the types of failure among all connections. Only the maximum deformations observed during experiments are illustrated here. Figures 4.1(a) and (b) show the front and back views of connection after failure, respectively. The deformation of columns A and B is illustrated in Figures 4.2 (a) and (b), respectively. The deformation of the beam the connector is shown in Figure 4.3. The deformation of tabs in the connectors ‘A’ and ‘B’ is illustrated in Figures 4.4 (a) and (b), respectively.

(a)

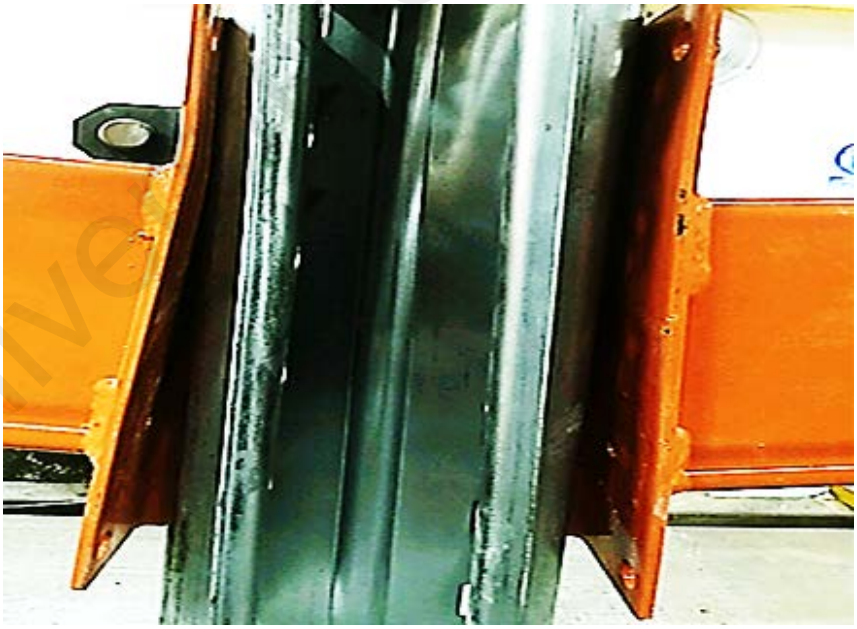

(b)

(a) Front view, (b) Back view

Figure 4.1: Connection failure of specimen A

(a)

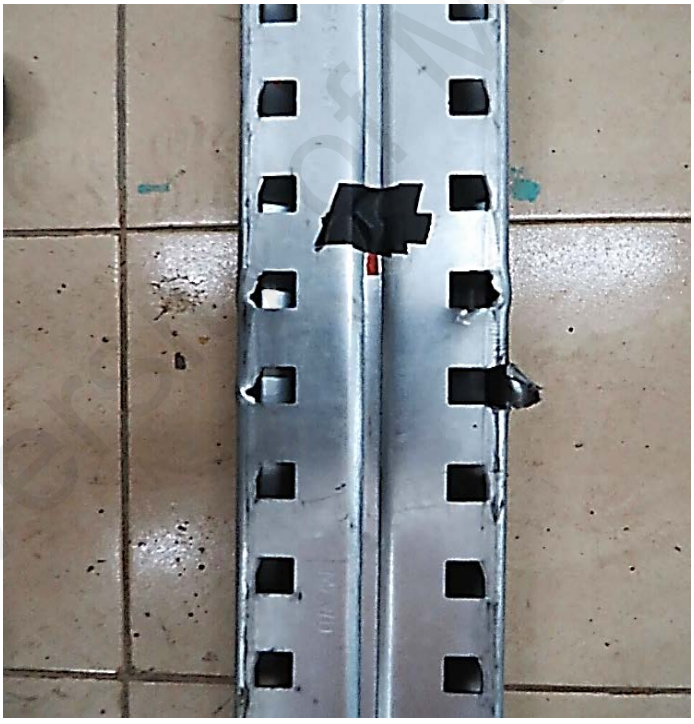

(b)

(a) Column A, (b) Column B

Figure 4.2: Deformation of columns

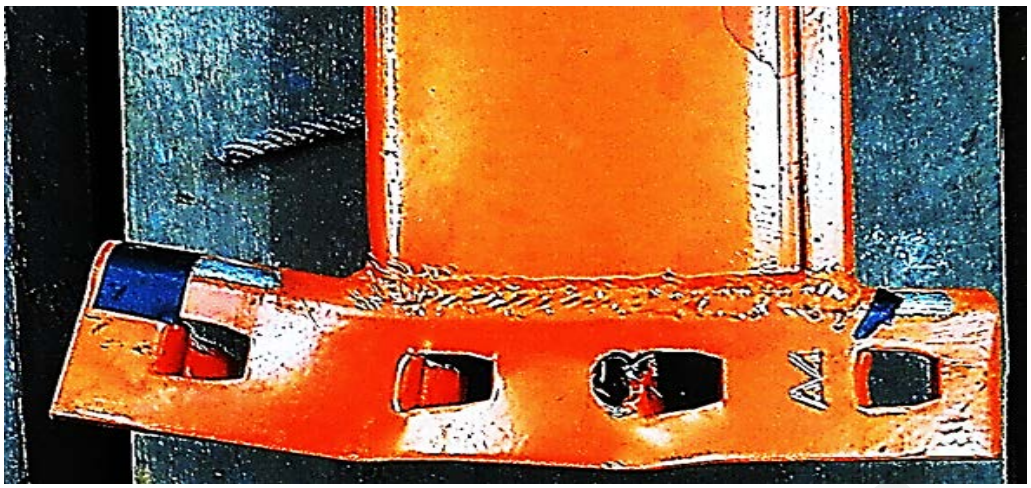

Figure 4.3: Deformation of the beam end connector

(a)

(b)

(a) Deformation of tabs in connector 'A', (b) Deformation of tabs in connector 'B'

Figure 4.4: Deformation of tabs

4.2.2 Load-Strain Relationship

The load-strain behavior based on the applied load to the column and the strain recorded by the strain gauges was measured. In most of the tests, the strain gauges pasted in column showed that at the complete connection failure, the column experienced higher stress near the tension zone of the beam end connector. However, an increase in the thickness of the column, made the tabs on the beam end connector to experience larger deformation due to the in-plane moment. The S3 and S4 locations showed that, in majority of the tests, the welded joint for the beam and beam end connector promoted an uneven force distribution in the relatively shallow beams. Whereas, the specimens with larger beam depths, had a comparatively uniform force distribution. The behavior of the specimens with same column thickness and number of tabs in the beam end connector but different beam depths showed that the ratio of the beam depth to the depth of beam end connector in the beams with smaller depth was larger, which means that both the top and bottom tabs are closer to the top flange and bottom flange of the beam, respectively. In reality, the forces in the tabs were not evenly transferred to the beam, but transferred primarily to the portions of the flange and the outside web closer to the tab. The effect of this eccentricity was found to have considerable influence on the specimens with a smaller ratio between the beam depths to connector depths.

For the tests involving beams B1 and B2, three strain gauges were fixed. One strain gauge (S1) is pasted in the column web near the top surface of the beam end connector to estimate the tensile strain. The other two strain gauges (S3 and S4) are pasted near the bottom slot of the beam end connector in the tension region. For beams B3 and B4, four strain gauges were installed. Three strain gauges were placed in the same position as for B1 and B2, whereas an additional strain gauge (S2) was pasted in the lower portion of column web near the bottom surface of the beam end connector. Readings from the loading apparatus and strain gauges were recorded onto the computer system and the

load-strain graphs were developed. These results were used to determine the failure load for the test. It was observed that with the increase in the sizes of the specimens, the failure load increased. As an example, Figure 4.5 demonstrates the failure load for the specimen 'A'. The average failure load for all the specimens is given in Table 4.1.

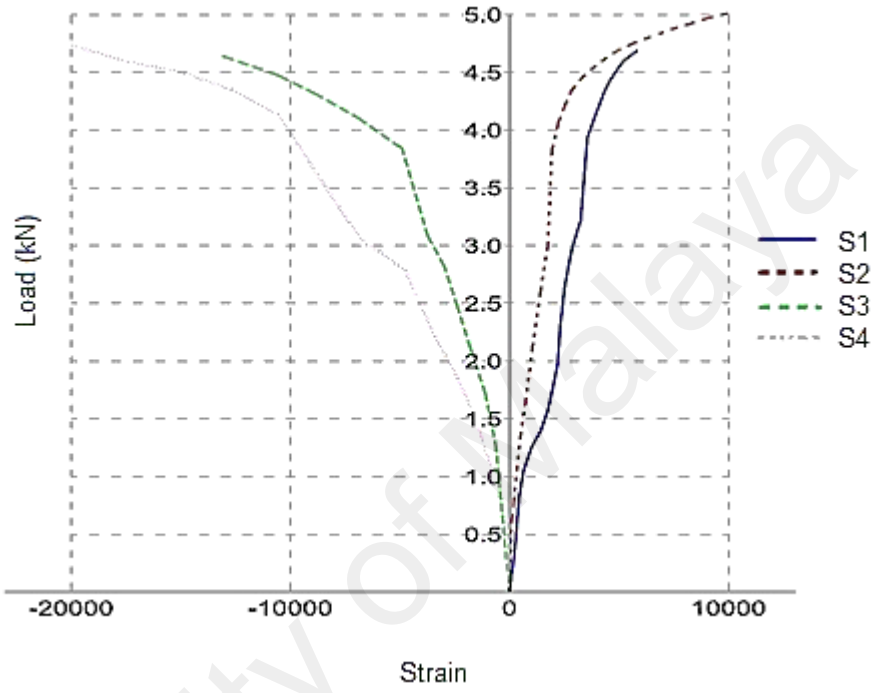

Figure 4.5: Load-strain graph for specimen 'A'

4.2.3 Moment-rotation (M-θ) relationship

The moment was calculated by the following equation:

$$\text{Moment } (M) = \frac{P}{2} \times \left\langle \frac{L}{2} - \frac{w}{2} \right\rangle \qquad (4.1)$$

L is the length between the supports, *w/2* is the half width of the column; as the bending moment is to be calculated in the beam end connector, the half width of the column is subtracted from *L/2*.

In total, eight sets of specimens were tested. The M-θ curves are based on the mean values of the strength and stiffness of both the left and right hand side connectors as

recommended in Annex A.2.4.3 of EN15512 (2009).The average M-θ curves for each set of specimens are presented in Figure 4.6. For a clarified representation, the curves are divided into Figures 4.6 (a) and (b) based on the difference in column thickness.

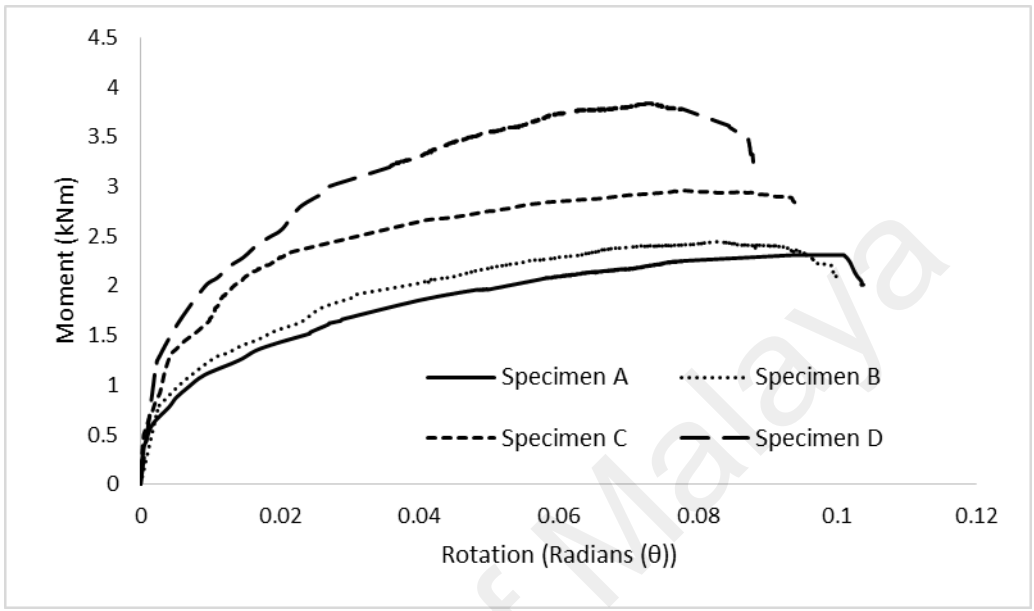

(a)

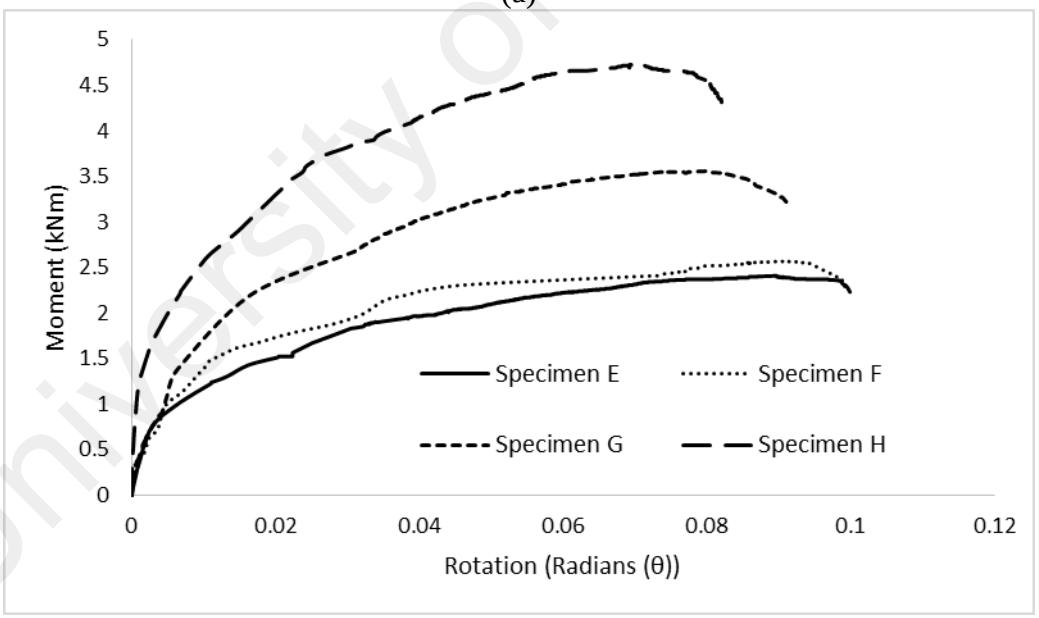

(b)

(a) M-θ graphs for specimens with column A,
(b) M-θ graphs for specimens with column B

Figure 4.6: Average M-θ graphs for each set of specimens

Contrary to an idealized graph of connections, these curves indicate non-linear behavior from the starting point. The major reasons for this overall non-linear behavior

is due to the relative slippage between the column and the beam end connector, yielding of the tabs, or some points on the end-connector or the column perforation walls due to localized stress concentration, and geometrical non-linearity. The initial imperfection of the specimens plays a major role in initiating the M-θ graphs with minor kinks (Prabha et al., 2010). The average results of experimental testing are given in Table 4.1.

Table 4.1: Average test results

Specimen	Failure Load (kN)	Ultimate Moment Capacity (kNm)	Rotation at failure (Radians)
A	4.89	2.31	0.10
B	5.19	2.45	0.10
B	6.27	2.96	0.094
D	8.05	3.80	0.088
E	5.17	2.44	0.10
F	5.44	2.57	0.10
G	7.54	3.56	0.091
H	10.04	4.74	0.082

4.2.4 Stiffness

For designing a rack structure, the performance of the beam end connector is essential and thus the calculation methods require an accurate estimate of the beam end connector's stiffness and strength. The criteria to calculate the stiffness of SPR BCCs is different in the current design codes. For the purpose of linear analysis, the RMI (2012) suggest that the stiffness should be calculated as the slope of a line passing through the origin and a point on the M-θ curve at 85% of the maximum moment. EN15512 (2009) suggests that the rotational stiffness of the connector should be obtained as the slope of a line through the origin which isolates equal areas between it and the experimental curve, below the design moment corrected for yield and thickness. In addition, a variety of methods are adopted to measure the stiffness of the beam end connector. This study compares three different methodologies available in the literature to calculate the connection stiffness (Godley, 1991). These methods are the initial stiffness, slope to half-ultimate moment and equal area methods that can be used to calculate the connection stiffness of any SPR BCC.

The stiffness for the tested specimens was evaluated using the initial stiffness method, slope to half-ultimate method and equal area method and is given in Table 4.2. The mean stiffness of the all four specimens in each set and the variance in the set data was calculated to predict the reliability of all three methods compared in this study. A small variance indicates that the data points tend to be very close to the mean (expected value) and hence to each other, while a high variance indicates that the data points are very spread out around the mean and from each other.

Table 4.2 shows that there is always an increase in the connection stiffness by increasing the thickness of column and number of tabs in the beam connectors for one particular type of column.

The analysis of the stiffness values obtained using the three methods shows that the initial stiffness method constantly gives an over-estimated value of stiffness. The slope to half-ultimate moment method showed high variance in the stiffness among the same size specimens in a given set of specimen. As compared to the initial stiffness and slope to half-ultimate moment methods; the equal area method has shown more consistent stiffness values among the specimens in each identified set. Moreover; based on the lowest variance in the set population as compared to the other two methods, the equal area method has provided relatively precise stiffness of the tested connections.

Table 4.2: Comparison of the Initial stiffness, Slope to half-ultimate moment and equal area methods

Set	Initial stiffness method			Slope to half-ultimate moment method			Equal Area method		
	Stiffness of four specimens (kNm/rad)	Mean Stiffness (kNm/rad)	Variance	Stiffness of four specimens (kNm/rad)	Mean Stiffness (kNm/rad)	Variance	Stiffness of four specimens (kNm/rad)	Mean Stiffness (kNm/rad)	Variance
A	79.02	72.81	67.48	55.65	60.78	210.12	31.7	32.3	0.27
	61.50			63.87			32.1		
	71.97			79.02			32.9		
	78.75			44.6			32.5		
B	82.75	83.92	8.73	70.80	70.71	13.68	35.3	36.2	3.08
	84.80			75.65			38.1		
	80.60			66.78			34.3		
	87.53			69.61			37.3		
C	90.86	89.13	48.03	79.80	77.21	22.90	57.82	54.29	5.57
	81.85			82.45			52.91		
	85.89			71.90			53.08		
	97.94			74.69			53.35		
D	101.32	110.7	167.13	89.12	89.90	38.44	79.40	79.21	13.48
	115.6			82.70			83.68		
	126.7			97.83			79.17		
	99.15			89.91			74.69		
E	85.50	73.60	63.85	42.60	36.67	33.41	31.23	35.9	11.97
	70.50			40.40			39.57		
	68.30			30.34			36.7		
	70.10			33.34			35.8		
F	76.14	85.10	38.86	88.60	77.21	59.50	39.2	42.8	7.79
	90.40			72.46			41.83		
	87.80			72.45			45.03		
	86.06			75.33			44.92		
G	78.60	82.85	536.91	88.60	79.97	51.69	70.72	69.54	27.60
	121.8			73.46			72.65		
	131.1			74.67			73.20		
	117.9			83.15			61.9		
H	147.9	143.66	430.16	114.6	120.47	142.14	101.4	97.86	68.70
	151.86			121.2			107.8		
	161.2			136.8			89.8		
	113.7			109.3			92.4		

4.2.5 Corrections in rotation and stiffness values

The routine calculation for stiffness usually ignores the deflection of the beam and the beam end connector, and a minimal error may exist. Abdel Jaber et al. (2006) developed theoretical equations to determine the effect of the error due to the flexural and shear deformations on the total measured experimental rotation and stiffness values. The details of the developed equations are given in Abdel Jaber et al. (2006). In this study, the transducers were placed in a vertical direction only; thus, the equation developed by Abdel Jaber et al. (2006) for vertical correction was solely applied. The values of distance between the column and inclinometers and between inclinometers and LVDTs; as well as the applied load value were used according to the experimental data used in this study. After the measured rotation was corrected, the values of mean rotational stiffness were

rectified. Table 4.3 presents the rotation and mean stiffness values corrected for the effects of flexural and shear deformations and the respective percentage differences for all tested specimens along with other test results.

Table 4.3: Corrected stiffness and rotation for all eight sets

Specimen	Experimental Stiffness (kNm/rad)	Flexural correction	% difference	Shear correction	% difference	Corrected stiffness
A	32.3	32.78	1.48	32.56	0.80	33.03
B	36.2	36.91	1.93	36.50	0.84	37.20
C	54.29	55.11	1.51	54.73	0.81	55.54
D	79.21	80.81	2.01	79.96	0.94	81.54
E	35.9	36.38	1.33	36.16	0.72	36.63
F	42.8	43.7	2.10	43.1	0.70	43.99
G	69.54	70.91	1.97	70.15	0.88	71.52
H	97.86	100.23	2.42	98.78	0.94	101.14

4.2.6 Effect of parameters on connection performance

The effect of various parameters on the strength and stiffness of the tested connections is presented in this section. The reference stiffness is the stiffness obtained by the equal area method.

4.2.6.1 Effect of varying beam depth with constant column thickness and tabs in the connector

The rate of increase in the moment capacity of the connection by varying the depth of beams with same number of tabs in the beam end connectors was not much different for both columns, ‘A’ and ‘B’. In the case of connector A, for a constant column thickness of 2.0 mm, changing the beam depth from 92 mm showed a 6% increase in moment capacity for a depth of 110 mm, as shown in Figure 4.7. However, the stiffness was increased by 11%. The rate of percentage increase in the moment capacity and stiffness was almost similar for column B. Changing the beam depth from 92 mm to 110 mm for a constant column thickness of 2.6 mm, resulted in an increase in the moment capacity and stiffness of the connection by 6% and 16%, respectively.

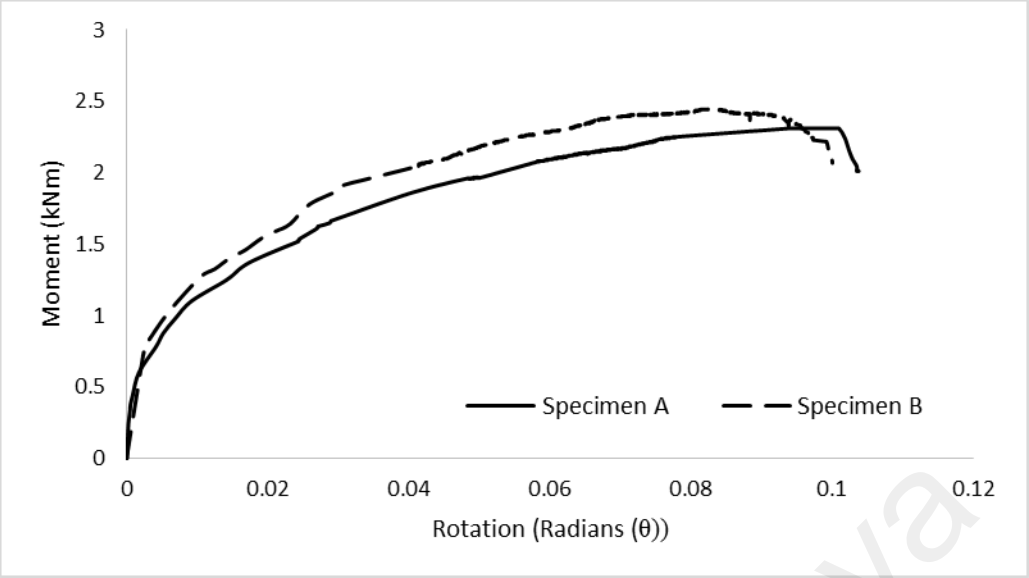

Figure 4.7: Effect of varying beam depth with constant column thickness and number of tabs in the beam end connector

In the case of connector B, by keeping the thickness of the column constant at 2.0 mm, the effect of varying beam depth was considerable. The increased beam depth enabled the connection to sustain higher moments. By keeping the column thickness constant at 2.0 mm, increasing beam depth from 125 mm to 150 mm increased the moment capacity and stiffness of the connection by 22% and 31%, respectively. Changing the beam depth from 125 mm to 150 mm for a constant column thickness of 2.6 mm, resulted in the increase in the moment capacity and stiffness of the connection by 24% and 29%, respectively. This reveals that a higher increase in beam depth, increased the performance of the connection at a greater ratio. A progressive increase in the beam depth caused significant change in the moment capacity and stiffness.

4.2.6.2 Effect of column thickness on connection behavior

The resultant M-θ curve of connector 'A' with beam depth 92 mm and varying column thickness is presented in Figure 4.8. For B1, increasing the column thickness from 2.0 mm to 2.6 mm resulted in a marginal increase of 6% in the moment capacity of the connection. The stiffness was increased by 10%. For B2, increasing the column thickness from 2.0 mm to 2.6 mm resulted in an increase of 6% and 15% in the moment capacity

and stiffness, respectively, indicating the influence of greater column thickness on connection performance.

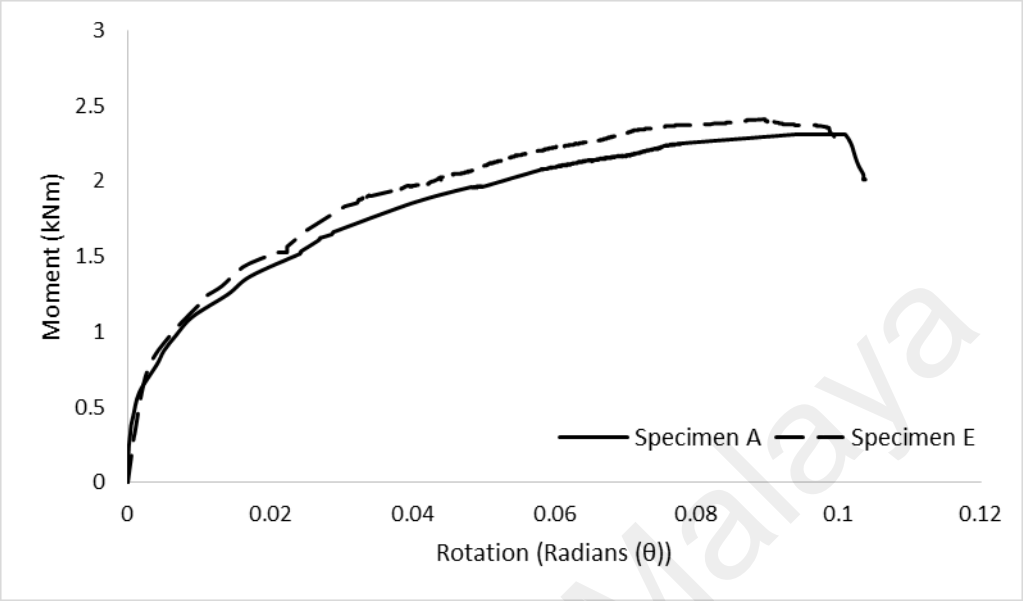

Figure 4.8: Effect of varying column thickness with constant beam depth and number of tabs in the beam end connector

4.2.6.3 Combined effect of variation in the geometry of beam end connector and beam depth

During experimental investigations, the effect of number of tabs in the beam end connector was associated with the difference in beam depths. Therefore, the effect of connector geometry could be identified for the columns of same thickness only. For column 'A', changing the number of tabs from four to five (for increased beam depth from 92 mm to 125 mm) resulted in a 22% increase in the moment capacity, as shown in Figure 4.9. The stiffness of the connection was increased by 40%. For column 'B', increasing the number of tabs from four to five (for increased beam depth from 92 mm to 125 mm) increased the moment capacity and stiffness of the connection by 31% and 48%, respectively. This demonstrated that increasing the number of connector tabs sufficiently enhanced the strength and stiffness of the connection.

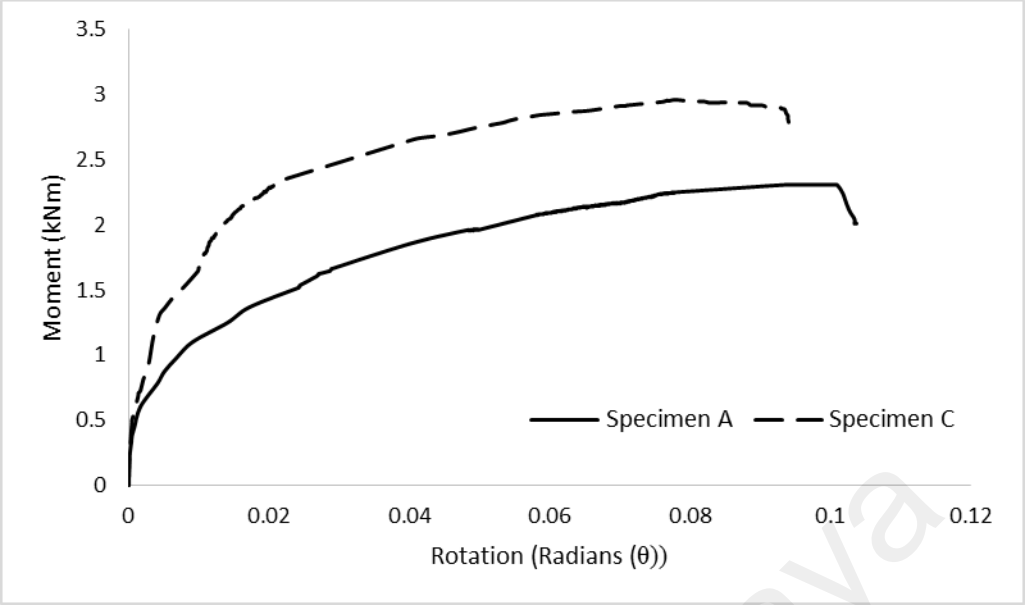

Figure 4.9: Effect of the geometry of the beam end connector

4.2.7 Ductility

The ductility of a connection plays an important role in moment redistribution and is considered as a key parameter when the deformations are concentrated in the connection elements, as in the case of the BCCs tested in this study. The American Institute of Steel Construction (AISC, 2010) recommends that if the value of connection rotation at the maximum moment is ≥ 0.02 radians, the connection is considered as ductile, otherwise it should be considered as brittle. In the case of semi-rigid connections, the rotational capacity may effectively help in designing the connected beam. If the rotational capacity of a semi-rigid connection is sufficient to develop an effective hinge at mid-span of the connected beam, the beam can be designed plastically.

In this study, at connection failure, the deformation in the connector 'B' was considerably lesser than that observed for connector 'A'. Table 4.1 shows changing the number of tabs from four to five along with a progressive increase in beam depth, showed a maximum difference of 12% in the rotational capacity of the connection at failure moment. By keeping the number of tabs and column thickness constant and considering the effect of beam depth on the connection performance, maximum 10% difference was

observed in the rotational capacity at ultimate moment in the case of specimens 'G' and 'H'. An increase in column thickness did not show any considerable change on the maximum rotation of the connection. Collectively, all the connections tested in this study showed ductile behavior.

4.3 FE analysis results at ambient temperature

FE simulations were performed to evaluate the structural behavior of SPR BCCs. A 3D nonlinear FE model of the column, beam, and beam end connector assembly was developed using the commercial FE software ABAQUS (Simulia, 2011) for both four- and five-tab connectors.

4.3.1 Failure modes

The FE model exhibited close agreement with the experimental results. Similar to the experimental investigations, deformation of almost all tabs was observed in the specimens with relatively shallow beams and thin columns, however, for deeper beams the tabs in the tension zone experienced higher stress and attempted to tear down the column slots. Moreover, the deformation of the beam end connector observed in the experimental and FE results were similar. The FE model also captured the distortion of the column web and the phenomenon of tabs attempting to exit column slots. However, the distortion of column slots captured in the FE model was less intense than that in the experimental investigation. A comparison of failures in both investigations, namely, experimental and FE analysis, is presented in Figures 4.10 (a) and (b). In order to show the closer response of those tabs which were engaged with the column perforations, a front view of connection is presented in Figure 4.10 (c). The von Mises stress distribution and the failure of the beam end connector A in the FE model is shown in Figure 4.10 (b) and (c) to compare them with the experimental results. The beam on one side of the column is eliminated to show the response of column holes.

(a)

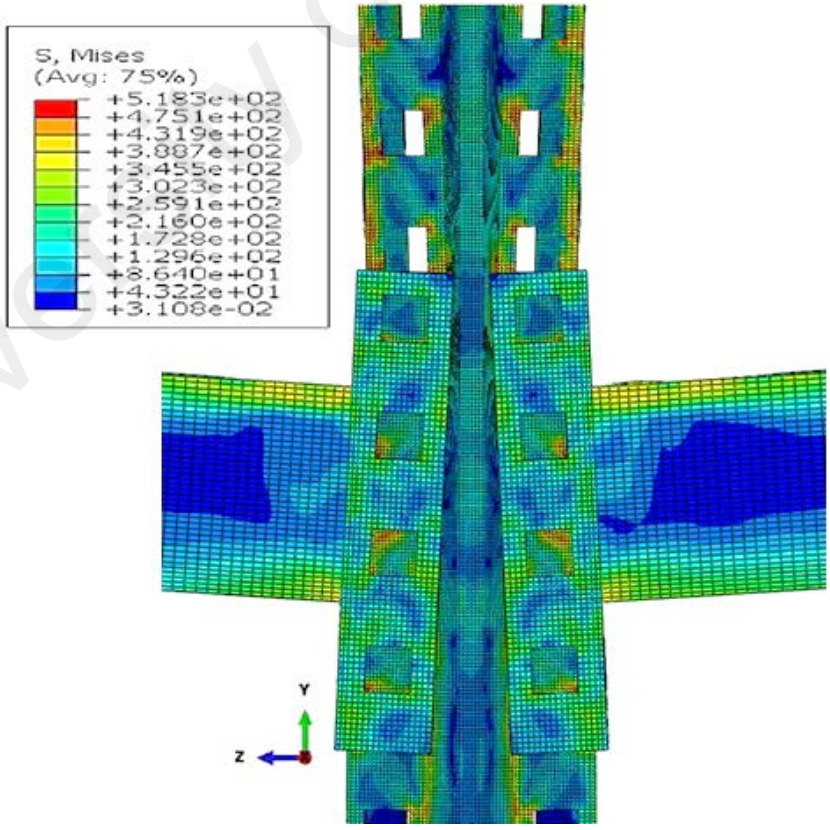

(b)

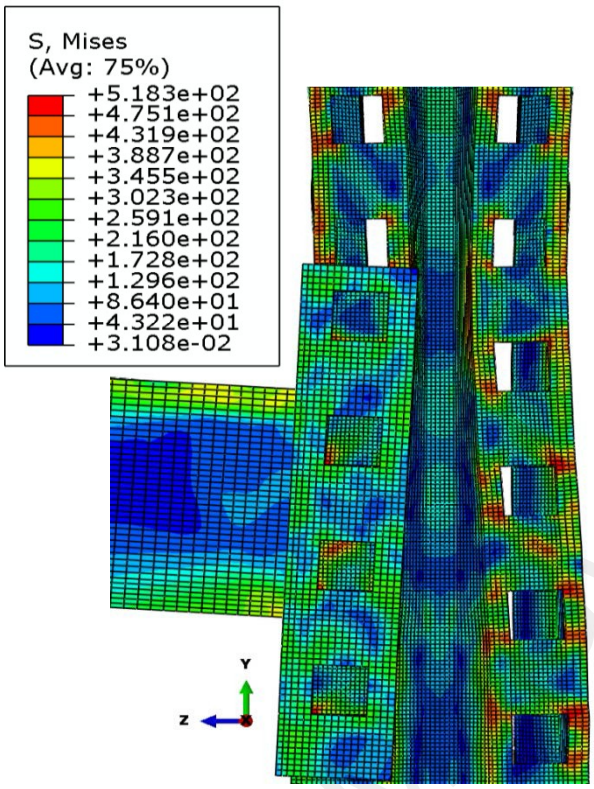

(c)

(a) Experimental failure, (b) FE analysis failure, (c) response of tabs and column holes in a front view

Figure 4.10: Comparison of the connection failure

4.3.1.1 Failure of the beam end connector

Similar to the experimental investigations, the FE analysis indicated that the beam end connector experienced a noticeable deformation in the tension zone. The gradually increased loading increased the gap between the column and the tension zone of the beam end connector at connection failure. Figure 4.11 (a) and (b) show the failure of the beam end connector 'A' during experimental and FE investigations, respectively.

(a)

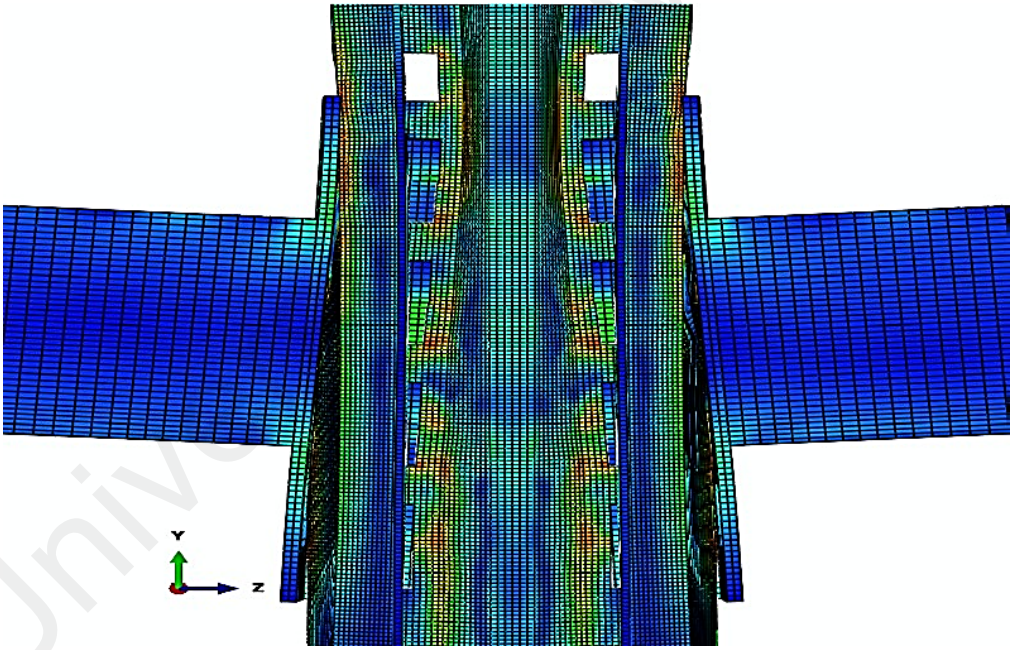

(b)

(a) Experimental failure, (b) FE analysis failure

Figure 4.11: Comparison of failure of the beam end connector 'A'

4.3.1.2 Failure of Tabs

The FE model was unable to predict the complete rupture of top tabs for both specimens A and B, however a noticeable deformation of top tabs was observed as shown

in Figure 4.12. The distortion levels at the bottom tabs were almost similar to those observed in experimental testing. The only difference between the two types of specimens (A and B) was the failure load. An increased beam depth (110 mm) caused the specimen to sustain a marginally large loading magnitude. The FE models prepared for rest of the specimens predicted the same level of deformation of tabs as observed in the experimental investigations.

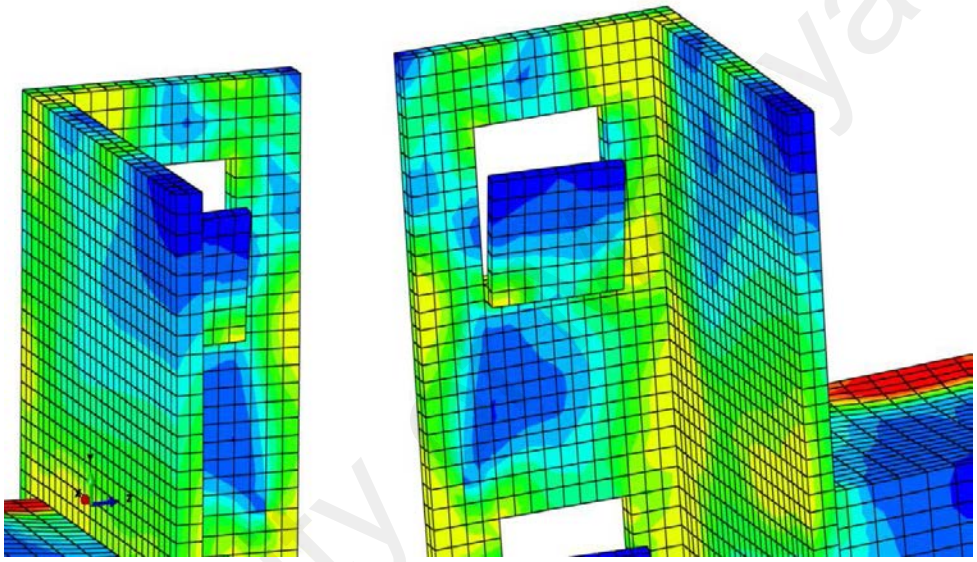

Figure 4.12: Failure of tabs

4.3.1.3 Failure of column

The third type of failure observed in the experimental investigations was the tearing of column flange and cut in the holes. According to von Mises stress distribution, the column was under high stress in the tension zone of the connection. Consequently, the portion of the column near the tension zone of the beam end connector experienced higher stress than that in the compression zone. The tabs were reversely inserted into the column perforations. Thus, a large stress concentration was observed at the portion of the column where the tab came in contact with the column slot in the tension zone, as opposed to other parts of the column web.

During experimental investigations, for almost all specimens, the tabs in tension zone slit the column slots and clearly came out by tearing the column. The FE analysis predicted the tearing of column slots, however the intensity of tearing was less than that observed in the experimental testing. Maximum column deformation at the connection failure occurred in the tension zone. A comparison of column failures during experimental and FE investigations and stress distribution observed in FE analysis is provided in Figures 4.13 (a) and (b).

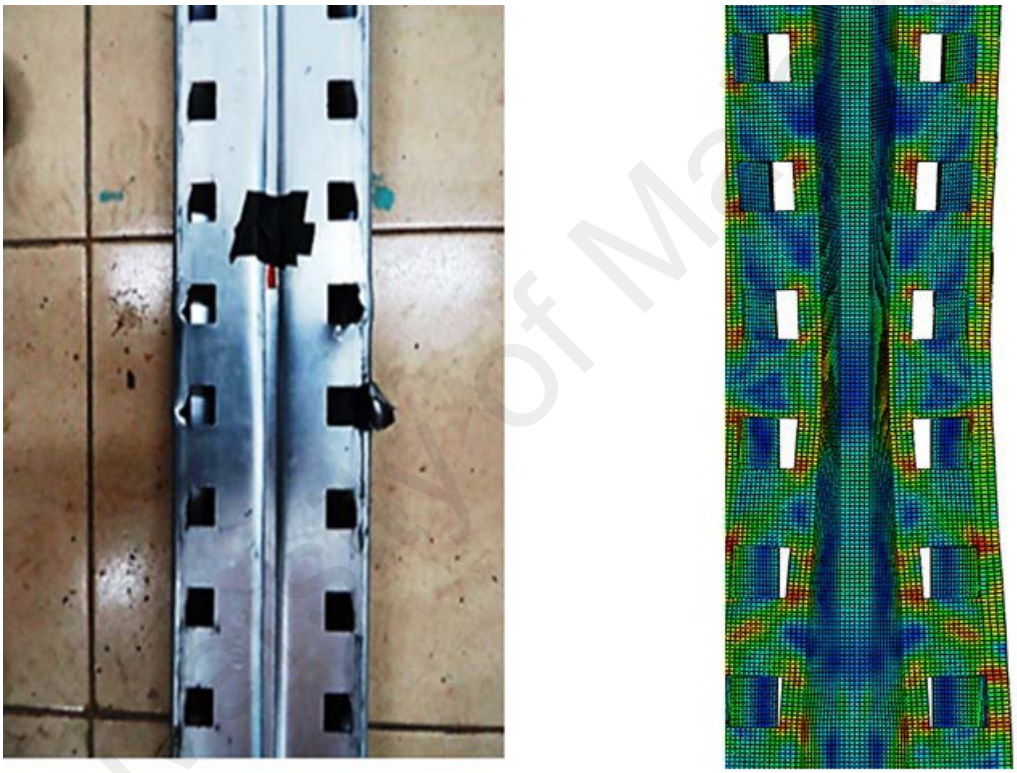

(a) (b)

(a) Experimental failure, (b) FE failure

Figure 4.13: Comparison of the maximum deformation of the column at the connection failure

4.3.2 Moment-Rotation (M-θ) behavior and stiffness

The FE model predicted the experimental behavior to a large extent. The stiffness of the specimens matched well with that in the experimental test result. However, the ultimate moment capacity of the connection obtained through the FE model for specimen A was slightly higher than that obtained through the experiments. This is because the

rupture of top tabs was not captured by the FE model. Further, a slight difference between the column slot failures in the two types of investigations increased the moment capacity of the connection predicted by the FE model. Load is gradually applied on top of the column section in steps, and the corresponding rotations of the connector were monitored using four nodes as shown in Figure 4.14.

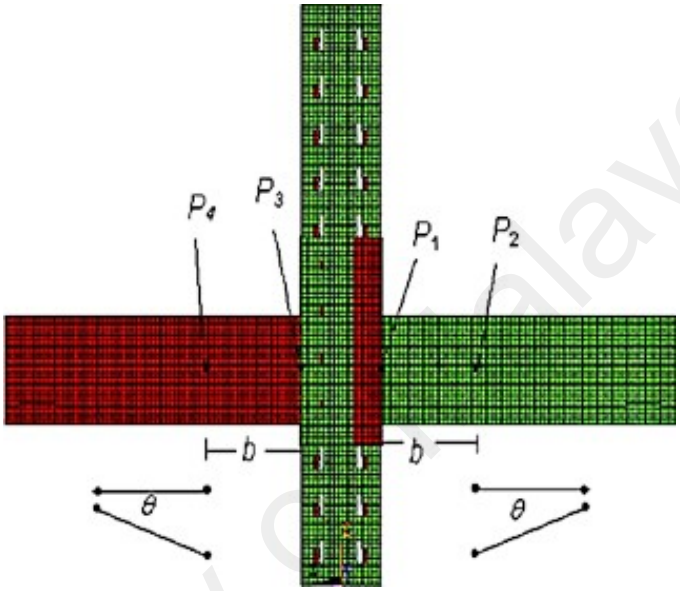

Figure 4.14: Four nodes monitored to determine the rotation

A comparison of the M–θ graphs plotted for the experimental and FEM investigations is provided in Figures 4.15 (a-d). Four specimens with varying column thickness values, beam depths, and numbers of tabs in the beam end connector were compared to illustrate the agreement between the experimental and FE analysis results. The major difference between the two types of curves is the increased moment capacity in ultimate stage of most of the FE curves which is because the less intensity of column slots failure was predicted by FE model. The FE curve of specimen A showed a different behavior from its initial stages as compared to the experimental curve because the FE model could not captured the complete rupture of tabs at connection failure. Table 4.4 shows comparison between the moment capacity and stiffness obtained from the experimental and FE investigations.

Table 4.4: Comparison of the moment capacity and stiffness of the tested connection in the experimental and FE investigations

Specimen ID	Ultimate Moment Capacity (kNm)		Stiffness (kNm/rad)	
	Experimental	FEA	Experimental (corrected)	FEA
A	2.31	2.49	33.03	37.93
D	3.80	3.93	51.54	82.89
E	2.44	2.63	36.63	44.02
H	4.74	5.02	101.14	101.4

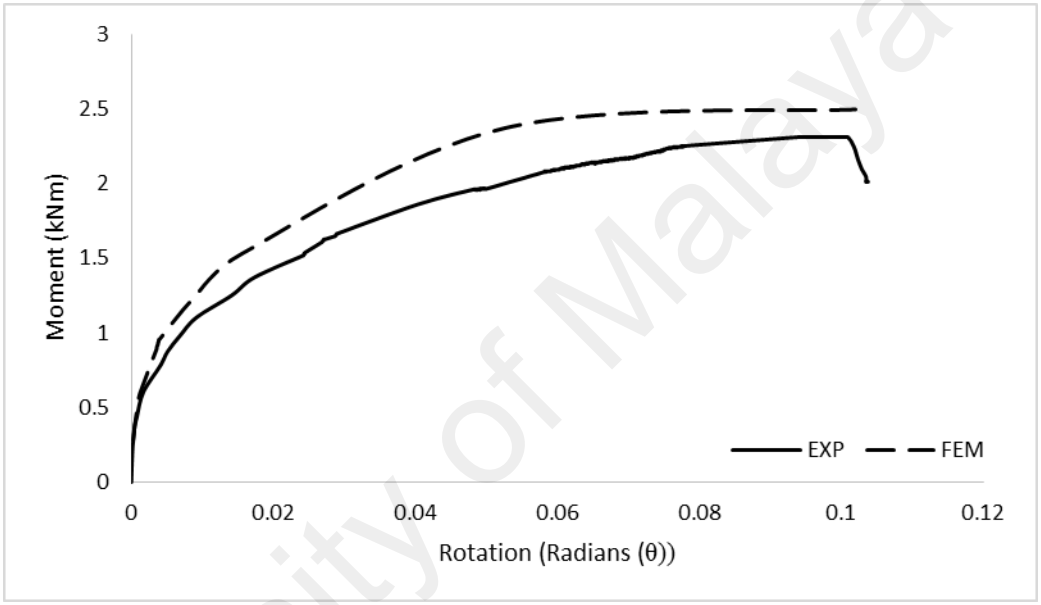

(a)

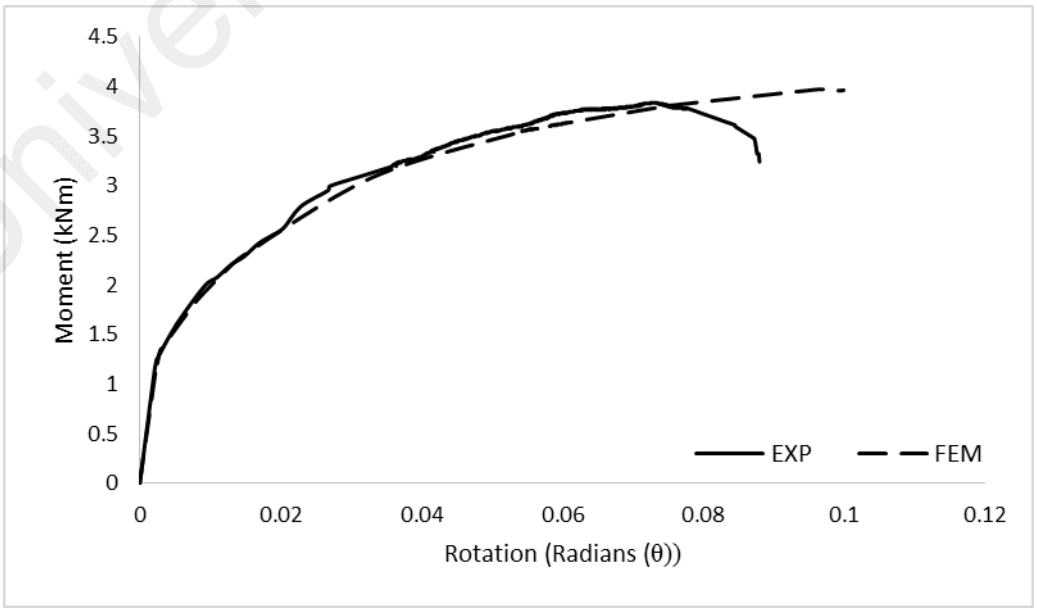

(b)

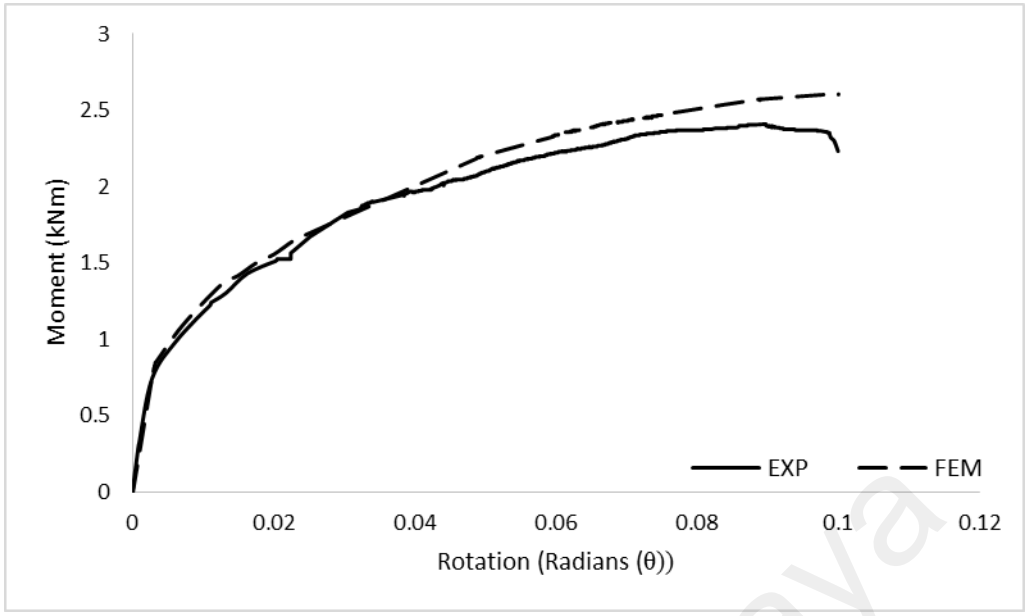

(c)

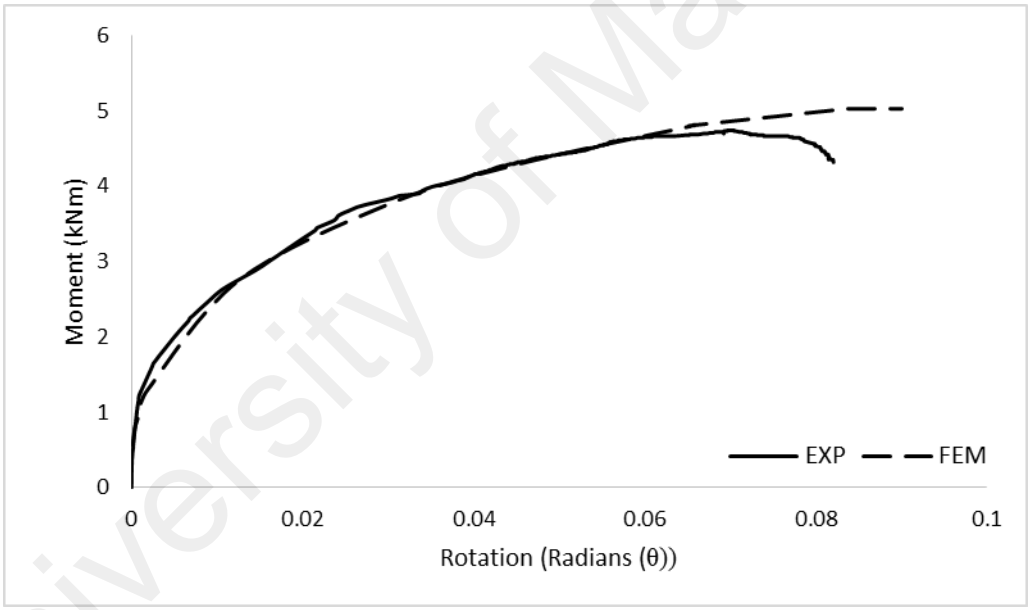

(d)

(a) specimen A, (b) specimen D, (c) specimen E, (d) specimen H

Figure 4.15: Comparison of the M-θ graphs of the experimental and FE investigations

4.4 Parametric analysis

The FE model that was developed to validate the experimental testing was further extended for parametric analysis. The analyzed parameters are as follows: variation in column thickness, beam depth and number of tabs in the beam end connector, variation

in the thickness of the beam end connector, variation in the welding position of beams to the beam end connector, and variation in the spacing between the tabs to keep the depth of the connector similar to that during the experimental test. Different sizes of specimens were chosen for parametric analysis to observe the connection response for various connection types.

4.4.1 Effect of varying column thickness, beam depth and number of tabs in the beam end connector

Figure 4.16 and Table 4.4 shows the effect of variations in column thickness, beam depth, and number of tabs in the connector, as observed through FEM. The FEM results indicated that increasing the sizes of the members resulted in increased strength and stiffness of the connection.

According to the FEM results, by keeping the depth of beam and number of tabs constant, comparison of specimens A and E showed that by increasing the column thickness from 2.0 mm to 2.6 mm, the moment capacity and stiffness of the connection increased by 6% and 14%, respectively. By keeping the column thickness constant, comparison of specimens A and D showed that a combined effect of increasing beam depth (from 92 mm to 150 mm) and the number of tabs (from four to five) showed an increase of 37% and 54% in the moment capacity and stiffness of the connection, respectively.

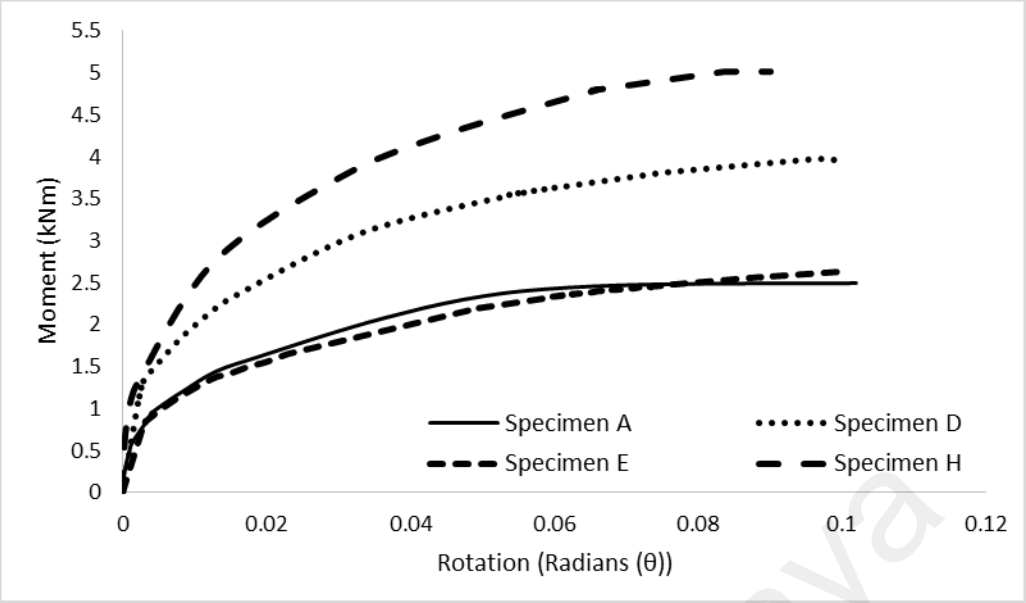

Figure 4.16: Effect of variation in parameters on the M–θ behavior (FE analysis)

4.4.2 Effect of variation in the thickness of the beam end connector

The thickness of the beam end connector was 4 mm for all the specimens tested in the experiment. The FE analysis was performed by varying the thickness of the beam end connector by ±50%, that is, 2 mm- and 6 mm-thick beam end connectors were used. The geometries of the remaining connection components were the same as those for the experimental testing of specimen H. The letter IDs 'I' and 'J' were assigned to the specimens with 2 mm- and 6 mm- thick beam end connectors, respectively.

Reducing beam end connector thickness from 4 mm to 2 mm (specimen I) significantly affected the failure mode of the beam end connector. The FE analysis showed that the failure of the beam end connector was the major failure mode along with an increased level of deformation of the last two tabs on either side in the tension zone of the beam end connector. The fourth tab from the top was more deformed as compared to the deformation observed during experimental testing of specimen H. Figure 4.17 (a) shows the failure mode of the 2 mm-thick beam end connector.

Figure 4.17 (b) shows the response of the specimen ‘J’ after the FE analysis. Increasing the thickness of the beam end connector from 4 mm to 6 mm improved the connection’s performance and significantly minimized the deformation of the beam end connector and tabs while keeping all other dimensions the same as those of the experimentally tested specimen H. The stress was higher in the top two tabs in the compression zone and bottom tabs in the tension zone. The failure mode was the deformation of bottom tabs. However, the deformation of tabs captured by FE analysis was less than that observed during experimental testing of specimen H.

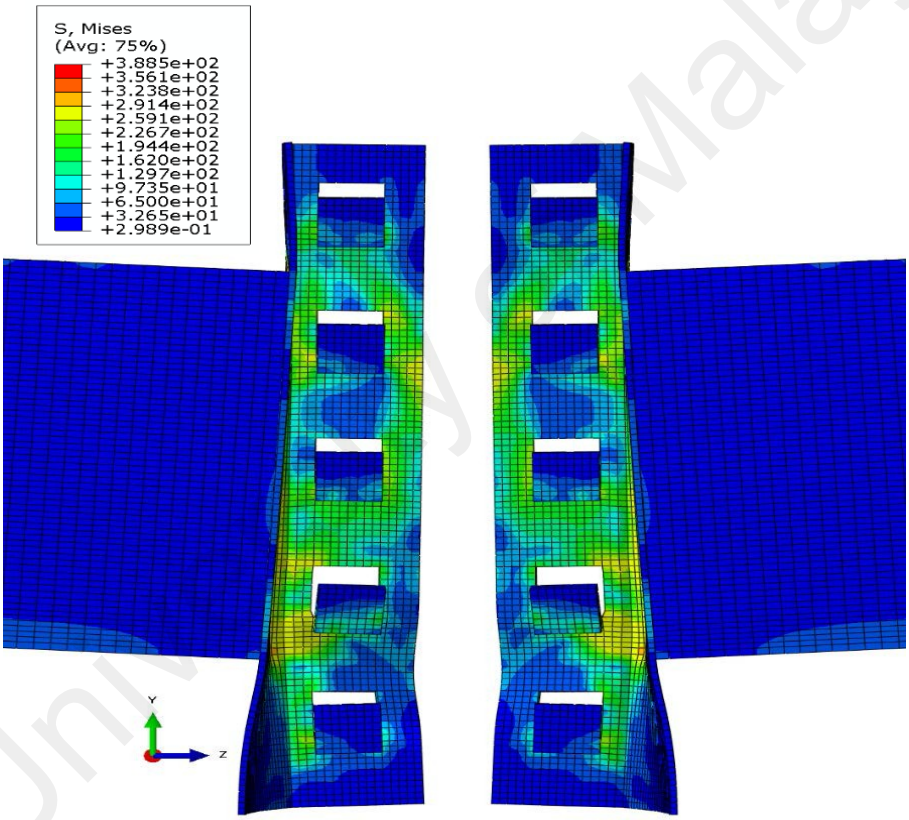

(a)

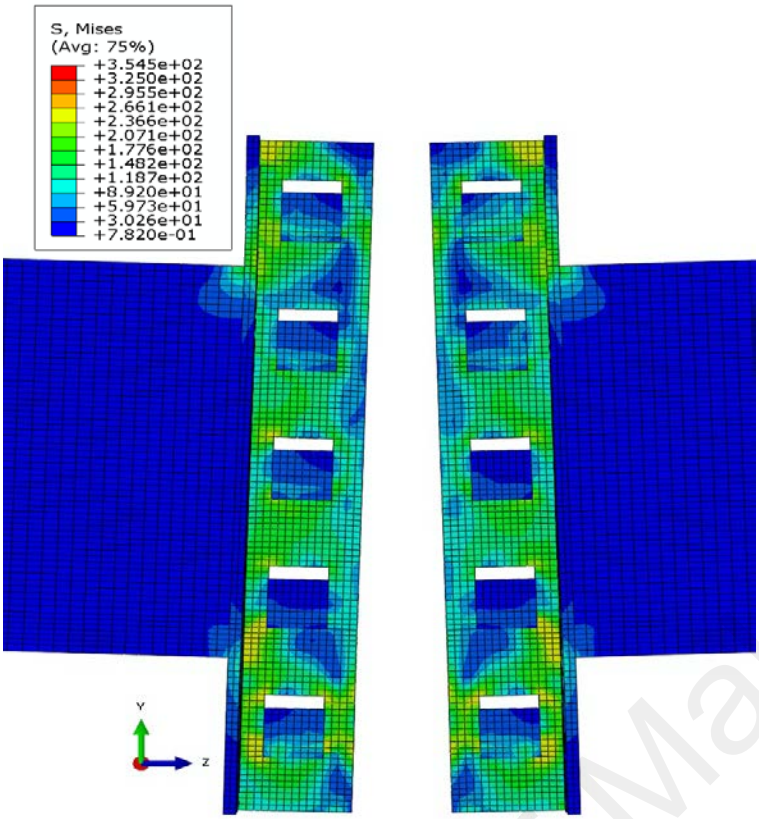

(b)

(a) Specimen I, (b) Specimen J

Figure 4.17: Failure of the beam end connectors

Figure 4.18 shows a comparison of the M–θ graphs for the specimens H, I and J. The influence of the dimensional changes of the beam end connector highly influenced the stiffness of the connection. Taking 4 mm thickness of the beam end connector as a base, a 50% decrease in the thickness of the beam end connector decreased the moment capacity and stiffness of the connection by 18% and 42%, respectively. An increase in the thickness of the beam end connector by 50% increased the moment capacity and stiffness of the connection by 14% and 49%, respectively.

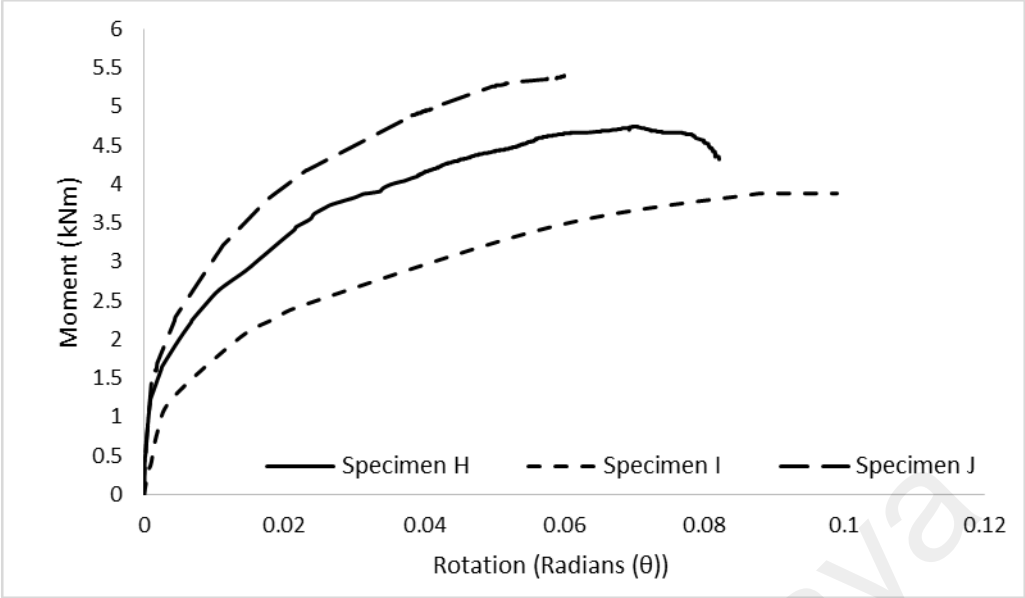

Figure 4.18: M-θ graphs of the variation in the thickness of the beam end connector

4.4.3 Effect of welding position of beam to the beam end connector

Simulating the experimental investigations involving specimen E, where the position of tabs was reversed and the distance of top flange of beam was 40 mm from the top of the beam end connector, parametric analysis was performed on specimen E in order to assess the effect of welding position of beam to the beam end connector.

For parametric analysis, several models were developed and the top flange of beam was welded at different distances from the top of the beam end connector. Keeping the rest of the dimensions of the connection similar to specimen E, the welding distance of top flange of beam from the top of the beam end connector was changed from 40 mm to 10 mm (specimen K), 30 mm (specimen L), and 70 mm (specimen M). In specimens K and L, the beam was up-welded whereas in specimen M, the beam was down-welded. According to Markazi et al., (1997), a beam is considered up-welded when the horizontal axis of symmetry of the beam is off set upwards from the beam end connector's mid height. A beam is considered down-welded when the horizontal axis of symmetry of the

beam is off set from the beam end connector's mid-height, either below or just above it (Markazi et al., 1997).

Welding the beam 10 mm below the top surface of the beam end connector led to a premature failure of the connection, as shown in Figure 4.19 (a). The tabs in compression zone were highly distorted at relatively lower value of failure load. The bottom two tabs were less distorted than the tabs in the compression zone. The stress distribution in the top tabs was highly non-linear and considerably critical at the weld between the beam and the beam end connector near the second tab from the top. The distortion in the beam end connector was significant in the compression zone. In addition, a highly non-uniform stress distribution near the second tab from top to the bottom flange of the beam was observed which influenced the behavior of weld between the beam and the beam end connector. The governing failure mode in this type of specimen was a pre-mature failure of the tabs and the beam end connector in the compression zone. FE analysis of specimen L showed a slight variation in failure mode compared with that of the specimens E and K. The failure of connection occurred due to significant distortion of second tabs from the top. The deformation of the beam end connector in the tension zone was also noticeably higher than that observed for the specimens E and K, as shown in Figure 4.19 (b). Specimen M showed a relatively even distribution of load between the tabs in tension and compression zones; hence the performance of the tabs was better. Further, the beam end connector was remained in contact with the face of the column at the connection failure and deformation was minimized as compared to the reference specimen E. The major failure mode was the deformation of tabs. The failure of specimen M is shown in in Figure 4.19 (c). The ultimate moment capacity and the stiffness of the specimens with different welding position of beam to the beam end connector obtained through the M-θ curves are tabulated in Table 4.5.

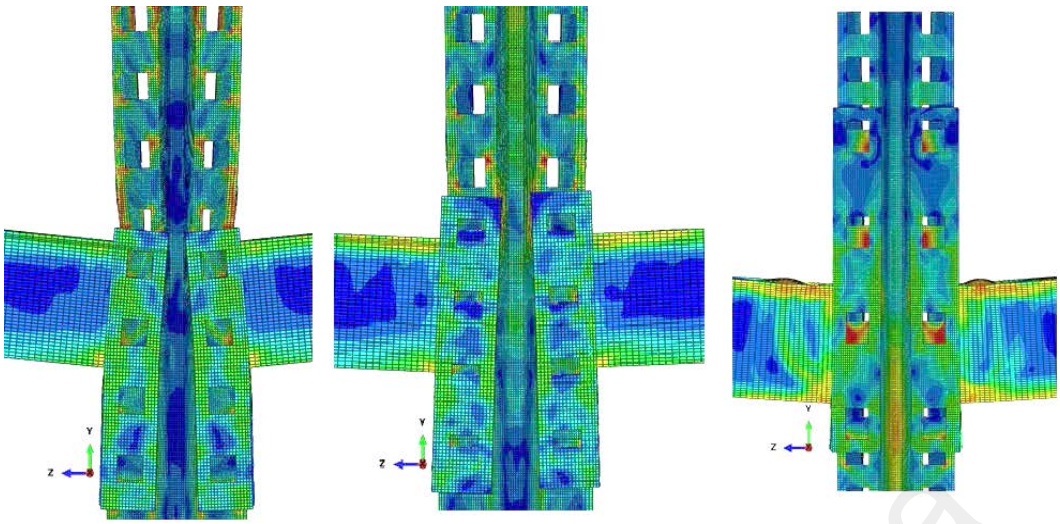

(a) Specimen K, (b) Specimen L, (c) Specimen M

Figure 4.19: Failure modes of the specimens with various welding positions of beam to the beam end connector

Table 4.5: Strength and stiffness of the specimens with various welding positions of beam to the beam end connector

Specimen	Ultimate Moment capacity (kNm)	Stiffness (kNm/rad)
K	1.73	23.28
L	2.21	29.8
M	2.81	55.04

4.4.4 Spacing between the tabs in the beam connector

Spacing between the tabs in the beam end connector was 50 mm for all the specimens used in the experimental investigation. The FE analysis was performed by reducing the spacing between the tabs in the beam end connector by 20%, that is, 40 mm, and by keeping the connector depth the same as that of the specimen E used in the experimental test. The distance between the column perforations was also adjusted according to the selected spacing between the tabs. The effect of decreased spacing only was analyzed. Increase in spacing between tabs by 20% results in increased connector depth. The geometries of the remaining connection components were kept the same as those for the

experimental testing of specimen E and the specimen with 40 mm tab spacing is named as ‘specimen N’.

Reducing the spacing between tabs from 50 mm to 40 mm (specimen N) improved the distortion intensity of the top two tabs compared with the FEM results achieved for specimen E. However, a significant increase in failure intensity of the beam end connector and the tabs in tension zone was observed. Both edges of the beam end connector (inner and exposed) were significantly distorted, which caused a drop in failure moment and influenced the stiffness of the connection. Figure 4.20 shows the M-θ behavior of specimen ‘N’. Taking specimen E as a reference, a 20% decrease in the tab spacing reduced the ultimate moment capacity and stiffness of the connection by 8% and 32%, respectively. Based on the observations of this study, a spacing of 50 mm between tabs is suitable for a beam end connector depth of 200 mm.

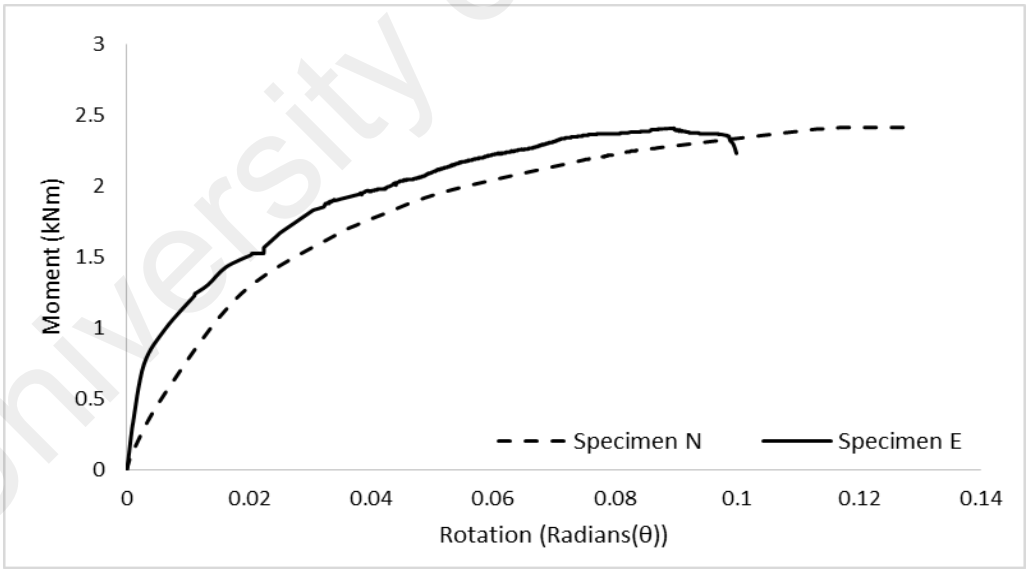

Figure 4.20: M-θ behavior of specimen N and specimen E

4.5 Experimental results of elevated temperature testing

4.5.1 Failure Modes

To minimize heat loss, the whole surface of the specimen was insulated with mineral wool. Therefore; the real time failure during test was not exactly observed; however, the maximum possible closer observation of failure modes during tests and the failure modes after the removal of wool was observed.

At 450°C and 550 °C, the failure of specimens with shallow beams and thin columns showed a similarity with the failure of same specimens tested at ambient temperature. The top two tabs in compression zone were completely ruptured. The bottom tabs in tension zone were critically distorted and disengaged from the column slots by tearing the column flange. The major dissimilarity between the failure of specimens ‘A’ and ‘B’ was the value of failure load. At 700 °C, the pre-dominant failure mode was the out of plane buckling of column web which significantly affected the amount of failure load and compelled the tabs in compression zone to distort at relatively early stage after applying the load. The failure of tabs and the beam end connector was also observed with an increased intensity as compared to that observed at 450 °C and 550 °C.

For the specimens with deep beams and greater column thickness, at 450 °C and 550 °C, the modes of failure were quite similar to each other, but different from the specimens with shallow beams and thin columns. The tabs in compression zone also showed a dissimilar behavior as compared to the ambient temperature testing. The splitting of column flange by the compression tabs was not observed and the top tabs in compression zone ruptured themselves. With an increase in mechanical load, the flexural deformation of column web occurred which increased the tensile stress in the lower tabs of the beam end connector. The bottom tabs in tension zone disengaged from the column slots and slit the column flange. For the compression zone in the beam end connector, the redistribution

of stresses was influenced by deformation of column web. This was governed by normal force and bending moment in the column. A typical failure of the connection as well as out of plane buckling of the column at elevated temperature is presented in Figure 4.21. The deformation of the tabs is shown in Figure 4.22. The deformation of the beam end connector is shown in Figure 4.23.

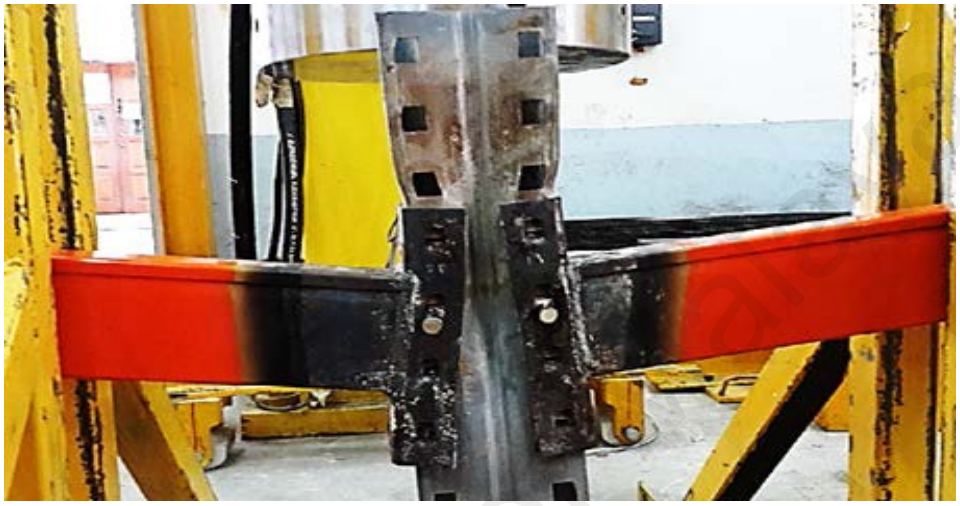

Figure 4.21: Typical failure of connection

Figure 4.22: Deformation of tabs

Figure 4.23: Deformation of the beam end connector

4.5.2 Moment-Rotation (M-θ) Behavior and Stiffness

The moment was calculated using Eq. 4.1. The end rotations of the beams were obtained as the relative LVDTs' displacements divided by the separation between them. The rotation was calculated for the beams on both left and right sides of the column, and the mean value was used to plot the M-θ curve. The rotation for each side of the connection was calculated as follows:

$$\text{Rotation } (\theta) = \frac{\delta_1 - \delta_2}{d}, \tag{4.2}$$

Where

δ_1 = deflection measured by LVDT: D1 and D2 for the right and left hand sides beams, respectively

δ_2 = deflection measured by LVDT: D3 and D4 for the right and left hand sides beams, respectively

d = distance between the LVDTs placed on identical beams

Comparison of M-θ curves for the each set of specimens tested at different temperature ranges as well as with the M-θ curves obtained for the ambient temperature testing of SPR BCCs is presented in Figures 4.24 (a-g). From these M-θ curves, the characteristics of BCCs, such as the moment capacity, Mc (peak moment), and the rotation at the maximum moment, θc, and the stiffness, K0, can be determined. The connections tested in this study showed an intermediate level of elasticity and behaved as semi-rigid connections. This semi-rigid behavior was caused by the distortion of the column wall and perforations and the deformation of the beam end connector. Almost all of the specimens showed nonlinear behavior from the starting point. Due to the temperature effects, the specimens became more flexible and a highly non-linear behavior was achieved. The curves for all the specimens tested under elevated temperature also showed a minor effect of initial looseness at their initiating point. It should be noted that SPR BCCs are adjustable type of connections and such connections more often than not lead to a certain amount of looseness of the connections. Special considerations to account for looseness of connection should be included in the analysis of overall rack structure. The M-θ test results are presented in Table 4.6. A comparison with ambient temperature test results is also provided.

The stiffness was calculated according to the equal area method. The values of experimentally measured rotation and stiffness for specimens tested at elevated temperatures were also corrected for the error due to the flexural and shear deformation. The values of distance between the column and LVDTs and between LVDTs themselves as well as the applied load value were used according to the experimental data used in this study. Given that the tensile coupon test at elevated temperature was not performed, the values of the flexural rigidity of the beams and the beam end connector were calculated based on the reduction factor of the elastic modulus provided in EC 3 (2005b). The respective values of shear rigidity were calculated using the reduced values of the

elastic modulus. After the measured rotation was corrected, the values of rotational stiffness were rectified. The experimental stiffness and the corrections are presented in Table 4.7.

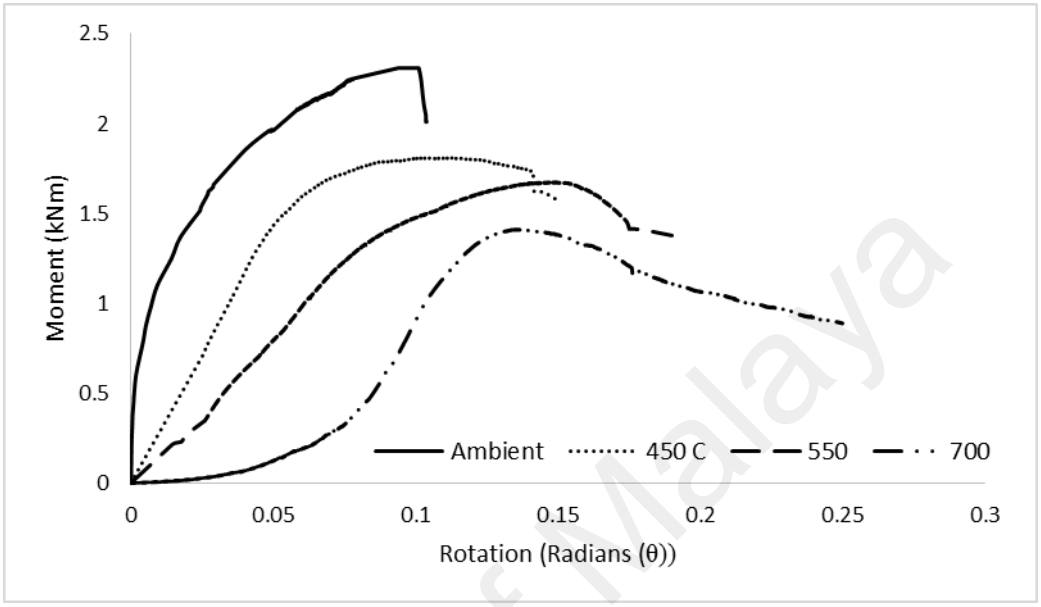

(a) Specimen A

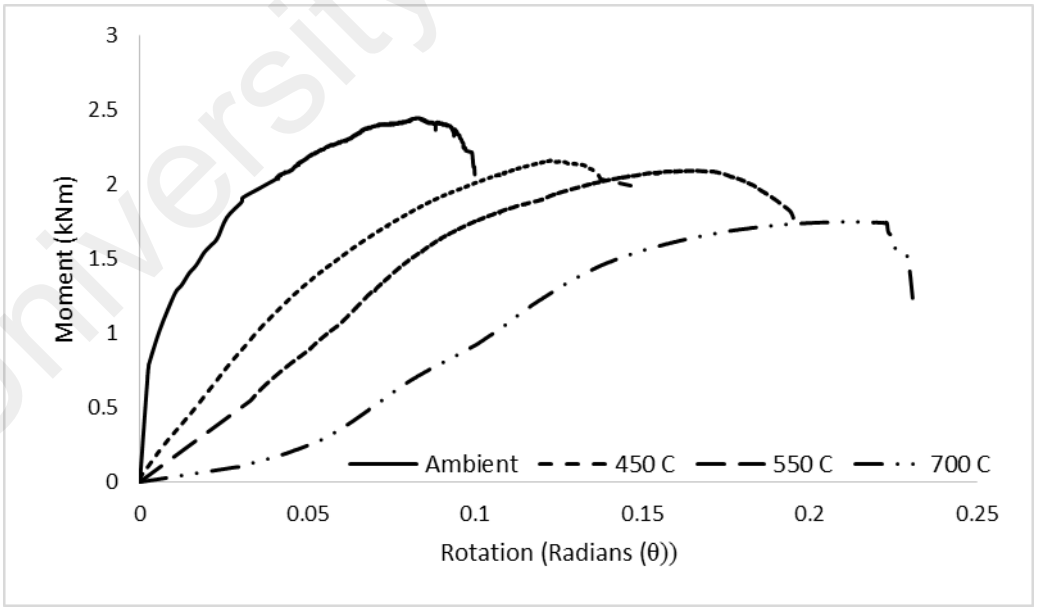

(a) Specimen B

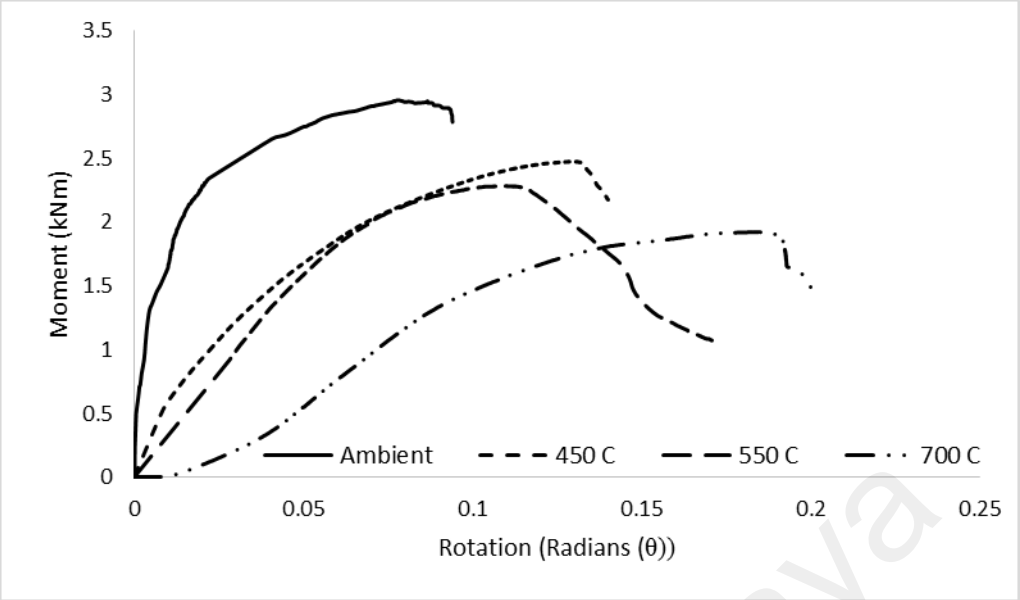

(c) Specimen 'C'

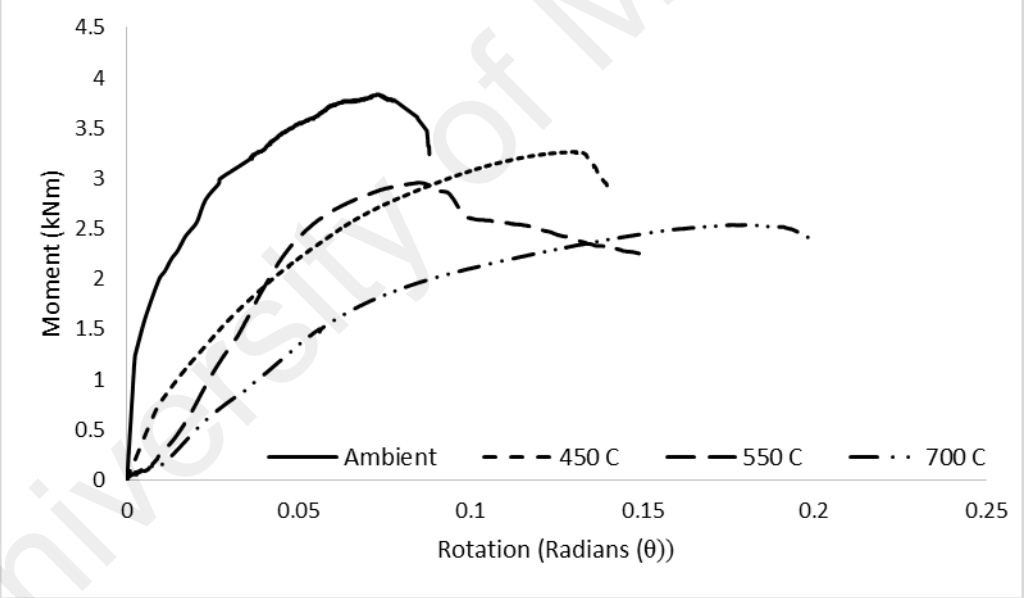

(d) Specimen 'D'

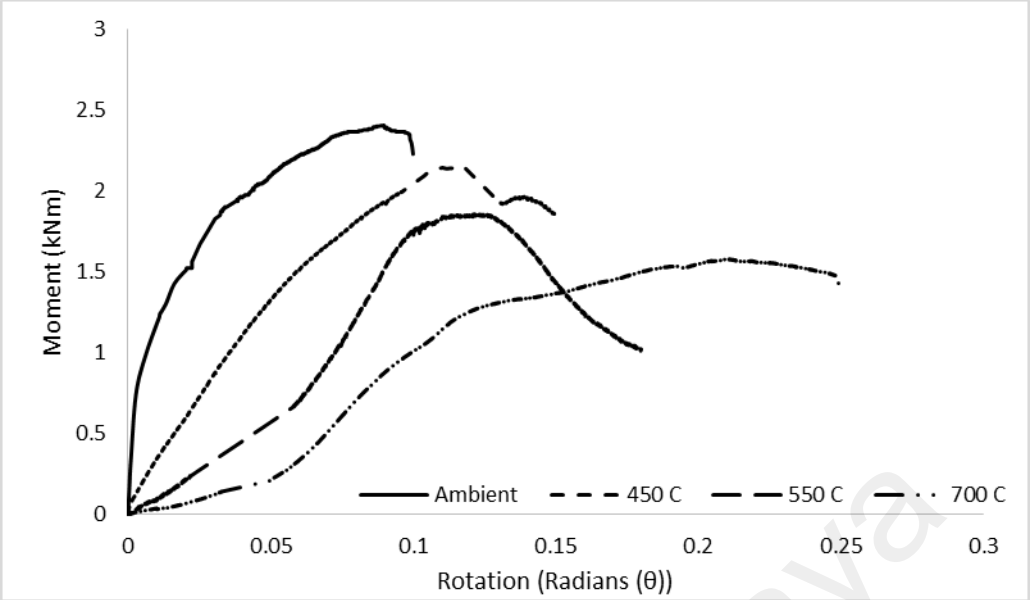

(e) Specimen ‘E’

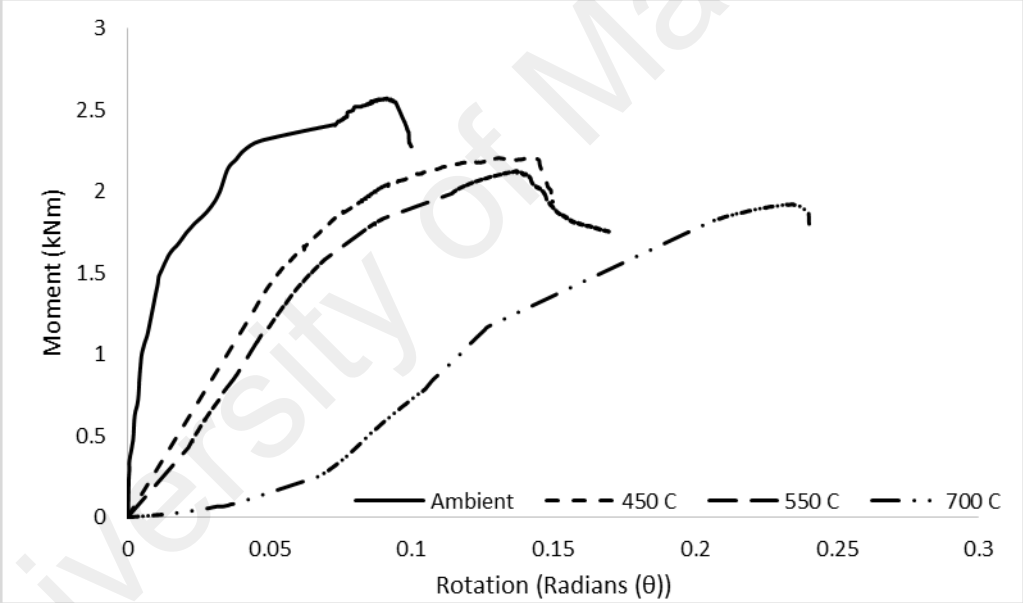

(f) Specimen ‘F’

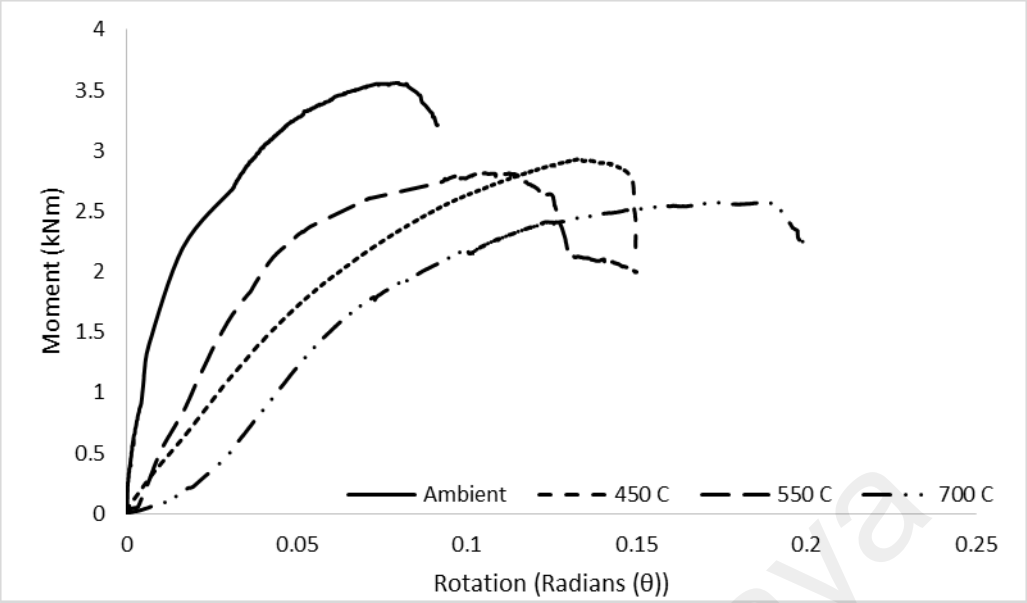

(g) Specimen ‘g’

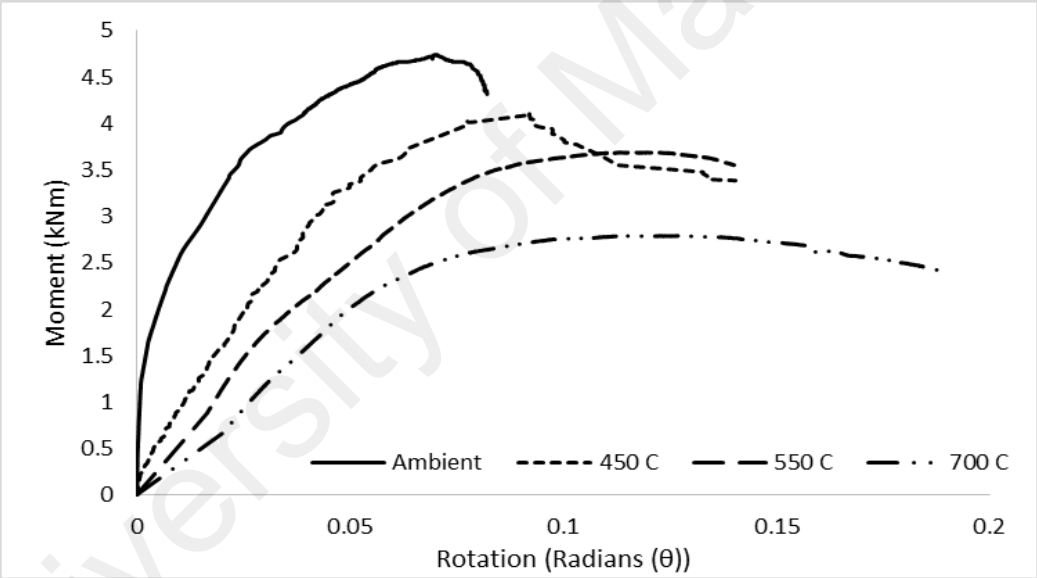

(h) Specimen ‘H’

Figure 4.24: M-θ curves for tested specimens

Table 4.6: M-θ results of the tested specimens

Specimen	Temperature	Moment (kNm)	Rotation (radians (θ))
A	Ambient	2.31	0.1
	450° C	1.80	0.15
	550° C	1.67	0.19
	700° C	1.41	0.25
B	Ambient	2.45	0.1
	450° C	2.16	0.15
	550° C	2.09	0.19
	700° C	1.75	0.23
C	Ambient	2.96	0.094
	450° C	2.48	0.14
	550° C	2.27	0.17
	700° C	1.92	0.20
D	Ambient	3.80	0.088
	450° C	3.26	0.14
	550° C	2.99	0.15
	700° C	2.54	0.20
E	Ambient	2.44	0.1
	450° C	1.98	0.15
	550° C	1.82	0.18
	700° C	1.56	0.25
F	Ambient	2.57	0.10
	450° C	2.21	0.15
	550° C	2.13	0.17
	700° C	1.82	0.24
G	Ambient	3.56	0.091
	450° C	2.96	0.15
	550° C	2.81	0.15
	700° C	2.57	0.20
H	Ambient	4.74	0.082
	450° C	4.09	0.14
	550° C	3.68	0.14
	700° C	2.80	0.19

Table 4.7: Experimental stiffness and corrections

Specimen	Temperature	Experimental Stiffness (kNm/radians)	Flexural correction	% difference	Shear correction	% difference	Corrected stiffness
A	Ambient	32.3	32.78	1.48	32.56	0.80	33.03
	450° C	22.90	23.22	1.39	23.07	0.74	23.38
	550° C	13.58	13.76	1.32	13.67	0.66	13.84
	700° C	7.59	7.69	1.31	7.63	0.52	7.72
B	Ambient	36.2	36.91	1.93	36.50	0.84	37.20
	450° C	24.20	24.65	1.86	24.39	0.77	24.83
	550° C	15.97	16.29	2.00	16.11	0.87	16.42
	700° C	9.39	9.52	1.38	9.46	0.74	9.58
C	Ambient	54.29	55.11	1.51	54.73	0.81	55.54
	450° C	38.74	39.51	1.98	39.08	0.87	39.84
	550° C	28.02	28.53	1.82	28.23	0.74	28.73
	700° C	12.85	13.02	1.32	12.94	0.70	13.10
D	Ambient	79.21	80.81	2.01	79.96	0.94	81.54
	450° C	41.51	42.32	1.95	41.87	0.86	42.67
	550° C	32.6	33.17	1.74	32.87	0.82	33.43
	700° C	18.01	18.27	1.44	18.14	0.73	18.4
E	Ambient	35.9	36.38	1.33	36.16	0.72	36.63
	450° C	23.74	24.08	1.43	23.93	0.80	24.26
	550° C	15.80	16.03	1.45	15.91	0.70	16.13
	700° C	8.87	8.98	1.24	8.93	0.67	9.03
F	Ambient	42.8	43.7	2.10	43.1	0.70	43.99
	450° C	29.64	30.13	1.65	29.88	0.80	30.36
	550° C	17.76	17.98	1.23	17.88	0.68	18.09
	700° C	10.96	11.09	1.18	11.03	0.64	11.15
G	Ambient	69.54	70.91	1.97	70.15	0.88	71.52
	450° C	43.09	43.80	1.64	43.38	0.67	44.08
	550° C	36.01	36.64	1.74	36.29	0.77	36.91
	700° C	20.02	20.26	1.19	20.15	0.64	20.38
H	Ambient	97.86	100.23	2.42	98.78	0.94	101.14
	450° C	62.97	64.13	1.84	63.44	0.74	64.59
	550° C	42.31	43.03	1.70	42.6	0.68	43.32
	700° C	30.44	30.85	1.34	30.65	0.68	31.05

For the specimens tested at elevated temperatures, it can be seen from Figure 4.24 and Table 4.6 that the change in the mechanical properties affected the plastic behavior of the specimens and stiffness has been affected with variation in the temperature. High temperatures made the specimens flexible and the specimens showed less resistance to mechanical load. The stiffness decreased at a higher rate with the increase in temperature as compared to the strength of the connection. This phenomenon was different from the one that was observed in the case of specimens tested at ambient temperature, where the strength was affected at a relatively higher rate than stiffness with the variation in the sizes of the connection components. This may be due to the fact that the steel loses its strength and begins to elongate with the increase in temperature.

The connection designs at ambient temperature generally consider only the ultimate moment and stiffness, whereas ductility and failure modes are important for connections in fire when large deformations are generally experienced. Ductility is simply defined as

the angle of rotation achieved at the maximum load. The ductile behavior of steel connections ensures that a sufficient rotation or deformation capacity is available to allow the selection of either the elastic or plastic analysis. All connections tested at elevated temperatures showed a ductile behavior by exhibiting a clear non-linearity of the M-θ curves with a large plateau before fracture. Moreover, no abrupt decline of load was shown, especially for the specimens with deep beams, great column thickness, and high number of tabs in the beam end connector. No beam failure was observed, but connection failure occurred when the deformation of tabs gradually increased. The beam end connector experienced a noticeable twist at failure. Compared with moment, the higher increasing rate of the rotation increased the ductility of the connection but affected its stiffness.

4.5.3 Effect of Temperature on Connection Performance

The results of the tested BCCs can be made from Table 4.6. In order to discuss the behavior of connection under different temperature ranges, the specimen 'A' is selected as an example for comparison and its behavior at different temperature ranges is conversed in this section.

Referring to Figure 4.24 and Table 4.6, it can be seen that increasing the temperature from 25 ° C to 450 ° C resulted in a decrease of 22% and 29% in the moment capacity and the stiffness of the connection, respectively. Increasing the temperature from ambient to 550 ° C, caused a decrease of 28% and 58% in the moment capacity and stiffness of connection, respectively. When temperature reached at 700 °C, a comparison of strength and stiffness from the specimen tested at ambient temperature, the moment capacity of connection was decreased by 39% and the stiffness was decreased by 76%.

4.6 Results of FE analysis at elevated temperature

4.6.1 Failure Modes

The FE model exhibited a very close agreement with the experimental results. Similar to the experimental investigations, the FE model for specimen ‘A’ showed that failure occurred due to the deformation of the tabs. The FE model captured a high level deformation in top tabs in compression, however, again, the FE model was unable to capture the complete rupture of top tabs. The behavior of tabs in tension zone captured by FE model was quite similar to that observed during experimental testing. The tabs in the tension zone experienced more stress and came out tearing the column slots. Thus, the dominant failure mode in the FE analysis was the distortion of tabs. The FE model successfully predicted the out of plane buckling of column web and also captured the distortion of column wall and the phenomenon of tabs trying to come out of the column slot. However, the intensity of column deformation observed in the FE analysis was not exactly same to that observed in the experimental investigations because the distortion of column slots captured in the FE model was a less intense. The failure of the connection with connector A for both experimental and FE investigations at 700° C is presented in Figures 4.25 (a) and (b), respectively. The failure of the beam end connector and the stress distribution in the tabs is presented in Figure 4.26, whereas, Figure 4.27 shows the stress distribution in the column.

(a)

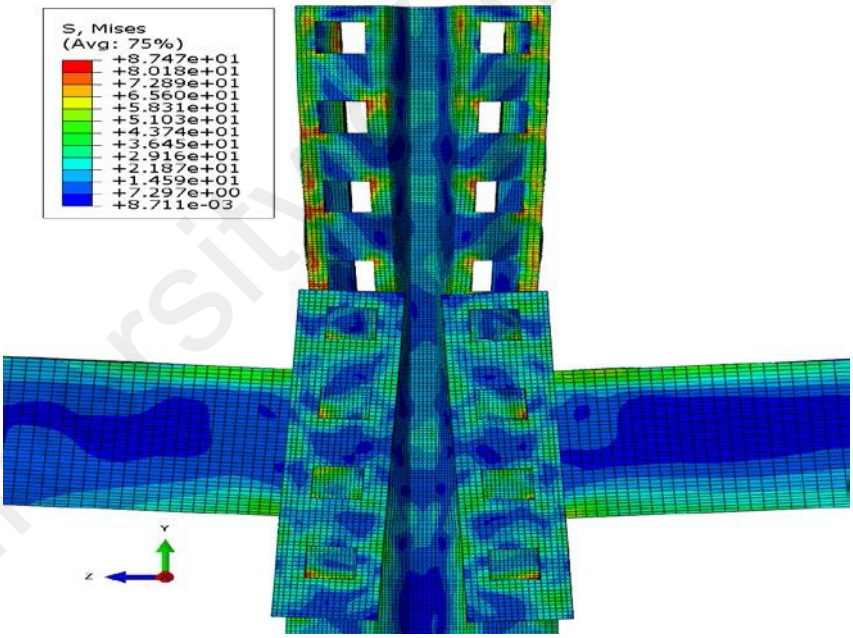

(b)

(a) Experimental failure, (b) FE Failure

Figure 4.25: Failure of connection at 700 °C

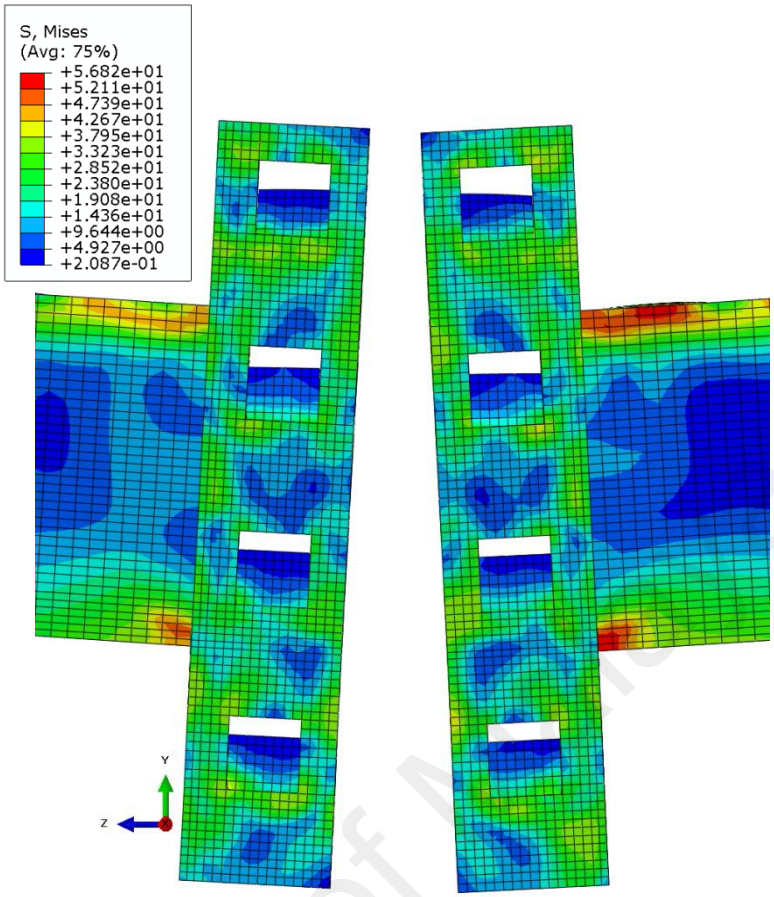

Figure 4.26: Failure of connection at 700 °C

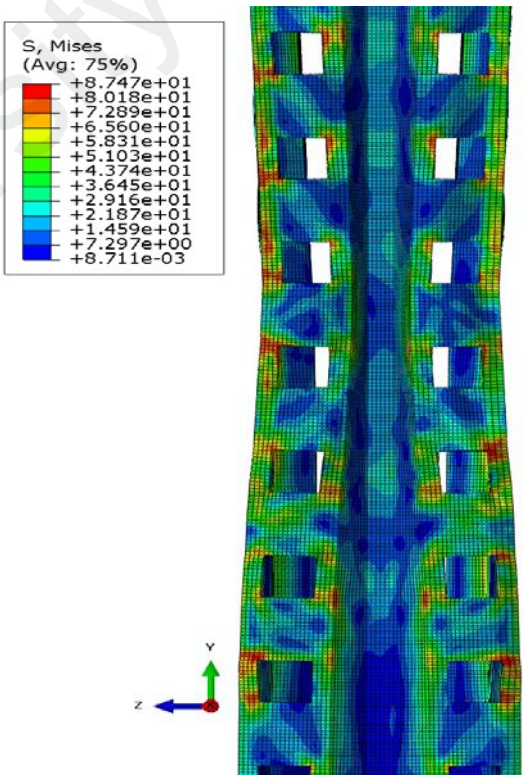

Figure 4.27: Failure of column

4.6.2 M-θ Behavior and Stiffness

The bi-linear FE model used for the analysis of connections tested at ambient temperature resulted in a higher ultimate moment capacity. This may be due to the reason that the bi-linear material model is defined for all components of connector assembly. In this, tangent modulus is calculated (as normally in case of steel alloys) through connecting yield and ultimate tensile stress. This consideration may overestimate strain hardening. Once strain hardening is increased, moment capacity of the whole assembly will increase. Thus, the model may overestimates experimental results. Therefore, for FE analysis of connections tested at elevated temperatures, the bi-linear model was converted into a multi-linear model and a comparison is made among the experimental and FE results of elevated temperature testing and the FE results of bi-linear and multi-linear models which are presented in Figure 4.28 (a). Figure 4.28 (b-d) shows the comparison of the M-θ graphs for specimen A tested at 450 °C, 550 °C, and 700 °C.

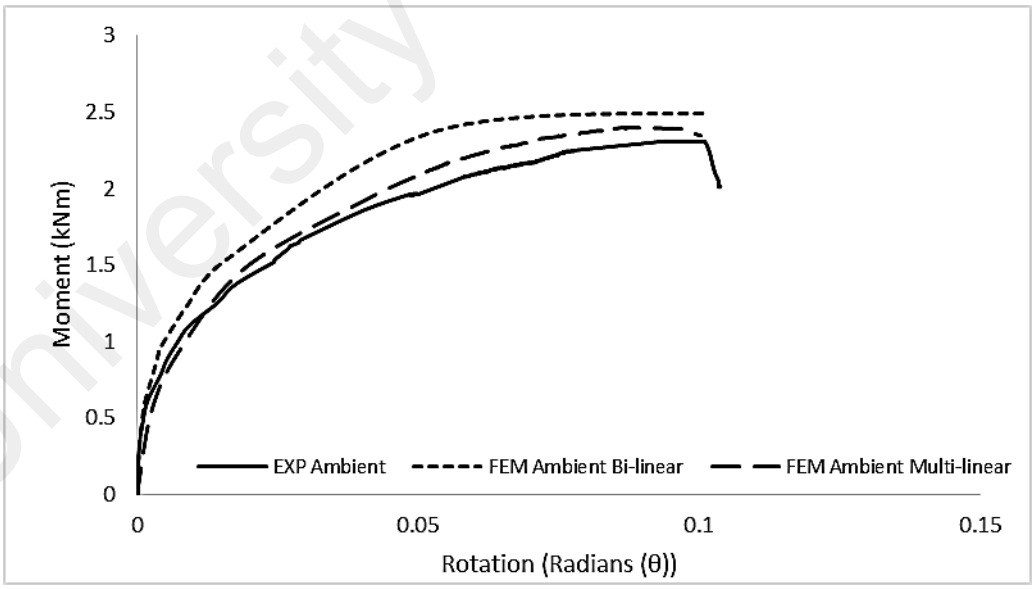

(a) Comparison of experimental and FE models' results for specimen 'A'

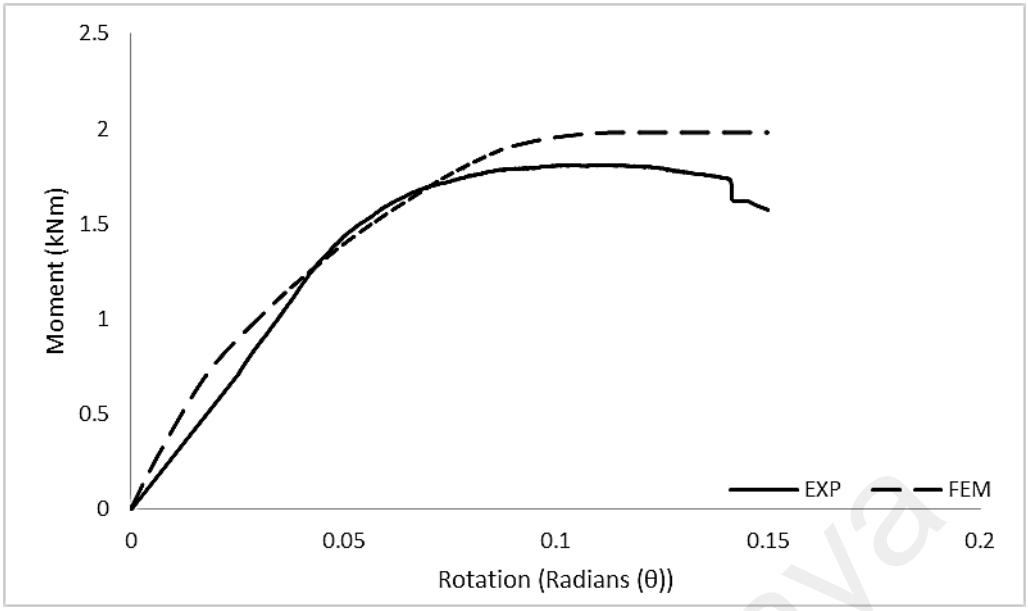

(b) Specimen 'A' at 450 °C

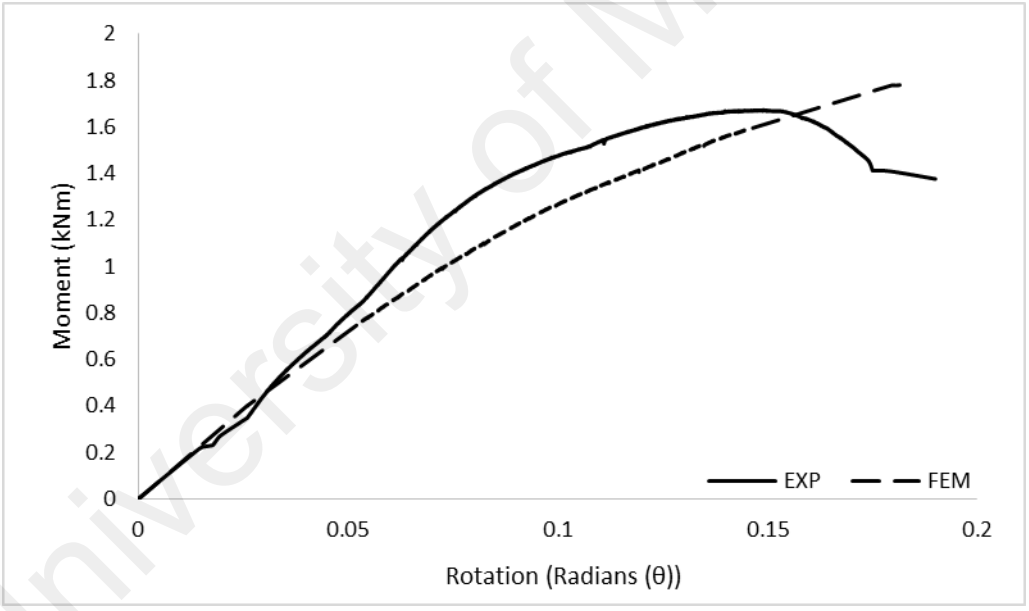

(c) Specimen 'A' at 550 °C

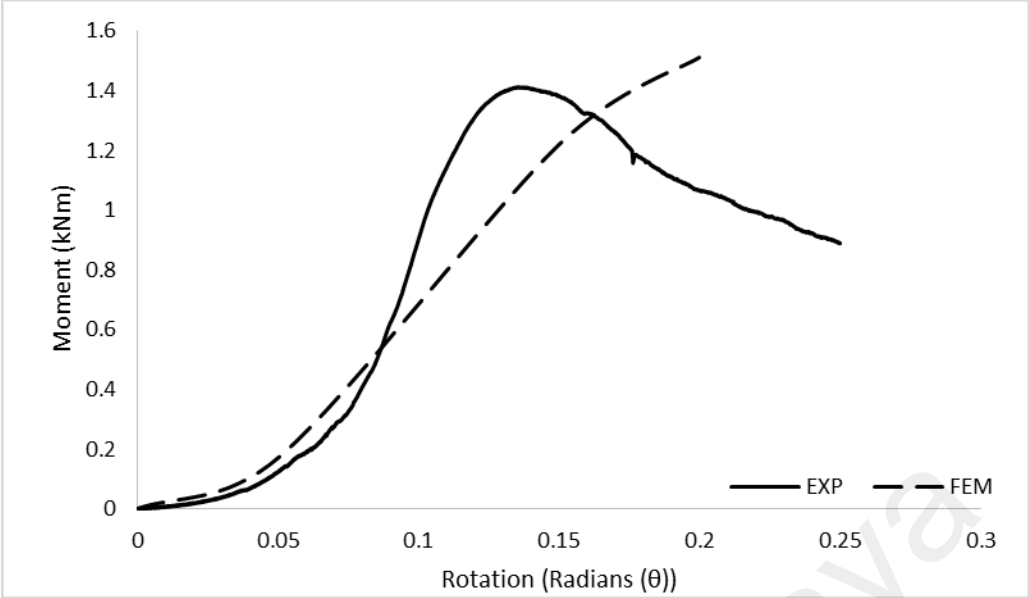

(d) Specimen 'A' at 700 °C

Figure 4.28: M-θ curves comparison of experimental and FE investigations for Specimen 'A' at various temperature ranges

Table 4.8: Comparison of Experimental and FEM results for specimen A

Temperature Range	Ambient Temperature			450 °C		550 °C		700 °C	
Investigation type	EXP	FEM (Bi-linear model)	FEM (Multilinear model)	EXP	FEM	EXP	FEM	EXP	FEM
Ultimate Moment (kNm)	2.31	2.49	2.40	1.80	1.85	1.67	1.78	1.41	1.50
Stiffness (kNm/radians)	33.03	37.93	34.01	23.38	23.71	13.84	14.06	7.72	8.13

Similar to the experimental results, the M-θ curves obtained through the FE model showed a nonlinear behavior. It is evident from Figure 4.28 (a-d) that simulation results are initially in good agreement with experimental observation but show overestimation at higher rotation angles. The ultimate moment capacity of the connection was similar up to half of the peak moment for both types of investigations. After that, the ultimate moment capacity of the connection obtained through the FE model was increased gradually till the failure of the connection. By contrast, after reaching the peak moment, the experimental curves show a gradual decrease in the moment capacity. However, the final values of

strength and stiffness of the specimens matched well with that of the experimental test results. A slight increase in the ultimate moment capacity achieved by the FE model is due to a minor difference between the column slot failures in the two types of investigation.

The variation in the behavior of experimental and FE curves may be attributed to a number of reasons, In FE model, all materials in connector assembly (beam, column, and beam-end connector) are considered as homogenous and free of imperfections. In real materials, deformation behavior may represent low value of yield and ultimate strength due to the presence of defects and non-homogenous nature, as minor kinks due to specimens' imperfection can be seen in the initial stage of M-θ curves presented in Figure 4.24. Once the overall strength of beam-connector assembly obtained by FE model is higher, the moment capacity of the system will be higher. Therefore, FE model slightly overestimates the overall deformation behavior of connector assembly. Other possible reasons may include the shape of tabs. In FE model, the geometry of tabs and column perforations was idealized as L-cross-section and frictionless contact conditions between the tabs and column were considered. These assumptions in FE model were considered to reduce the complexity and increase the probability of solution convergence. It is recommended that the relaxations in the current model may be included in future works to reduce the difference between simulation and experimental results.

While designing the CFS connections under fire, it is much helpful to understand how strength and stiffness degradation has been occurred with respect to the temperature variation at various values of rotation. Normalized M-θ-t curves are an efficient way to describe the strength and stiffness degradation with increasing temperature. In this study, these curves are developed at different values of rotation for the values of temperature selected in this study for experimental testing. No data was available in between 25 ºC

and 450 ºC, thus, the presented curves shows the strength degradation rate among selected temperature ranges. For strength reduction, the curves are normalized by dividing the ultimate moment at elevated temperature by the ultimate moment at ambient temperature at selected rotation values. For stiffness reduction, the curves are obtained by dividing the initial stiffness at elevated temperatures by the initial stiffness at ambient temperature. Figure 4.29 represents the strength degradation with increasing temperature for all eight sets of specimens at different values of rotation in the form of normalized strength degradation curves. Figure 4.30 represents the stiffness degradation with increasing temperature for all eight sets of specimens at different values of rotation in the form of normalized stiffness degradation curves.

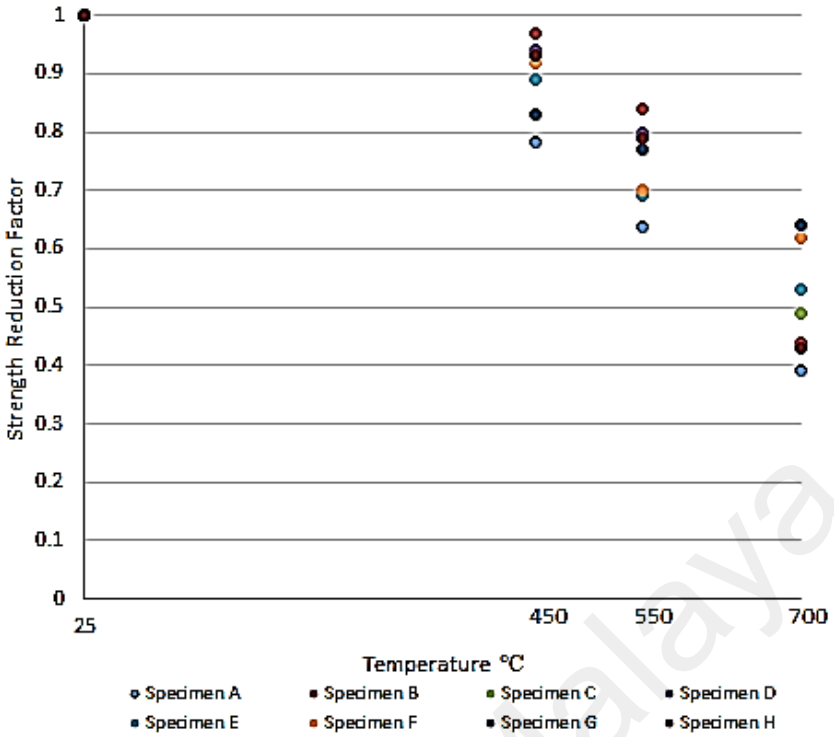

Figure 4.29: Normalized strength degradation curves for all eight sets of specimens

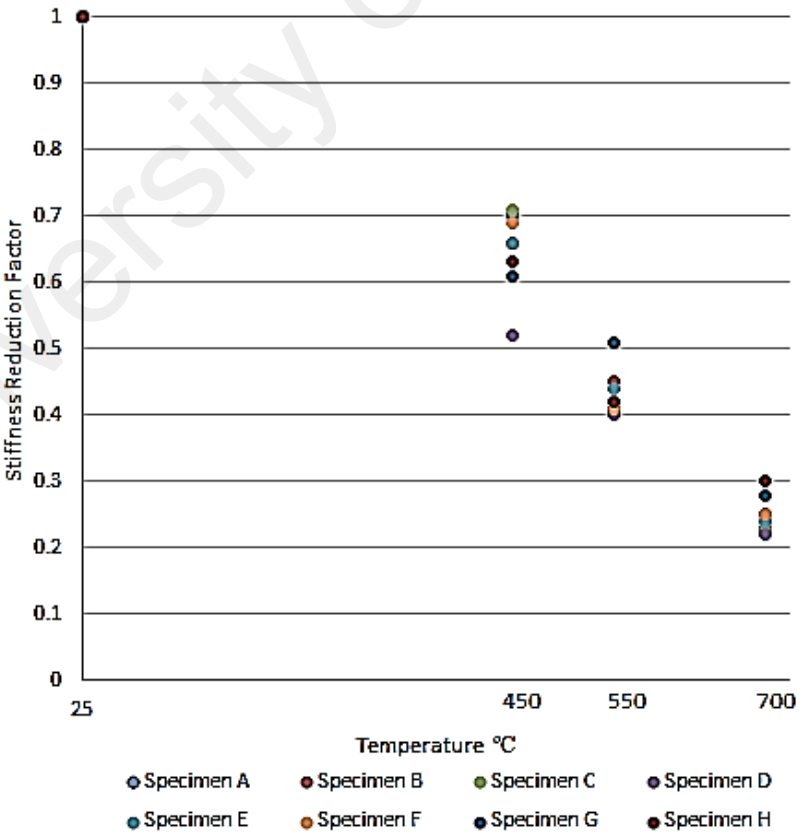

Figure 4.30: Normalized stiffness degradation curves for all eight sets of specimens

It can be seen from Figures 4.29 and 4.30 that the degradation rate of strength and stiffness has a higher rate when temperature increased from 25 ºC to 450 ºC. The rate of degradation has marginal difference when temperature raised from 450 ºC to 550 ºC. However, above 550 ºC, the degradation rate of both the strength and the stiffness was again critical. The specimens became highly flexible at 700 ºC.

With regards to sizes of specimens, increased number of tabs influenced the strength of the connection. The degradation in the specimens with greater number of tabs showed a relatively lesser rate of strength and stiffness degradation with the rise in temperature as compared to the specimens with shallow beams, thin column and lesser number of tabs.

CHAPTER 5: CONCLUSION AND FUTURE RECOMMENDATIONS

Because of the special nature of SPRs, their design presents many problems that cannot be handled routinely within existing design specifications. One of these special problems are the semi-rigid boltless readily adjustable connections used as BCCs in SPRs. The ingenious configuration of BCCs, which differ among different manufacturers, hampers the development of a generalized approach to obtain identical M-θ relationship for each connection. Thus, the design structural analysis is carried out by adopting a semi-continuous sway frame model, i.e. unbraced frame with semi-rigid joints under the guidelines of recent design codes. The design of such boltless connections becomes more complex in the event of fire. The presence of great quantity of combustible gases represents the main cause of possible developments of fire in a warehouse or storage building where the goods are placed on SPRs. Further, it is revealed by the literature review that the down-aisle stability of SPRs depends upon the BCCs in both ambient and elevated temperature cases. Despite the availability of research focusing the overall behavior of SPRs subjected to various types of loadings, the behavior of SPR BCCs solely at ambient temperatures is not well recognized in the literature. Several full scale experimental and numerical investigations on SPRs were developed however, most of the investigations do not provide complete details about the effect of geometrical properties of connection members on the behavior of BCC. Particularly, there is no research available discussing the behavior of SPR BCCs at elevated temperatures. In pallet racks, high temperature urges the moment transfer from members to connections. Lack of knowledge on the fire behavior of SPR BCCs may lead to a poor design of SPR structure, which consequently result in an unexpected structural failure. The literature brings to light that the collapse of high rise SPRs has resulted in lives and property loss. Taking into account these criteria, the moment resistance and stiffness of SPR BCCs must be verified

at elevated temperatures. Given the lack of research on the fire behavior of SPR BCCs, it is essential to predict the behavior of SPR BCCs subjected to elevated temperatures.

The main goal of this research was to understand the structural and mechanical behavior of SPR BCCs subjected to ambient and elevated temperatures using experimental and numerical investigations. The connection parameters covered by experimental investigations are (i) column thickness (ii) beam depth (iii) number of tabs in the beam end connector. The observations collected include the M-θ behavior, load-strain relationship, major failure modes and effects of various parameters on the performance of connection. The study has undertaken the double-cantilever test method only and thirty-two specimens were tested at ambient temperature whereas twenty-four specimens were tested at elevated temperatures. The results of ambient temperature testing were validated using FE modeling on a commercial software ABAQUS. The validated FE model is further extended to parametric studies in order to evaluate the effects of those parameters which were not tested during experimental investigations.

The following conclusions are made based on the investigations performed in this study:

- The failure of the connection was initiated with the failure of the tabs. The tabs tried to tear the column web slot. A complete rupture of tabs was noticed in the case of specimen with relatively shallow beams and thin column. The intensity of this failure was minimized in connections with deep beam sections and a large number of tabs in the beam end connector.

- The initial looseness of the connection gave rise to lateral deformation. Imperfections in the specimens tends to make the M-θ curve behave non-linearly even from a very early stage. The localized failure effect of SPR BCCs may be attributed to

the wear and tear of the tool die. This is caused due to the repeated punching during the manufacturing of beam end connectors, which is the prime component in the connection. A slight variation in dimension in the component leads to a considerable variation in the value of connection strength and stiffness.

- An increase in the thickness of the column, made the tabs on the beam end connector experience a larger deformation due to the in-plane moment.

- The equal area method provided more consistent values of stiffness and lowest variance in the data set as compared to the other two methods. Thus, it may be a relatively reliable method to calculate connection stiffness.

- The variation in the geometrical features of BCCs tested at ambient temperature showed a more direct effect on the stiffness of connection. Increased size of parameters increased the stiffness of connection at a higher rate as compared to the strength. This indicates that elastic properties of SPR BCCs rely on geometrical parameters.

- Increased column thickness and greater beam depths enhanced the strength and stiffness of the connection. An increase in the number of tabs minimizes the deformation of the beam end connector. A combined effect of the higher number of tabs and greater beam depth is more influential as compared to varying the thickness of the column.

- The observed failure modes of SPR BCCs at elevated temperatures were deformation of tabs, deformation of column slots, deformation of the beam end connector and out of plane buckling of column web.

- In contrast to the low temperature testing where the governing failure mode was the distortion of tabs, at high temperatures the failure mode was switched to an out-of-plane buckling of column.

- A noticeable degradation in the strength and stiffness of the connection is observed due to with increasing temperature due to thermal action.

- Dissimilar to the phenomenon of variation in the sizes of connection parameters, the change in material properties affected the strength of SPR BCCs at much higher rate as compared to its stiffness. The specimens become more flexible and the M-θ curves showed highly non-linear behavior from the starting point.

- The strength and stiffness of the connector were not much different at 450 °C and 550 °C. However, the connection exhibited high level of deformation at 700 °C and the rotation became significantly increased with an increase in temperature.

- The FE analysis performed to validate the experimental results for both ambient and elevated temperatures showed a close agreement with experimental results.

- The failure modes of both types of investigations, namely, experimental and FE, were quite alike at both the ambient and elevated temperatures. Similar to the experimental results, the failure of connector tabs, deformation of column and deformation of the beam end connector were observed. The only difference was in the failure of the tabs for the specimens with shallow beams and thin columns in which the complete rupture of tabs was not captured by FE model.

- The M-θ curve obtained from the FE results were in close agreement with those obtained from the experimental results. The stiffness matched well with the experimental results, however, for most of the specimen, the FE results showed a slight increase in the ultimate moment capacity of the connection in the ultimate stage.

- The parametric analysis showed that an increase in beam end connector thickness enhanced the performance of the connection. Regarding the position of weld of beam to

the beam end connector, the findings revealed that the up-welding of beam causes a non-uniform stress distribution in the tabs which compels the connection towards a pre-mature failure. Thus, up-welding of the beam is detrimental and reduces the performance of the connection. Down-welding of beam resulted in a better performance of connection in terms of strength and stiffness. According to findings of this study, keeping the spacing between the tabs of the beam end connector approximately one-fourth of the total depth of the beam end connector may result in satisfactory performance of the connection.

5.1 Design recommendations

This study has examined the behavior of SPR BCCs at ambient and elevated temperatures using different types of investigations. A comparison of stiffness design method is also performed to highlight the most appropriate method to predict the connection stiffness. It was revealed that the equal area method provides reliable estimation of connection stiffness as compared to the initial stiffness method which is suggested by the EC3 (2005a) to calculate the connection stiffness. The method suggested in EC3 (2005a) overestimates the stiffness of the connection.

It was also observed that for modeling of SPR BCCs, the EN15512 suggests that the axial spring should be used instead of tabs to define the interaction between the column and the beam end connector. The FE results of this study showed close agreement with experimental results by modeling the tabs as compared to the studies performed in past that have used the axial spring approach. Thus, for FE modeling it is recommended that the tabs should be modeled instead of defining the axial spring to achieve the exact deformation behavior of the beam end connector as well as the ultimate moment capacity of the connection.

The routine calculation for stiffness suggested by the design codes for SPR BCCs ignores the deflection of the beam and the beam end connector, and a minimal error may

exist. This study has applied the equations developed by Abdel Jaber et al. (2010) to determine the effect of the error due to the flexural and shear deformations on the total measured experimental rotation and stiffness values and it was revealed that without considering the effect of error due to the deflection of the beam and the beam end connector, the accurate stiffness of SPR BCCs may not be achieved.

5.2 Recommendations for future research

This study has several limitations and based on those, some recommendations for future research are presented in this section. For experimental testing at ambient temperature, the study is limited to the influence of the selected parameters tested. The future study can be extended by investigating the influence of other various parameters on the performance of SPR BCCs using the double cantilever test method as well as the standard cantilever test method. For elevated temperature testing, it is suggested that the temperature ranges other than those used in this study should be selected for testing. Moreover, this study has applied the iso-thermal test condition only. Other types of fire testing may be used to evaluate time-temperature response of SPR BCCs. Furthermore, since advance research focuses on the performance based design of CFS connections, it is recommended that the full-scale SPR testing should be performed at elevated temperatures to further understand the behavior of SPR BCCs. For numerical testing, the FE analysis performed for elevated temperature testing can be improved by (i) incorporating coulomb's friction model (ii) use of coupling elements to describe the actual welding type between the beam and the beam end connector (iii) proper material testing should be carried out to determine the actual Young's Modulus, uniaxial yield stress, hardening gradient, plastic strain, etc. Since the literature has very less number of studies performing component modeling of SPR BCCs, one of the important recommendation for future research is to develop component model for SPR BCCs for both ambient and elevated temperatures.

REFERENCES

Abdel-Jaber, M., Beale, R., & Godley, M. (2005). Numerical study on semi-rigid racking frames under sway. *Computers & structures, 83*(28), 2463-2475.

Abdel-Jaber, M., Beale, R., & Godley, M. (2006). A theoretical and experimental investigation of pallet rack structures under sway. *Journal of Constructional Steel Research, 62*(1), 68-80.

Abreu, J. C. B., Vieira, L. M., Abu-Hamd, M. H., & Schafer, B. W. (2014). Review: development of performance-based fire design for cold-formed steel. *Fire Science Reviews, 3*(1), 1.

Affolter, C., Piskoty, G., Wullschleger, L., & Weisse, B. (2009). Collapse of a high storage rack. *Engineering Failure Analysis, 16*(6), 1846-1855.

Aguirre, C. (2005). Seismic behavior of rack structures. *Journal of Constructional Steel Research, 61*(5), 607-624.

AISC. (2010). 360--05, Specification for Structural Steel Buildings. *American Institute of Steel Construction, Chicago, IL, USA.*

Al-Jabri, K. (2004). Component-based model of the behaviour of flexible end-plate connections at elevated temperatures. *Composite structures, 66*(1), 215-221.

Al-Jabri, K., Burgess, I., Lennon, T., & Plank, R. (2005). Moment–rotation–temperature curves for semi-rigid joints. *Journal of Constructional Steel Research, 61*(3), 281-303.

Al-Jabri, K., Burgess, I., & Plank, R. (2000). *Recent Developments in the Behaviour of Steel and Composite Connections in Fire.* Paper presented at the Proc. International Conference on Steel Structures of the 2000s, Istanbul.

Al-Jabri, K., Seibi, A., & Karrech, A. (2006). Modelling of unstiffened flush end-plate bolted connections in fire. *Journal of Constructional Steel Research, 62*(1), 151-159.

Al-Jabri, K. S. (1999). *The behaviour of steel and composite beam-to-column connections in fire.* University of Sheffield.

Al-Jabri, K. S., & Al-Alawi, S. M. (2007). Predicting the behaviour of semi-rigid joints in fire using an artificial neural network. *Steel Structures, 7*, 209-217.

Al-Jabri, K. S., Davison, J. B., & Burgess, I. W. (2008). Performance of beam-to-column joints in fire—a review. *Fire Safety Journal, 43*(1), 50-62.

AS4084. (2012). Steel Storage Racking. *Standards Australia*.

Bajoria, K., & McConnel, R. (1984). *Progressive Collapse of Warehouse Racking.* Paper presented at the Space Structures, Third International Conference.

Bajoria, K., & Talikoti, R. (2006). Determination of flexibility of beam-to-column connectors used in thin walled cold-formed steel pallet racking systems. *Thin-Walled Structures, 44*(3), 372-380.

Bajoria, K. M., Sangle, K. K., & Talicotti, R. S. (2010). Modal analysis of cold-formed pallet rack structures with semi-rigid connections. *Journal of Constructional Steel Research, 66*(3), 428-441.

Baldassino, N., & Bernuzzi, C. (2000). Analysis and behaviour of steel storage pallet racks. *Thin-Walled Structures, 37*(4), 277-304.

Beale, R., & Godley, M. (2001). *Problems arising with pallet rack semi-rigid base-plates.* Paper presented at the 1st international conference on steel and composite structures.

Bernuzzi, C., & Castiglioni, C. A. (2001). Experimental analysis on the cyclic behaviour of beam-to-column joints in steel storage pallet racks. *Thin-Walled Structures, 39*(10), 841-859.

Bernuzzi, C., Gobetti, A., Gabbianelli, G., & Simoncelli, M. (2015a). Unbraced pallet rack design in accordance with European practice–Part 1: Selection of the method of analysis. *Thin-Walled Structures, 86*, 185-207.

Bernuzzi, C., Gobetti, A., Gabbianelli, G., & Simoncelli, M. (2015b). Unbraced pallet rack design in accordance with European practice–Part 2: Essential verification checks. *Thin-Walled Structures, 86*, 208-229.

Bravery, P. (1993). Cardington large building test facility, Construction details for the first building. *Building Research Establishment, Internal paper, Watford*, 158.

BS5950. (1990). Structural use of steelwork in building, Part 8, Code of practice for fire resistant design. *British Standards Institution, London*.

Burgess, I., Davison, J. B., Dong, G., & Huang, S.-S. (2012). The role of connections in the response of steel frames to fire. *Structural Engineering International, 22*(4), 449-461.

Cai, Y., & Young, B. (2014). Behavior of cold-formed stainless steel single shear bolted connections at elevated temperatures. *Thin-Walled Structures, 75*, 63-75.

Cai, Y., & Young, B. (2015). High temperature tests of cold-formed stainless steel double shear bolted connections. *Journal of Constructional Steel Research, 104*, 49-63.

Cai, Y., & Young, B. (2016). Bearing factors of cold-formed stainless steel double shear bolted connections at elevated temperatures. *Thin-Walled Structures, 98*, 212-229.

Casafont, M., Pastor, M. M., Roure, F., & Peköz, T. (2011). An experimental investigation of distortional buckling of steel storage rack columns. *Thin-Walled Structures, 49*(8), 933-946.

Chen, C., Scholl, R., & Blume, J. (1980). *Earthquake simulation tests of industrial steel storage racks.* Paper presented at the Proceedings of the Seventh World Conference on Earthquake Engineering, Istanbul, Turkey.

Chen, J., & Young, B. (2006). Corner properties of cold-formed steel sections at elevated temperatures. *Thin-Walled Structures, 44*(2), 216-223.

Chen, J., & Young, B. (2007). Experimental investigation of cold-formed steel material at elevated temperatures. *Thin-Walled Structures, 45*(1), 96-110.

da Silva, L. S., Santiago, A., & Real, P. V. (2001). A component model for the behaviour of steel joints at elevated temperatures. *Journal of Constructional Steel Research, 57*(11), 1169-1195.

EC3. (2005a). EN-1993-Design of steel structures-Part 1-8: Design of joints. *European Committee for Standardization, Brussels, Belgium*.

EC3. (2005b). EN-1993-Design of steel structures–Part 1-2: General rules–Structural fire design. *European Committee for Standardization, Brussels, Belgium*.

Ellobody, E., & Young, B. (2005). Structural performance of cold-formed high strength stainless steel columns. *Journal of Constructional Steel Research, 61*(12), 1631-1649.

EN15512. (2009). Steel static storage systems– Adjustable pallet racking systems– Principles for structural design. *European Committee for Standardization*.

FEM. (1997). Recommendations for the design of steel static pallet racking and shelving. Section X. *Fédération Européenne de la Manutention, Brussels, Belgium*.

Filiatrault, A., Bachman, R. E., & Mahoney, M. G. (2006). Performance-based seismic design of pallet-type steel storage racks. *Earthquake spectra, 22*(1), 47-64.

Filiatrault, A., Higgins, P. S., & Wanitkorkul, A. (2006). Experimental stiffness and seismic response of pallet-type steel storage rack connectors. *Practice Periodical on Structural Design and Construction, 11*(3), 161-170.

Filiatrault, A., Higgins, P. S., Wanitkorkul, A., & Courtwright, J. (2007). Experimental stiffness of pallet-type steel storage rack tier drop connectors. *Practice Periodical on Structural Design and Construction, 12*(4), 210-215.

Filiatrault, A., Higgins, P. S., Wanitkorkul, A., Courtwright, J. A., & Michael, R. (2008). Experimental seismic response of base isolated pallet-type steel storage racks. *Earthquake spectra, 24*(3), 617-639.

Filiatrault, A., & Wanitkorkul, A. (2004). Shake-table testing of frazier industrial storage racks *Report no. CSEE-SEESL-2005-02, Structural Engineering and Earthquake Simulation Laboratory, Departmental of Civil, Structural and Environmental Engineering*: University at Buffalo, State University of New York.

Freitas, A. M., Souza, F. T., & Freitas, M. S. (2010). Analysis and behavior of steel storage drive-in racks. *Thin-Walled Structures, 48*(2), 110-117.

Freitas, A. M. S., Freitas, M. S. d. R., & Souza, F. T. d. (2005). Analysis of steel storage rack columns. *Journal of Constructional Steel Research, 61*(8), 1135-1146.

Garlock, M. E., & Selamet, S. (2010). Modeling and behavior of steel plate connections subject to various fire scenarios. *Journal of Structural Engineering, 136*(7), 897-906.

Gilbert, B. P., & Rasmussen, K. J. (2009). Experimental test on steel storage rack components *TUoS School of Civil Engineering, Australia (Ed.), School of Civil Engineering, The University of Sydney, Australia*.

Gilbert, B. P., & Rasmussen, K. J. (2011a). Determination of the base plate stiffness and strength of steel storage racks. *Journal of Constructional Steel Research, 67*(6), 1031-1041.

Gilbert, B. P., & Rasmussen, K. J. (2011b). Drive-in steel storage racks I: Stiffness tests and 3D load-transfer mechanisms. *Journal of Structural Engineering, 138*(2), 135-147.

Gilbert, B. P., & Rasmussen, K. J. (2011c). Impact tests and parametric impact studies on drive-in steel storage racks. *Engineering Structures, 33*(5), 1410-1422.

Gilbert, B. P., Rasmussen, K. J., Baldassino, N., Cudini, T., & Rovere, L. (2012). Determining the transverse shear stiffness of steel storage rack upright frames. *Journal of Constructional Steel Research, 78*, 107-116.

Gilbert, B. P., Teh, L. H., Badet, R. X., & Rasmussen, K. J. (2014). Influence of pallets on the behaviour and design of steel drive-in racks. *Journal of Constructional Steel Research, 97*, 10-23.

Godley, M. (1991). Storage racking-chapter 11. *Design of Cold Formed Steel Members. Ed. Rhodes*.

Godley, M. (1997). Plastic design of pallet rack beams. *Thin-Walled Structures, 29*(1), 175-188.

Godley, M., & Beale, R. (2008). Investigation of the effects of looseness of bracing components in the cross-aisle direction on the ultimate load-carrying capacity of pallet rack frames. *Thin-Walled Structures, 46*(7), 848-854.

Godley, M., Beale, R., & Feng, X. (1998). *Rotational stiffness of semi-rigid baseplates.* Paper presented at the Proceedings of the 14th International Specialty Conference on Cold-Formed Steel Structures.

Godley, M., Beale, R., & Feng, X. (2000). Analysis and design of down-aisle pallet rack structures. *Computers & structures, 77*(4), 391-401.

Hancock, G. J. (1985). Distortional buckling of steel storage rack columns. *Journal of Structural Engineering, 111*(12), 2770-2783.

Harris, E. (2007). *Sway behaviour of high rise steel storage racks.* (Doctoral Thesis), University of Sydney, Sdney.

Harris, E., & Hancock, G. J. (2002). *Sway stability testing of high rise rack sub-assemblages.* Paper presented at the Sixteenth international specialty conference on cold-formed steel structures, Florida, USA.

Hu, Y., Davison, B., Burgess, I., & Plank, R. (2009). Component modelling of flexible end-plate connections in fire. *International Journal of Steel Structures, 9*(1), 1-15.

Kaitila, O. (2002). *Finite element modelling of cold-formed steel members at high temperatures*: Helsinki University of Technology.

Kankanamge, N. D. (2010). *Structural behaviour and design of cold-formed steel beams at elevated temperatures*: Queensland University of Technology, Brisbane.

Kankanamge, N. D., & Mahendran, M. (2011). Mechanical properties of cold-formed steels at elevated temperatures. *Thin-Walled Structures, 49*(1), 26-44.

Kilar, V., Petrovčič, S., Koren, D., & Šilih, S. (2011). Seismic analysis of an asymmetric fixed base and base-isolated high-rack steel structure. *Engineering Structures, 33*(12), 3471-3482.

Koen, D. J. (2008). *Structural capacity of light gauge steel storage rack uprights.* (Master of Engineering), University of Sydney, Sydney.

Kozłowski, A., & Ślęczka, L. (2004). *Preliminary component method model of storage rack joint.* Paper presented at the Proceedings of Connections in Steel Structures V, Amsterdam.

Krawinkler, H., Cofie, N., Astiz, M., & Kircher, C. (1979). Experimental Study on the Seismic Behavior of Industrial Storage Racks Report No. 41. The John A. Blume Earthquake Engineering Center, Department of Civil and Environmental Engineering: Stanford University California.

Kwarteng, K., Beale, R., Godley, M., & Thomson, S. (2012). *The Effects of Seismic Loading on Pallet Rack Semi-Rigid Joints.* Paper presented at the Proceedings of the Eleventh International Conference on Computational Structures Technology, Scotland.

Laím, L., & Rodrigues, J. P. C. (2016). Numerical analysis on axially-and-rotationally restrained cold-formed steel beams subjected to fire. *Thin-Walled Structures, 104*, 1-16.

Laím, L., Rodrigues, J. P. C., & Craveiro, H. D. (2016). Flexural behaviour of axially and rotationally restrained cold-formed steel beams subjected to fire. *Thin-Walled Structures, 98,* 39-47.

Lau, H. H. (2002). *The influence of column base connectivity on the stability of columns and frames.* Oxford Brookes University.

Lawson, R. (1990). Behaviour of steel beam-to-column connections in fire. *Structural Engineer, 68*, 263-271.

Lee, J. H., Mahendran, M., & Makelainen, P. (2003). Prediction of mechanical properties of light gauge steels at elevated temperatures. *Journal of Constructional Steel Research, 59*(12), 1517-1532.

Lee, Y. H., Tan, C. S., Mohammad, S., Md Tahir, M., & Shek, P. N. (2014). Review on Cold-formed steel Connections. *The Scientific World Journal, 2014*.

Leston-Jones, L. C. (1997). The influence of semi-rigid connections on the performance of steel framed structures in fire.

Mahoney, M. (2008). Performance-based seismic design of pallet-type steel storage racks. *Earthquake spectra, 22*(1), 47-64.

Makelainen, P., & Miller, K. (1983). Mechanical Properties of Cold-Formed Galvanized Sheet Steel Z32 at Elevated Temperatures. *Helsinki University of Technology, Finland*.

Mao, C., Chiou, Y.-J., Hsiao, P.-A., & Ho, M.-C. (2009). Fire response of steel semi-rigid beam–column moment connections. *Journal of Constructional Steel Research, 65*(6), 1290-1303.

Markazi, F., Beale, R., & Godley, M. (1997). Experimental analysis of semi-rigid boltless connectors. *Thin-Walled Structures, 28*(1), 57-87.

Markazi, F., Beale, R., & Godley, M. (2001). Numerical modelling of semi-rigid boltless connectors. *Computers & structures, 79*(26), 2391-2402.

Moen, C. D., & Schafer, B. (2009). Elastic buckling of cold-formed steel columns and beams with holes. *Engineering Structures, 31*(12), 2812-2824.

Ng, A., Beale, R., & Godley, M. (2009). Methods of restraining progressive collapse in rack structures. *Engineering Structures, 31*(7), 1460-1468.

Outinen, J., & Makelainen, P. (2001). *Effect of high temperature on mechanical properties of cold-formed structural steel.* Paper presented at the Tubular Structures-International Symposium.

Prabha, P., Marimuthu, V., Saravanan, M., & Jayachandran, S. A. (2010). Evaluation of connection flexibility in cold formed steel racks. *Journal of Constructional Steel Research, 66*(7), 863-872.

Ramberg, W., & Osgood, W. R. (1943). Description of stress-strain curves by three parameters.

Ranawaka, T., & Mahendran, M. (2006). *Finite element analyses of cold-formed steel columns subject to distortional buckling under simulated fire conditions.* Paper presented at the Proceedings of the international colloquium on stability and ductility of steel structures.

Ranawaka, T., & Mahendran, M. (2009a). Distortional buckling tests of cold-formed steel compression members at elevated temperatures. *Journal of Constructional Steel Research, 65*(2), 249-259.

Ranawaka, T., & Mahendran, M. (2009b). Experimental study of the mechanical properties of light gauge cold-formed steels at elevated temperatures. *Fire Safety Journal, 44*(2), 219-229.

Ranawaka, T., & Mahendran, M. (2010). Numerical modelling of light gauge cold-formed steel compression members subjected to distortional buckling at elevated temperatures. *Thin-Walled Structures, 48*(4), 334-344.

RMI. (2012). Specification for the design, testing and utilization of industrial steel storage rack- Material Handling Industry, MH16.1. *Rack Manufacturing Institute*.

Roure, F., Somalo, M. R., Casafont, M., Pastor, M. M., Bonada, J., & Peköz, T. (2013). Determination of beam-to-column connection characteristics in pallet rack structures: a comparison of the EN and ANSI methods and an analysis of the influence of the moment-to-shear ratios. *Steel Construction, 6*(2), 132-138.

Sangle, K. K., Bajoria, K. M., & Talicotti, R. S. (2012). Elastic stability analysis of cold-formed pallet rack structures with semi-rigid connections. *Journal of Constructional Steel Research, 71*, 245-262.

Sarawit, A. T., & Pekoz, T. (2002). *Design of industrial storage racks.* Paper presented at the Sixteenth international specialty conference on cold-formed steel structures, USA.

Sarawit, A. T., & Peköz, T. (2006). Notional load method for industrial steel storage racks. *Thin-Walled Structures, 44*(12), 1280-1286.

SEMA. (1985). Code of practice for the design of static racking. *Storage Equipment Manufacturers' Association, Birmingham United Kingdom*.

Sideris, P., & Filiatrault, A. (2009). *Dynamic analysis of rigid bodies on inclined plane surfaces: application to prediction of merchandise response in steel storage racks under earthquake excitation.* Paper presented at the COMPDYN 2009, ECCOMAS Thematic Conference on Computational Methods in Structural Dynamics and Earthquake Engineering.

Sideris, P., Filiatrault, A., Leclerc, M., & Tremblay, R. (2010). Experimental investigation on the seismic behavior of palletized merchandise in steel storage racks. *Earthquake spectra, 26*(1), 209-233.

Sidey, M., & Teague, D. (1988). Elevated temperature data for structural grades of galvanized steel. *British Steel (Welsh Laboratories) Report, UK*.

Simulia, D. (2011). Abaqus 6.11 analysis user's manual. *Abaqus 6.11 Documentation*, 22.22.

Sleczka, L., & Kozłowski, A. (2007). Experimental and theoretical investigations of pallet rack connections. *Advanced Steel Construction, 3*(2), 607-627.

Spyrou, S., Davison, J., Burgess, I., & Plank, R. (2004a). Experimental and analytical investigation of the 'compression zone'component within a steel joint at elevated temperatures. *Journal of Constructional Steel Research, 60*(6), 841-865.

Spyrou, S., Davison, J., Burgess, I., & Plank, R. (2004b). Experimental and analytical investigation of the 'tension zone'components within a steel joint at elevated temperatures. *Journal of Constructional Steel Research, 60*(6), 867-896.

Stark, J. W., & Tilburgs, K. (1978). European research on pallet, drive-in and drive-through racks. Netherland: Delft University of Technology.

Stoddart, E., Byfield, M., & Tyas, A. (2012). Blast modeling of steel frames with simple connections. *Journal of Structural Engineering, 140*(1), 04013027.

Sun, R., Burgess, I. W., Huang, Z., & Dong, G. (2015). Progressive failure modelling and ductility demand of steel beam-to-column connections in fire. *Engineering Structures, 89*, 66-78.

Teh, L. H., Hancock, G. J., & Clarke, M. J. (2004). Analysis and design of double-sided high-rise steel pallet rack frames. *Journal of Structural Engineering, 130*(7), 1011-1021.

Wang, T., Zhao, X.-z., & Chen, Y.-y. (2010). State of the Art on Assembled Steel Storage Racks [J]. *Progress in Steel Building Structures, 6*, 004.

Wei, C., & Jihong, Y. (2012). Mechanical properties of G550 cold-formed steel under transient and steady state conditions. *Journal of Constructional Steel Research, 73*, 1-11.

Winter, G., & Pekoz, T. (1973). *Cold-formed steel rack structures.* Paper presented at the Second specialty conference on cold-formed steel structures, USA.

Yu, H., Burgess, I., Davison, J., & Plank, R. (2008). Numerical simulation of bolted steel connections in fire using explicit dynamic analysis. *Journal of Constructional Steel Research, 64*(5), 515-525.

Zhang, H., Gilbert, B. P., & Rasmussen, K. J. (2011). Drive-in steel storage racks. II: Reliability-based design for forklift truck impact. *Journal of Structural Engineering, 138*(2), 148-156.

Zhao, X., Wang, T., Chen, Y., & Sivakumaran, K. (2014). Flexural behavior of steel storage rack beam-to-upright connections. *Journal of Constructional Steel Research, 99*, 161-175.

LIST OF PUBLICATIONS AND PRESENTED PAPERS

S.NO	Authors, title, journal details and year of publication	ISI Thomas Reuters Web of Science category
1.	**Shah, S. N. R.,** Sulong, N. R., Shariati, M., Khan, R., &Jumaat, M. Z. (2016). Behavior of steel pallet rack beam-to-column connections at elevated temperatures. ***Thin-Walled Structures***, 106, 471-483.	Q1
2.	**Shah, S. N. R.,** Sulong, N. R., Jumaat, M. Z., & Shariati, M. (2016). State-of-the-art review on the design and performance of steel pallet rack connections. ***Engineering Failure Analysis***, 66, 240-258.	Q2
3.	**Shah, S. N. R.,** Sulong, N. R., Shariati, M., & Jumaat, M. Z. (2015). Steel rack connections: identification of most influential factors and a comparison of stiffness design methods. ***PloS one***, 10(10), e0139422.	Q1
4.	**Shah, S. N. R.,** Sulong, N. R., Khan, R., Jumaat, M. Z., & Shariati, M. (2016). Behavior of industrial steel rack connections. ***Mechanical Systems and Signal Processing***, 70, 725-740.	Q1
5.	**Shah, S.N.R.,** Sulong, N.H.R., & Jumaat, M.Z. (2015). Effect of column thickness on the strength and stiffness of steel pallet rack connections. Proceedings of the 7th Asia Pacific Young Researchers and Graduates Symposium, 20-21 August, Kuala Lumpur, Malaysia	Conference paper